PHYTOCHEMICAL STUDIES ON THE MASTIC GUM OF *PISTACIA LENTISCUS* VAR. *CHIA* COLLECTED FROM KARABURUN PENINSULA AND BIOACTIVITIES OF ISOLATES

A Thesis Submitted to the Graduate School of Engineering and Sciences of İzmir Institute of Technology in Partial Fulfillment of the Requirements for the Degree of

MASTER OF SCIENCE

in Biotechnology

by
Mehmet DEMİR

December 2021
İZMİR

ACKNOWLEDGMENTS

I would like to express my endless thanks to my supervisor Prof. Dr. Erdal BEDİR for his continuous direction, support, guidance, and motivation in all time of my master thesis and related research. I am grateful to him for his encouragement, patience, and immense knowledge.

I would like to thank my co-adviser Prof. Dr. Petek BALLAR KIRMIZIBAYRAK for her direction and experimental aids.

I also want to thank Ünver KURT for structure elucidation studies and his assistance. He always shared his knowledge and helped me throughout my experiments.

I'm grateful to Göklem ÜNER for support and assisting the bioactivity studies.

I would like to thank my officemates Berivan Dizmen, Eyüp Bilgi, Gamze Doğan, Gülten Kuru, Melis Küçüksolak and all BEDİR group members for their valuable friendship, comment, and support.

I would like to thank Mustafa Özer and Madlen Staaf Kura for providing us with the mastic gum

I also want to thank Assoc. Prof. Muhittin AYGÜN for X-ray diffraction analysis.

Finally, and most importantly, I strongly thank my family for supporting during my education and social life. Also, I am grateful of my parents for their patience, love, and support throughout my life.

ABSTRACT

PHYTOCHEMICAL STUDIES ON THE MASTIC GUM OF *PISTACIA LENTISCUS* VAR. *CHIA* COLLECTED FROM KARABURUN PENINSULA AND BIOACTIVITIES OF ISOLATES

Pistacia lentiscus L. is an evergreen shrub or tree-like plant named as 'mastic tree'. The phytochemical studies of Chios mastic gum have revealed that it is a complex natural product comprising several organic ingredients like natural polymers, essential oils and triterpenic compounds. Triterpenes are the main components of mastic gum, and they are thought to be responsible for important biological activities such as anti-cancer, anti-ulcer, cytotoxic, antidiabetic, and anti-inflammatory.

Within the scope of this thesis, mastic gum collected from the mastic trees (*Pistacia lentiscus* var. *chia*) grown on the Karaburun peninsula of İzmir was investigated to reveal its phytochemical composition and neuroprotective effects of the isolates. Isolation and purification studies utilizing chromatographic methods are followed by structural elucidation of the isolates by spectroscopic methods (1D NMR, 2D NMR, MS and X-RAY). Detailed analysis of the obtained spectra helped us to establish structures of 14 molecules possessing triterpenic skeleton, and two of them turned out to be undescribed compounds. The bioactivity of selected compounds was screened for their neuroprotective effects against H_2O_2 induced oxidative stress on differentiated and undifferentiated SH-SY5Y cells. Two compounds showed neuroprotective effects against H_2O_2-induced cell death on undifferentiated SH-SY5Y cells at 5 and 10 µM concentrations, while the other compounds either showed little or no effect. This study provides promising new insights into the use of mastic gum or its components in the treatment of neurodegenerative diseases.

ÖZET

KARABURUN YARIMADASI'NDAN TOPLANAN *PİSTACİA LENTİSCUS* VAR. *CHİA* DAMLA SAKIZI ÜZERİNDE FİTOKİMYASAL ÇALIŞMALAR VE İZOLATLARIN BİYOAKTİVİTELERİ

Pistacia lentiscus L var. *chia*., 'sakız ağacı' adı verilen yaprak dökmeyen bir çalı veya ağaç benzeri bir bitkidir. Damla sakızının fitokimyasal çalışmaları, damla sakızının doğal polimer, uçucu yağ, uçucu ve triterpenik bileşikler gibi çeşitli organik bileşenlerden oluşan karmaşık bir doğal ürün olduğunu ortaya koymuştur. Triterpenler sakız sakızının ana bileşenleri olup, antikanser, anti-ülser, sitotoksik, antidiyabetik ve anti-inflamatuar gibi önemli biyolojik aktivitelerden sorumlu oldukları düşünülmektedir.

Bu tez kapsamında Karaburun Yarımadası'nda (İzmir) yetiştirilen sakız ağacından (*Pistacia lentiscus* var. *chia*) elde edilen damla sakızının fitokimyasal profili ve metabolitlerinin nöroprotektif etkisi araştırılmıştır. Kromatografik yöntemlerle gerçekleştirilen izolasyon ve saflaştırma çalışmalarını spektroskopik yöntemler ile (1D NMR, 2D NMR, MS ve X-Ray) yapı aydınlatma çalışmaları takip etmiştir. Elde edilen spektrumların detaylı analizi triterpen grubu toplam 14 bileşiğin yapısal karakterizasyonu ile sonuçlanmış ve bu bileşiklerden ikisinin yeni olduğu belirlenmiştir. Seçilen moleküllerin biyoaktivitesi, farklılaştırılmış ve farklılaştırılmamış SH-SY5Y hücrelerinin H_2O_2 kaynaklı oksidatif strese karşı nöroprotektif etkileri açısından taranmıştır. İki bileşik, 5 ve 10 μM konsantrasyonlarda farklılaşmamış SH-SY5Y hücreleri üzerinde H_2O_2 kaynaklı hücre ölümüne karşı nöroprotektif etkiler gösterirken, diğer bileşikler ya çok az etki göstermiş ya da hiç etki göstermemiştir. Bu çalışma, nörodejeneratif hastalıkların tedavisinde damla sakızı ve bileşiklerinin kullanım potansiyeli ile ilgili umut verici yeni bilgiler sunmaktadır.

TABLE OF CONTENTS

LIST OF FIGURES

Figure **Page**

LIST OF TABLES

LIST OF SPECTRA

Spectrum **Page**

Spectrum **Page**

Spectrum **Page**

ABBREVIATIONS

1D-NMR	One-Dimensional Nuclear Magnetic Resonance
2D-NMR	Two-Dimensional Nuclear Magnetic Resonance
^{13}C NMR	Carbon Nuclear Magnetic Resonance
^{1}H NMR	Proton Nuclear Magnetic Resonance
ACE	Acetone
ACN	Acetonitrile
CC	Column Chromatography
CH_2CI_2	Dichloromethane
C_5D_5N	Deuterated pyridine
$CHCI_3$	Chloroform
COSY	Correlation Spectroscopy
d	Doublet
DEPT	Distortionless Enhancement by Polarization Transfer
EtOAc	Ethyl Acetate
MeOH	Methanol
H_2O	Water
H_2SO_4	Sulfuric Acid
Hex	n-Hexane
HMBC	Heteronuclear Multiple Bond Coherence
HSQC	Heteronuclear Single Quantum Coherence
Fr.	Fraction
LC-MS	Liquid Chromatography-Mass Spectrometry
m	Multiple
MPLC	Medium Pressure Liquid Chromatography
NMR	Nuclear Magnetic Resonance
NOESY	Nuclear Overhauser Enhancement Spectroscopy
s	Singlet
q	Quartet
RP-VLC	Reverse Phase Vacuum Liquid Chromatography
TLC	Thin Layer Chromatography
UV	Ultraviolet

CHAPTER 1

INTRODUCTION

Anacardiaceae, a member of the sumac family of flowering plants, is one of the most common families worldwide, which grow mainly in coastal areas such as Turkey, Iran, China, Italy, and Brazil. Anacardiaceae family represents about 850 species belonging to 70 genera, including Anacardium, Holigarna, Mangifera, Pistacia, and Comocladia. The representatives of this family have several morphological types exhibiting characteristic roots, stems, sizes, and leaves.[1,2].

Pistacia lentiscus L., in the genus *Pistacia* in the family Anacardiaceae (Sumac) of the order Sapindales, is an evergreen shrub or tree-like plant. Also called 'mastic tree', it is a perennial plant with dense foliage. It is native to coastal areas of the Mediterranean region and generally grows in countries dominated by Mediterranean climates such as Turkey, Tunisia, Algeria, Italy, Iberia, and Greece. Although the mastic tree is widespread worldwide, mastic gum production is obtained only from male *Pistacia lentiscus* var. Chia trees grown in the southeastern parts of the Greek island Chios and Karaburun and Çesme peninsula of İzmir.[3,4]

Even though the first study on the chemical constituents of mastic gum was conducted in 1930, the chemical composition of the resin has not been fully determined yet. According to the European Health Agency's (EMA) mastic gum assessment report, the chemical composition of gum resin consists of natural polymers, triterpenes, monoterpene hydrocarbons, oxidized monoterpenes and sesquiterpenes, polyphenols, and phytosterols. Triterpenoids, which are important components of mastic gum, exhibit significant biological activities such as anti-cancer, anti-ulcer, cytotoxic, antidiabetic, and anti-inflammatory.[5,6]

Traditionally, *Pistacia lentiscus L*. has been used for medicinal purposes like phytotherapeutic remedy and cosmetic agents since ancient times was exploited for this purpose in the Mediterranean region. Furthermore, it is exploited in folk medicine to treat several diseases such as coughs, eczema, stomach pains, ulcers, and kidney stones.

Based on the studies performed on mastic gum, it has been shown that extract and triterpenic components of mastic gum have great importance in terms of exhibiting various biological activities. In the literature, since there are a few phytochemical studies and bioactivity screenings on mastic gum grown in Turkey, especially its triterpene-rich fractions profile and biological activity studies were not investigated. Also, there are still many unrevealed triterpenoids found in mastic gum and the bioactivities of isolates. For this reason, we aimed to reveal the triterpenoid constituents of Karaburun Peninsula mastic gum and to evaluate the neuroprotective effect of elucidated compounds.

1.1.Natural products

Since ancient times, humankind has exploited several natural products from plants, animals, microorganisms, and marine organisms for medicinal purposes. For centuries, they have been used for human, veterinary, and agricultural purposes to treat and alleviate diseases. With advances in chemical science towards the end of the 18th century, it became possible to study and identify the biologically active metabolites from natural sources. In particular, natural products, also called secondary metabolites, pose a huge structural and chemical variety that is not vital for the host's survival but provides the host with some advantages like defense. Due to these biologically active metabolites, natural products have been successfully employed in both traditional and modern medicine.[7,8]

1.2.Drug discovery from natural products

Natural products play a key role in drug discovery and development studies since many drugs have natural products or derived from natural products as active ingredients. The presence of more than 200000 biologically active metabolites shows how important natural products are in the discovery and development of new drugs. A study by Newman and Cragg (2016) showed that 70% of the total 1562 new drugs approved by the Food and Drug Administration (FDA) between 1981 and 2014 are of natural origin.[9]

One of the important sources of natural products is medicinal plants for new drugs and therapeutic agents. Throughout history, they have been utilized for the treatment of several diseases all over the world. The widespread use of plants in traditional medicine, especially in Chinese medicine, has led to the search for the bioactive compounds they

contain. Also, the uses of medicinal plants in traditional medicine can provide information on efficacy and safety. In addition to the pharmacological use of secondary metabolites from plants, they are also used in various fields such as sweeteners, essences, dyes, and foods.[10]

Phytochemical studies on plants have revealed bioactive compounds found in plants and complex chemicals that are difficult to obtain synthetically. Many drugs have been introduced to science by further clinical, pharmacological, and chemical studies of molecules obtained as a result of these studies. By far, the most famous and well-known example is aspirin, a natural product-derived anti-inflammatory drug. It was obtained from the synthesis of Salicin discovered from the bark of the willow tree *Salix alba L*. Another example is Taxol (Paclitaxel), discovered from the bark of Pacific yew (*Taxus brevifolia*), a natural product-based anti-cancer drug approved by the FDA in 2002. In addition to aspirin **(1)** and Taxol **(2)**, there are many drugs isolated from natural products such as morphine **(3)**, quinine **(4)**, pilocarpine **(5)**, artemisinin **(6)**. (Figure 1).

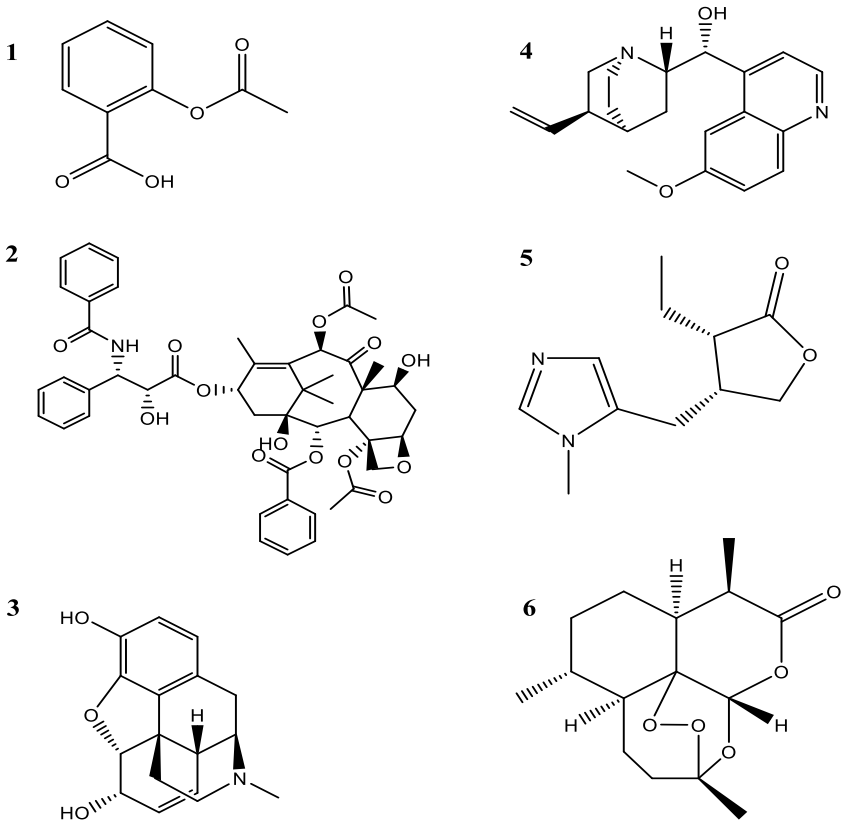

Figure 1. Some natural product-derived drugs

1.3. *Pistacia lentiscus* var. *chia* (Mastic tree)

Pistacia lentiscus var. *Chia* (mastic tree), which is in the genus Pistacia belonging to the Anacardiaceae family of the order Sapindales, is an evergreen shrub or tree-like plant that can grow up to 1 to 5 m in height (Figure 2). It is widely distributed in coastal countries of the Mediterranean and Aegean regions and as scrub vegetation in coastal areas up to 500 m above sea level up to The Canary Islands in the West, while in our country it spreads in the Aegean and Mediterranean regions, especially in the Cesme and Karaburun Peninsula. [3]

Although the distribution area in the world is quite broad, mastic gum production is only produced by the male chia trees grown in regions in the southeastern parts of Chios (Chios/Greece) and certain regions in the Çesme District of İzmir. Since this plant has an aromatic resin known as mastic resin or mastic gum, the plant has been called a 'mastic tree'. The mastic tree, which holds significant medicinal value, has already been utilized in traditional medicines such as Siddha Chinese and Ayurveda.[4,11]

Table 1. Taxonomical Classification[12]

KINGDOM	*Plantae*
DIVISION	*Tracheophyta*
CLASS	*Magnoliopsida*
ORDER	*Sapindales*
FAMILY	*Anacardiaceae*
GENUS	*Pistacia*
SPECIES	*Pistacia lentiscus*
BINOMIAL NAME	*Pistacia lentiscus* L.- Mastic tree

Figure 2. *Pistacia lentiscus* var. chia (mastic tree)

The commercially valuable mastic gum is harvested via efflux from scrapes formed on the trunk of the plant. The mastic tree grows very slowly in natural conditions and reaches maximum gum secretion efficiency after 10 years. A significant decrease in both gum secretion and gum quality is observed after the age of 70. Although both female trees and male trees produce mastic gum, the quality of gum harvested from male trees is higher. After taking the tree-like form, the mastic tree secretes gum to heal their wounds and strengthen their trunks. The harvested resins are named Pitta, Fliskri, Daktilidopetra, and Tear according to their secretion forms and sizes. The most valuable of them are Mastic tears (Figure 3). Freshly harvested mastic is colorless, but as a result of exposure to sunlight during harvest, the Mastic first turns slightly to yellow and then orange-yellow over the years. This color change can be explained by oxidation initiated by exposure to sunlight.[13–15]

A mastic tree produces about 1 kg of gum per year. According to the 2015 report, about 250 tons of gum are exported annually from the island of Chios. The mastic gum production is carried out commercially only on the Greek island of Chios and is registered by the European Union as a protected designation of origin and covered by EU financial support programs. In our country, although the mastic tree growing especially on the Çesme and Karaburun peninsula, it has more potential than in Greece where the production of mastic gum is very low. It should be encouraged to produce mastic gum in our country commercially since it has a price of about 70 Euros per kilogram. Due to the variety of chemical ingredients of mastic gum and the prevalence of its traditional use, it

is an important economic value and can be used for a wide range of areas with different purposes, such as the pharmaceutic, food, and chemical industry.[5,11]

Figure 3. Mastic tears from *Pistacia lentiscus* L.

Also, the leaves and fruits of the mastic tree have pharmacological importance and have been used for centuries as well as mastic gum. In recent years, the phytochemical studies on mastic gum showed that its metabolites have diverse bioactivities such as antidiabetic, anti-ulcer, anti-cancer, antiviral, and wound healing. But chemical ingredients of mastic gum and their specific bioactivities remain unclear.[4,16,17] Although it has been used for many years for different purposes, the production of mastic gum in our country is not appraised effectively.

1.3.1. Phytochemical studies of *Pistacia lentiscus* var. *chia*

The chemical constituents of *Pistacia lentiscus* var. chia have been studied by many researchers. Phytochemical studies on Chios mastic gum date back to the early 1900s.[5] These studies have demonstrated that mastic gum is a complex natural product consisting of various organic ingredients, including the natural polymer (approx. 25%), volatile compounds (approx. 5%), and triterpenoids (approx. 70%), the latter of which is the most abundant. Although more than 100 chemical compounds have been identified to date, its chemical content has still not been fully revealed.[11,18–21] Since Chios mastic gum

is insoluble in water, only nonpolar solvents such as hexane, chloroform, dichloromethane, and ethyl acetate can be used to dissolve the resin. Because of this property of the resin, identification and isolation of its chemical components are both difficult and costly but this is the nature of triterpenes in general.[11]

1.3.1.1. The natural polymer of the mastic resin

The chemical components of Chios mastic gum are held in a resin structure due to the presence of a natural polymer. In the study by Berg *et al*., the polymer of mastic gum was identified as *cis*-1,4-poly-*β*-myrcene with a molecular weight of 100.000 Da (Figure 4). When the resin leaks out from the tree, *β*-myrcene, a monoterpene, rapidly polymerizes and solidifies by radical chain reactions.[22] For the isolation of bioactive molecules from mastic gum, this polymer needs to be removed, by which purification process would be facilitated. Thus, the isolation of the polymeric substance is carried out by diluting the resin in DCM, followed by MeOH precipitation and Size Exclusion Chromatography (SEC). Spectral methods are used to elucidate the polymer structure, such as GC-MS, FT-IR, ^{1}H-NMR, ^{13}C-NMR, 2D NMR, DEPT-NMR. This is the first study reporting the naturally occurring polymer of a monoterpene, *β*-myrcene that was defined to be in both *cis*- and *trans*-configurations, and the cis-trans ratio was estimated to be 3/1. A similar method has been used by some other research groups to fractionate or separate the polymer substance from the mastic gum.[21,23,24] Recently, Xynos *et al*. carried out a novel separation process involving the use of Supercritical Fluid Extraction to remove the polymer from the Chios resin.[25]

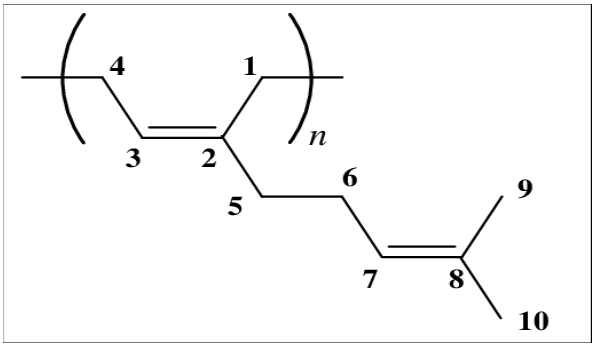

Figure 4. Chemical structure of monoterpene-based cis-1,4-poly-β-myrcene

1.3.1.2. Volatile compounds and essential oil

Volatile compounds consist of the main components of mastic essential oil, which accounts for about 3-5% of the weight of the harvested resin. The mastic oil can be obtained via hydrodistillation.[26] Recently, Supercritical Fluid Extraction has been proposed to the essential oil from mastic gum, as a different method to the traditional distillation method.[25]

The chemical constituents of the essential oil have been investigated by many researchers via several methods.[4,24,25,27–30] The major chemical constituents of which were found to be monoterpene hydrocarbons (50%), sesquiterpenes (25%), and oxygenated monoterpenes (20%).[25] To date, approximately 70 constituents have been determined, and the main compounds of mastic essential oil are α-pinene (30-75%), β-pinene (1-3%), and myrcene (3-60 %).[11,28] Moreover, unlike classic mastic essential oil, 15 of the volatile compounds have been obtained from mastic water that have not been identified from mastic resin or mastic oil previously.[25] Also, these compounds were found to be exhibiting several biological activities such as antibacterial[28], antimicrobial[31], antifungal[32], and antioxidant activities.[27]

1.3.1.3. Triterpenes

Triterpenes are secondary metabolites and synthesized from mevalonate and methylerythritol-phosphate (MEP) pathways, consisting of six isoprene units (C5). They are widely distributed in plant and animal sources. Also, they have several pharmacological activities such as anti-cancer, anti-inflammatory, antiviral, antimicrobial, etc.[33]

Triterpenes are the main components of Chios mastic gum and consist mostly of tetracyclic and pentacyclic triterpenes, which are derivatives of oleanane (**1**), euphane (**2**), lupane (**3**), and dammarane (**4**) skeleton-type (Figure 5).[20,30]

Previous studies have demonstrated that the major metabolites of Chios mastic gum are tirucallol, 28-norolean-17-en-3-one, oleanonic acid (OA), dammaradienone, moronic acid (MA), 24Z-isomasticadienonic acid (IMNA), 24Z-isomasticadienolic acid (IMLA), and their isomers (masticadienonic acid, masticadienolic acid), hydroxydammarenone, oleanonic aldehyde, and β-amyrone (Figure 6). [20,21,30]

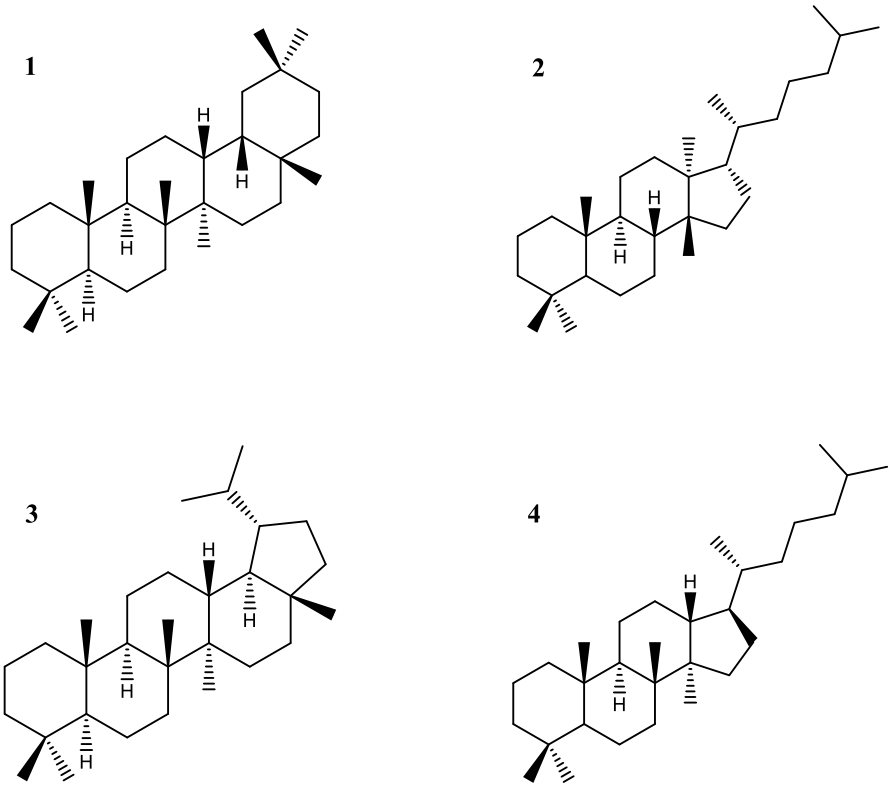

Figure 5. Some major triterpenoid skeletons in Chios mastic gum

In 1956, Barton *et al*. reported some triterpenes from Chios mastic gum for the first time.[18] They identified terpenes by fractionating mastic gum as acidic and neutral triterpenic fractions and subjected these fractions to a silica gel column separately, then eluted with several solvent systems. As a result of the process, a crystalline structure was obtained from the acidic fraction, identified as masticadienonic acid, and tirucallol was isolated from the neutral fraction.[18] Also, Seoane *et al*. isolated two other triterpenes, the oleanonic acid and isomasticadienonic acid.[34] Another study was established structures of several di-, tri, tetra-, and pentacyclic triterpenoids by spectroscopic methods, including dipterocarpol, lupeol, *β*-amyrin, *β*-amyrone, 3-oxo-dammara-20 (21), 24-diene, (8R)-3*β*,8-dihydroxy-polypoda-13E,17E,21-triene, and (3*β*-hydroxymalabarica-14 (26),17E,21-triene.[35] Moreover, Paraschos and colleagues identified the major compounds of Chios mastic gum by NMR and MS analysis, including 24Z-masticadienolic acid, and 24Z-isomasticadienolic acid, oleanonic acid, moronic acid, dammaradienone, 28-norolean12-en-3-one, oleanonic aldehyde, and oleanolic aldehyde.[2121,23,24,36,37] Most recently, 16 compounds having the tirucallene triterpenoid skeleton were identified, two of which had a 7(8 → 9)abeo-tirucallane skeleton unusual

in nature.[38] Phytochemical studies to determine the components of Chios mastic gum were carried out by other researchers following similar isolation processes.

1.3.1.4. Other compounds

Mastic gum, a remarkably complex resin, contains low amounts of phenolic compounds, as well as essential oils, polymer, and terpenoids. Kaliora *et al*. analyzed the metanol:water (MeOH: H_2O) extract of resin with HPLC and GC-MS to determine and identify the phenolic compound of Chios Mastic gum. As a result of this study, tyrosol and simple phenolic compounds such as p-hydroxybenzoic, p-hydroxy-phenylacetic, vanillic, gallic, and trans-cinnamon acids were identified in the extract.[39] Kivcak *et al*. reported the presence of α-tocopherol in mastic gum via chromatographic methods such as HPLC, TLC-densitometry, and colorimetry.[40]

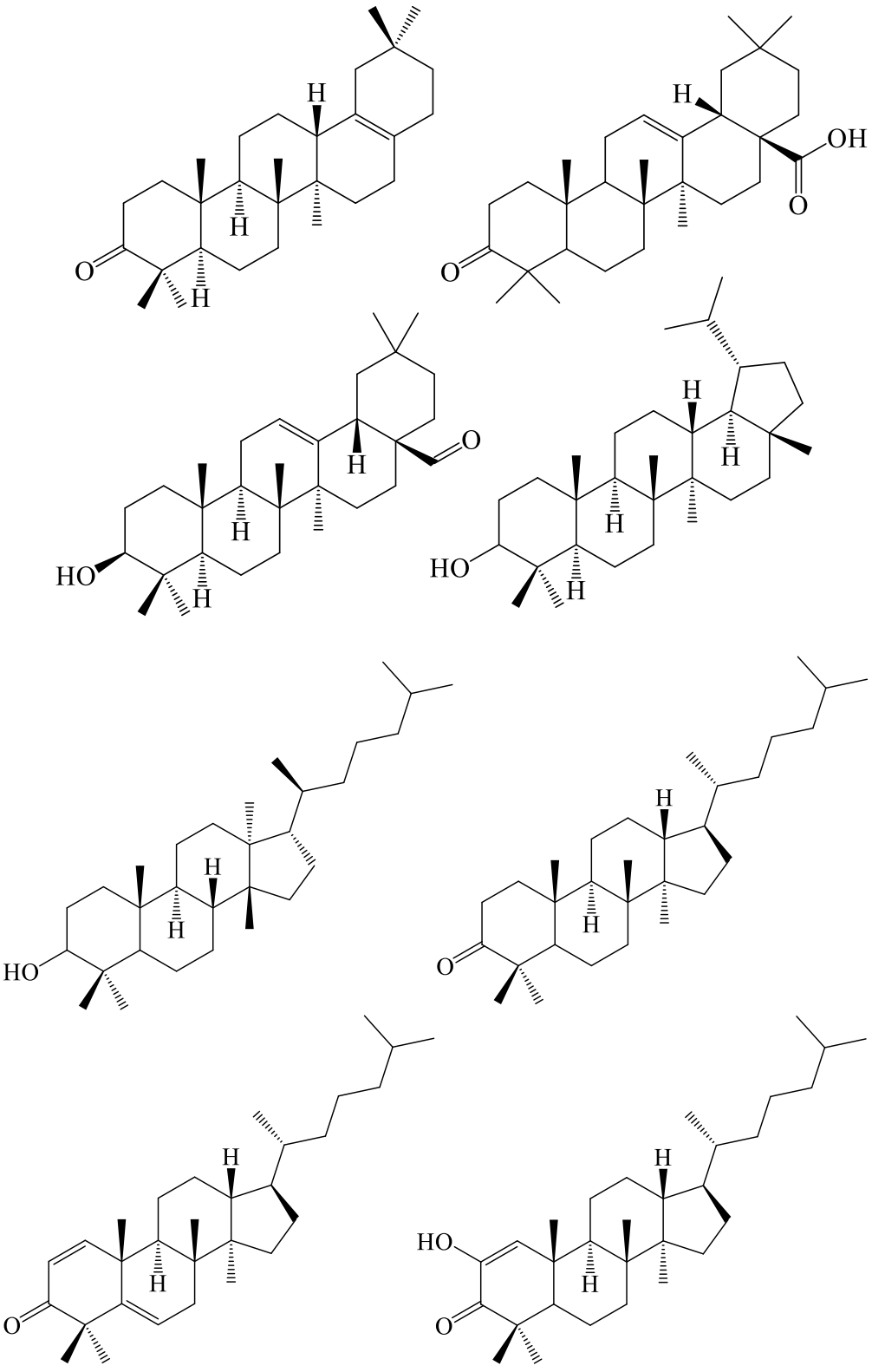

Figure 6. Some isolated triterpenes of Chios mastic gum

1.3.2. The biological activities of *Pistacia lentiscus* var. *chia*

1.3.2.1. Anti-inflammatory activity

Mastic gum was reported in several studies to be effective against inflammation due to its rich chemical profile. Qiao and colleagues investigated the production of inflammatory cytokines and the migration of eosinophilia into the airway in an ovalbumin-induced mouse asthma model. They demonstrated that mastic gum (50 or 100 mg/kg dissolved in 1% DMSO) significantly inhibited eosinophilia migration and reduced the secretion of inflammatory cytokines such as IL-5 and IL-13.[41] Also, it was demonstrated that mastic gum has a positive effect on the regulation of plasma inflammation in people with Crohn's disease and the clinical course of the disease. Mastic gum extract significantly reduced plasma interleukin-6 (IL-6) level, and C - reactive protein (CRP). The study suggests that mastic gum has a key role in the cure of Crohn's disease.[42] In another study, the effect of mastic gum on cytokine production of mononuclear cells in patients with Crohn's disease (CD) was evaluated. Researchers reported that mastic gum reduces TNF-alpha release and inhibits random migration and chemotaxis of macrophages.[43]

Furthermore, Zhou *et al*. investigated the mastic gum's ability to inhibit the production of pro-inflammatory factors like nitric oxide (NO) and prostaglandin E2 (PGE2) in mouse macrophage-like RAW264.7 cells. In the study, both the protein and mRNA levels for two genes were evaluated, which are in charge of the expression NO and PGE2, inducible NO synthase, and cyclooxygenase-2. Western Blot and RT-PCR analyses indicated that mastic gum inhibited both genes at the post-transcriptional level.[44] Loizou *et al*. investigated the anti-inflammatory effect of mastic gum hexane extract and tirucallol, one of its major compounds, in human aortic endothelial cells. As a result of the expression of endothelial adhesion molecules, the migration of cells to the vessel wall through binding leukocytes to the vascular endothelium causes atherogenesis. They studied the effects of mastic gum extract (25-200 µg/ml) and tirucallol (0.1-100 µM) on the expression of adhesion molecules (VCAM-1 and ICAM-1) and the attachment of monocytes (U937 cells) in TNF-α stimulated Human Aortic Endothelial Cells (HAEC). Researchers suggested that some mastic gum components may have potential antiatherogenic activity.[45]

In a randomized clinical trial, Mastic gum was administered to patients with inflammatory bowel disease who have an increase in plasma-free amino acids. The results of the study demonstrated that the increase in total cholesterol, LDL cholesterol, and amino acids like proline, glutamine, alanine, valine and tyrosine, serum IL-6 levels were observed only in the placebo group, and it was shown that mastic gum could limit the increase in free amino acids.[46]

1.3.2.2. Anti-cancer activity

Several reports have suggested the potential anti-cancer activity of Chios mastic gum against various types of cancer, such as prostate cancer, leukemia, lung cancer, and pancreatic cancer.

In 2006, He *et al*. studied the effect of the mastic gum on the activity of the androgen receptor (AR), which has an important role in the development and progression of prostate cancer. More specifically, the authors examined the expression of androgen-regulated genes like prostate-specific antigen (PSA), human kallikrein 2 (hK2), and NKX3.1 to determine the inhibitory effect of mastic gum on the function of AR. The results demonstrated that mastic gum (6–12 μg/ml) attenuated the expression and function of the AR by inhibiting the AR expression by the downregulation of both mRNA and protein levels. The study suggests that mastic gum has potential anti-cancer activity against prostate cancer.[47]

Another study examined the *in vivo* activity of hexane extract of mastic gum against human colon tumour in mice. They demonstrated that the hexane extract of mastic gum administered as 200 mg/kg per day for 4 days (followed by 3 days without administration) inhibited tumor growth by about 35 percent without causing toxicity at the end of 35 days. The results suggested that the hexane extract of mastic gum indicated antitumor activity against human colorectal cancer.[48]

It has been known that the combination of various chemotherapy drugs is used as an effective therapeutic strategy. Within this context, Huang and colleagues studied the combination of gemcitabine and mastic gum against pancreatic cancer cells. Gemcitabine (0.01– 100 mg/mL) induced apoptosis and inhibited cell proliferation in pancreatic cancer cells such as BxPC-3 and COLO 357. They showed that mastic gum at a concentration

of 40 mg/mL and gemcitabine at a concentration of 10 mg/mL notably promoted the antiproliferative and apoptotic effects. When cells are treated with a combination of mastic gum and gemcitabine, the Iκ-Bα level and the expression of Bax protein were substantially increased, whereas Bcl-2 protein was down-regulated, and NF-κB activation was reduced. The results indicated that the combination might be a potential therapeutic strategy for pancreatic cancer.[49]

1.3.2.3. Antibacterial and antifungal activities

It is well known that Chios mastic gum is used in traditional medicine for various diseases such as ulcers, gastritis, stomach pain, etc. Therefore, researchers have sought to reveal its antimicrobial and antibacterial properties through *in vitro* and *in vivo* studies. In early studies of Chios mastic gum on the gastrointestinal tract, researchers focused on the bacterium *Helicobacter pylori*, gram-negative bacteria, which is responsible for most gastrointestinal disorders.[50,51] In 2008, Kottakis *et al*. suggested that the likely cause of anti-*Helicobacter pylori* activity may be due to the presence of arabinogalactans, a hydrophilic protein. Aqueous extracts of mastic gum containing these proteins have shown an inhibition against *H. pylori*. However, they reported that further studies were required, as they were unable to observe a strong inhibitory effect.[52] Moreover, another study reported that isomasticadienolic acid, one of the triterpenic components of Chios mastic Gum, has a strong inhibitory effect against 11 *H. pylori* strains with MBC (Minimum Bactericidal Concentration) 0.202 mg/mL [0.443 mM].[21]

Aksoy *et al*. investigated the antibacterial activity of mastic chewing gum against *Streptococcus* and mutant *Streptococcus*, oral pathogens, both *in vitro* and *in vivo*. Significantly fewer bacteria were observed in saliva samples taken after chewing mastic gum (20 and 50 mg/ml) than in the control group. This study reported that mastic gum had notable antibacterial activity against oral pathogens, and it might be a beneficial adjunct in the prevention of caries.[53]

Furthermore, some studies have demonstrated that mastic gum may help with oral care by inhibiting or decreasing the growth of various pathogens which lead to dental decay. It has exhibited a significant effect against several oral microorganisms and particularly against Gram-negative bacteria. Thus, it could be exploited as a natural product for the prevention of oral infections. When the mastic gum extract solution in

DMSO was examined at the concentration range of 10 mg/mL to 0.02 mg/mL, the MBC values for Chios mastic gum were determined as 0.07–10 mg/mL.[54] Also, a more recent report suggested the antimicrobial properties of Chios mastic gum against several pathogens such as *Porphyromonas gingivalis*, *Aggregatibacter actinomycetemcomitans*, *Fusobacterium nucleatum*, and *Prevotella nigrescens* with the use of an agar disc diffusion test. The results demonstrated that mastic gum extract significantly inhibits tested oral pathogens compared to the hydrogen peroxide (H_2O_2) control group.[55]

1.4.Neurodegeneration and neurodegenerative diseases

Neurodegeneration is a complex process that causes loss of neuronal structure and function, leading to neuronal cell death. Progressive loss of neurons in the central nervous system (CNS) causes deficiencies in some brain functions such as movement, cognition, memory, which leads to neurodegenerative diseases. Since neurodegeneration is very complex, its mechanism is still not fully known.[56,57].

The loss of neurons in the brain leads to the emergence of neurodegenerative diseases such as Alzheimer's disease (AD), Huntington's disease, Parkinson's disease (PD), and Multiple sclerosis (MS). These diseases are especially one of the primary health problems of the age population. Recent studies have indicated that several biological processes, such as oxidative stress, neuroinflammation, mitochondrial dysfunction, and apoptosis, are involved in the progression of neurodegenerative disorders (Figure 7).[58,59]

Reactive oxygen species (ROS) produced in the cells of living organisms provide maintenance of cellular metabolism and contribute to ensuring cellular homeostasis. Moderate or lower ROS concentrations are critical for the immune system, cell life, and memory processes. However, as they are highly reactive, high ROS concentrations can disrupt the balance antioxidant and pro-oxidant levels, causing cell death or oxidative stress (OS). OS is observed in several pathological cases such as mitochondrial dysfunction, cellular damage, and DNA repair system impairment. Neuron cells in the brain are weak to oxidative stress and damage due to their high oxygen consumption and insufficient antioxidant defense, which accelerates the pathogenesis and progression of neurodegenerative diseases.[59–61]

In recent years, many researchers have focused on the therapeutic potential of natural products and their bioactive compounds in creating a neuroprotective effect in

neurodegenerative diseases.[62–64] Natural products against neurodegenerative diseases have an important place in treating and preventing these diseases without harmful side effects. New strategies/therapeutics (potential radical scavengers) derived-natural products can be developed to treat neuroprotective diseases.

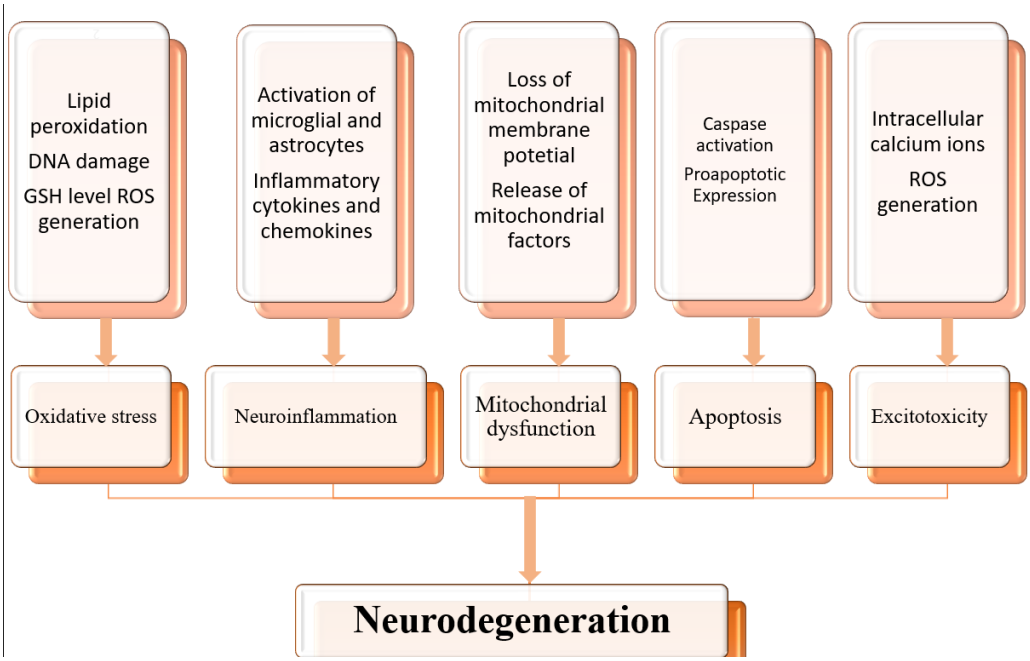

Figure 7. Some mechanisms associated with neurodegeneration

CHAPTER 2

MATERIALS AND METHODS

2.1. Materials

2.1.1. Plant material

Pistacia lentiscus L. (mastic gum) was harvested from Karaburun Peninsula, İzmir, Turkey in January 2020. A voucher specimen was deposited in the İzmir Institute of Technology, İzmir, Turkey. Karaburun Peninsula mastic gum was powdered by using a grinder and stored in a refrigerator at +4 °C. The powdered gum (100 g) was extracted with ethyl acetate (EtOAc) and methanol (MeOH) in a ratio of 3:1 (Total volume 400 ml).

2.1.2. Equipment and chemicals used in isolation studies

Equipment and chemicals used in isolation and purification studies are listed ;

CHEMICALS	EQUIPMENT
Acetonitrile: VWR Chemicals	Nuclear Magnetic Resonance Spectrometry: Varian AS 400; Bruker 500
Ethyl acetate: ISOLAB	Mass Spectrometry: Agilent 1200/6530 Instrument – HRTOFMS
Chloroform: VWR Chemicals	Ultrasonic Bath: Ultrasonic LC30
Methanol: Carlo Erba	Centrifuge: Labnet-Spectrafuge- Hettich Zentrifugen
n-Hexane: Sigma-Aldrich	UV Imaging system: Vilber Lourmat
Dichloromethane: VWR Chemicals	Vacuum pump: Labnet
Dimethyl Sulfoxide (DMSO): Sigma-Aldrich	Peristaltic Pump: Thermo
Acetone: Sigma-Aldrich	SpeedVac Concentrator: Thermo Scientific Savant SPD 121P

Sulfuric Acid: Merck

RP-C18: Merck

Sephadex LH-20: GE

Silica gel 60: Merck

Chloroform-$CDCl_3$: Merck

Pyridine-d5: Merck

Micropipette: Thermoelectron Finnpipet

Freeze Dryer: Labconco FreeZone Freeze Dry System

Rotary Evaporator: Heidolph Laborota 4001; ISOLAB

Homogenizer: Precelly 24, Bertin Corp

Medium pressure liquid chromatography (MPLC)

Vacuum liquid chromatography (VLC)

Nuclear Magnetic Resonance Spectrometry: Varian AS 400; Bruker 500

2.1.3. Bioactivity studies

MTT (Sigma-Aldrich, USA), DMEM (Gibco, USA), DMEM (Gibco, USA), Fetal Bovine Serum (FBS) (Panbiotech, Germany), 2-Mercaptoethanol (Sigma-Aldrich, USA), retinoic acid (Sigma-Aldrich, USA) L-glutamine (Thermo Scientific, USA) were purchased for bioactivity studies.

2.2. Methods

2.2.1. Extraction

The powdered Karaburun peninsula mastic gum (100 g) was extracted with ethyl acetate (EtOAc, 300 ml) and methanol (MeOH, 100 ml) by maceration technique, using an ultrasonic bath for 45 minutes at room temperature. The residual gum debris was discarded with paper filtration and then obtained clear extract was evaporated by rotary evaporator at 50°C under low pressure. After these processes, 92 g of crude resin was yielded, and 40 g of which was used for further studies.

2.2.2. Isolation and purification

The TLC analysis of the mastic gum was conducted utilizing silica gel 60 F254 and/or reverse-phase silica gel 60 RP-C18 coated aluminum plates. Chemical profiles were visualized by spraying 20% aq.H_2SO_4 on the TLC plates and then heating up to

120°C until spots were visible. After the TLC analysis, column chromatographies with reverse-phase silica gel (RP C-18, Merck), normal-phase silica gel 60 (Merck), and Sephadex LH-20 (GE Healthcare Life Sciences) were driven to obtain pure compounds. As described in Methods 2.2.1, isolation and purification studies were started with 40 g of mastic gum.

In general, solvent and/or solvent systems used in chromatographic studies and TLC controls are as follows;

I. Acetone: Water (ACE: H_2O)
II. Acetonitrile: Water (ACN: H_2O)
III. Chloroform ($CHCI_3$)
IV. Chloroform: Methanol ($CHCI_3$: MeOH)
V. Dichloromethane (CH_2CI_2)
VI. Dichloromethane: Methanol (CH_2CI_2: MeOH)
VII. Ethyl acetate: Methanol (EtOAc: MeOH)
VIII. n-Hexane: Ethyl acetate (Hex: EtOAc)
IX. Methanol (MeOH)
X. Methanol: Water (MeOH: H_2O)

The ratios of solvent systems are detailed in the isolation scheme.

Firstly, 40 g of resin (mastic gum) was dissolved in %100 EtOAc by heating up to 50°C. It was impregnated with 40 g of silica gel and dried. The dried silica-containing extract was subject to the silica gel (360 g) column and eluted with Hex-EtOAc gradient (%100:0 → 50:50), and then with EtOAc-MeOH gradient (90:10 → 0:100) yielding 41 fractions (Figure 8). The total solvent volume used was 5 liters. The fractions with similar TLC profiles were pooled, yielding 18 main fractions. The process of separating the main fractions was decided based on TLC profiles using different solvent systems.

Some of the main fractions, fractions 18, 20, 21-22, 23-25, 27, and 36, were chromatographed using normal and RP-C18 silica gel column chromatography methodologies with various solvent system mixtures. Silica gel and RP silica gel coated plates were employed for TLC to follow column chromatography. Spots of TLC were marked under the UV light at 365 nm. To visualize the spots was sprayed with 20% aq. H2SO4 and heated for a few minutes. All isolation and purification processes were carried out using similar chromatographic methods. As a result of the isolation procedures, a total of 14 molecules were obtained, Details of isolation procedures are shown in Figures 8-15.

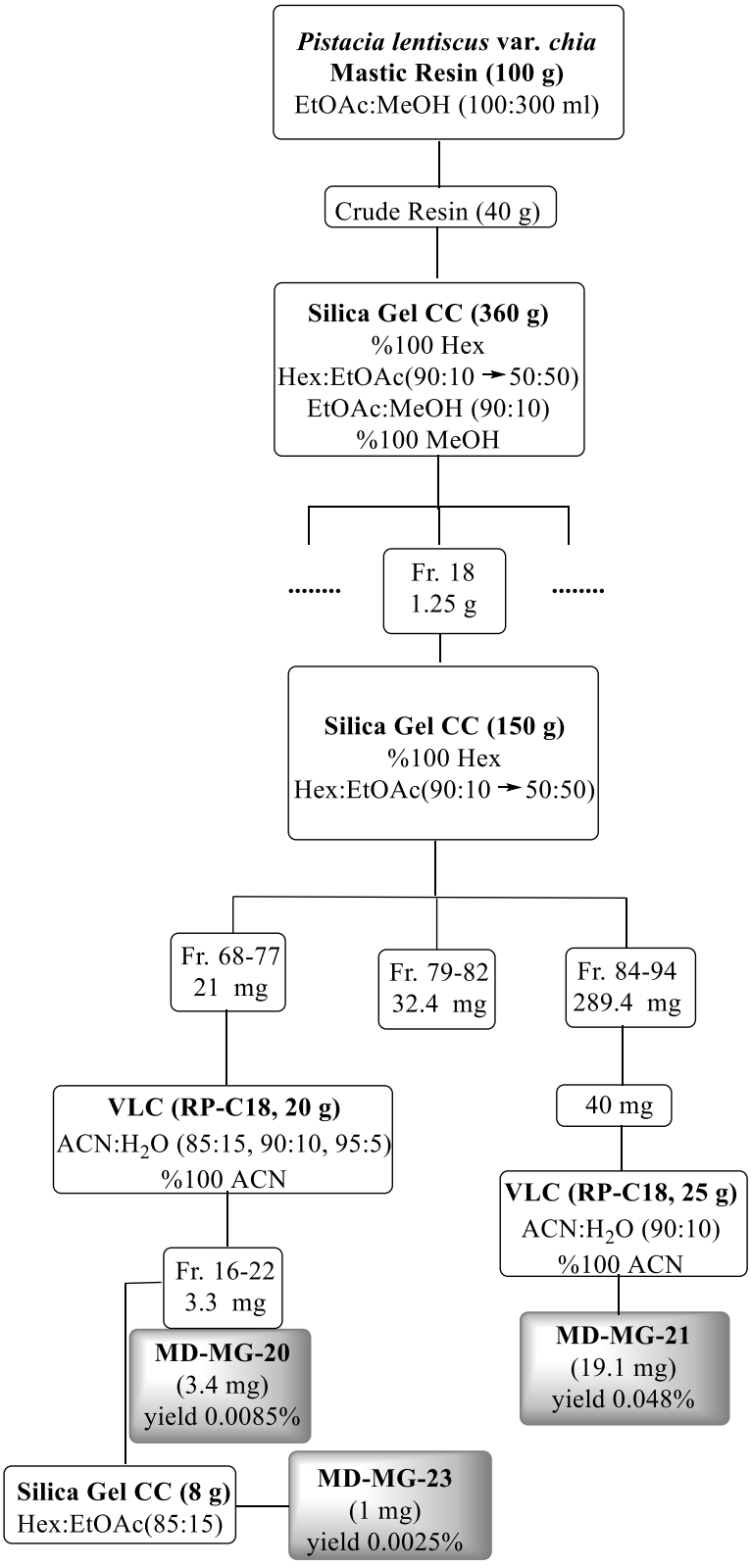

Figure 8. Isolation scheme of main fraction 18

(cont. on next page)

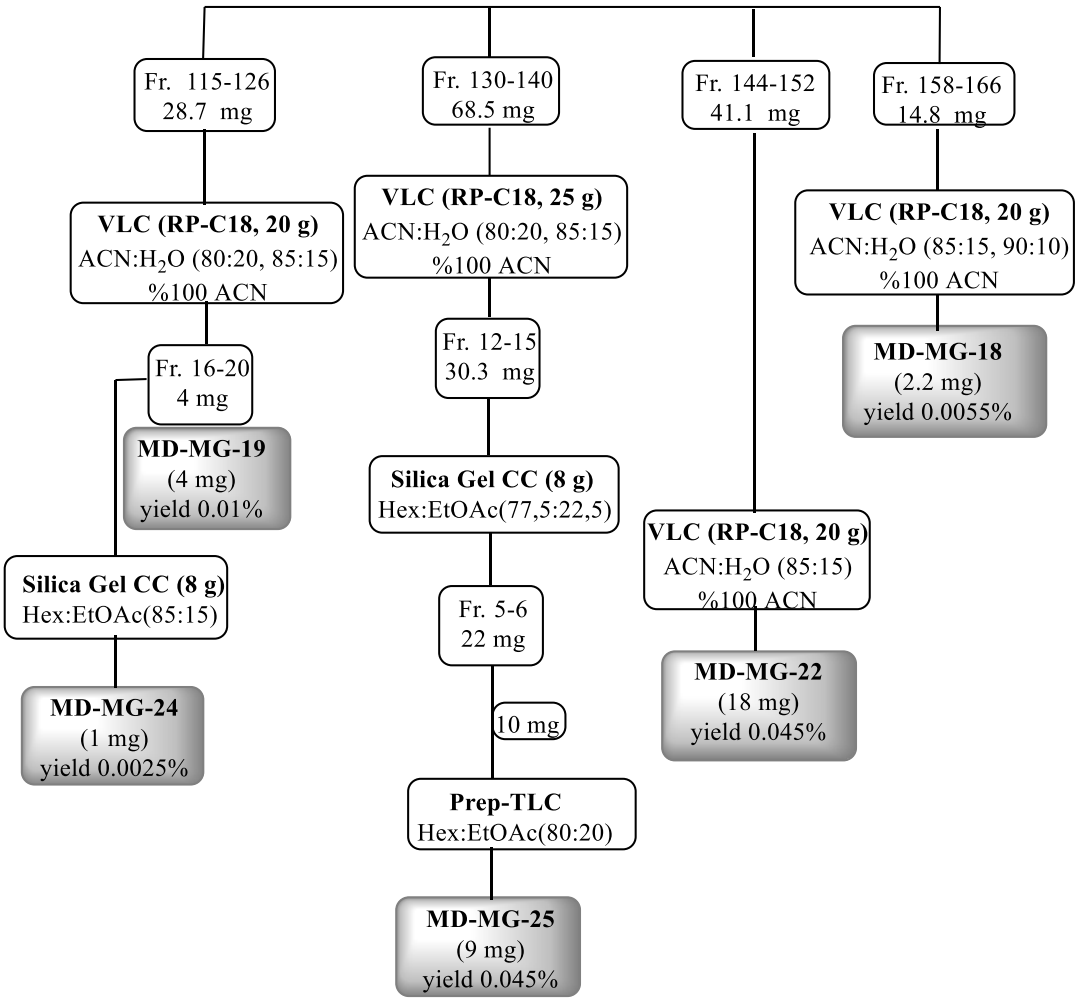

Figure 9. Isolation scheme of main fraction 18 (cont.)

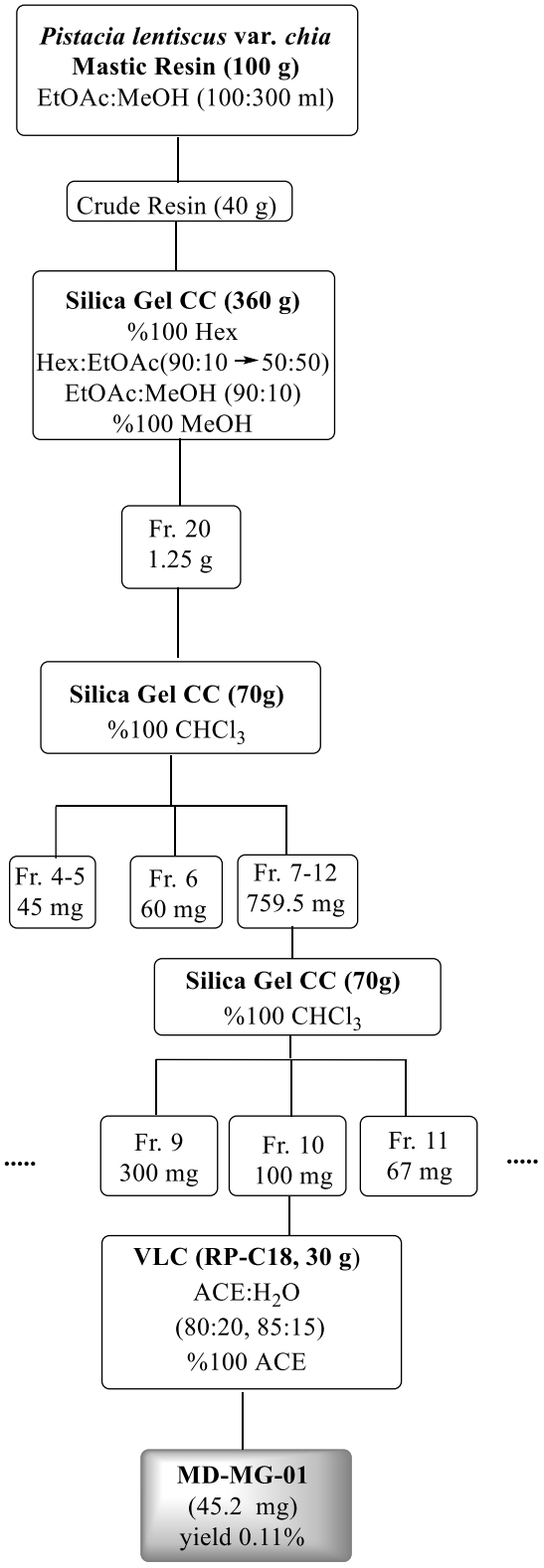

Figure 10. Isolation scheme of main fraction 20

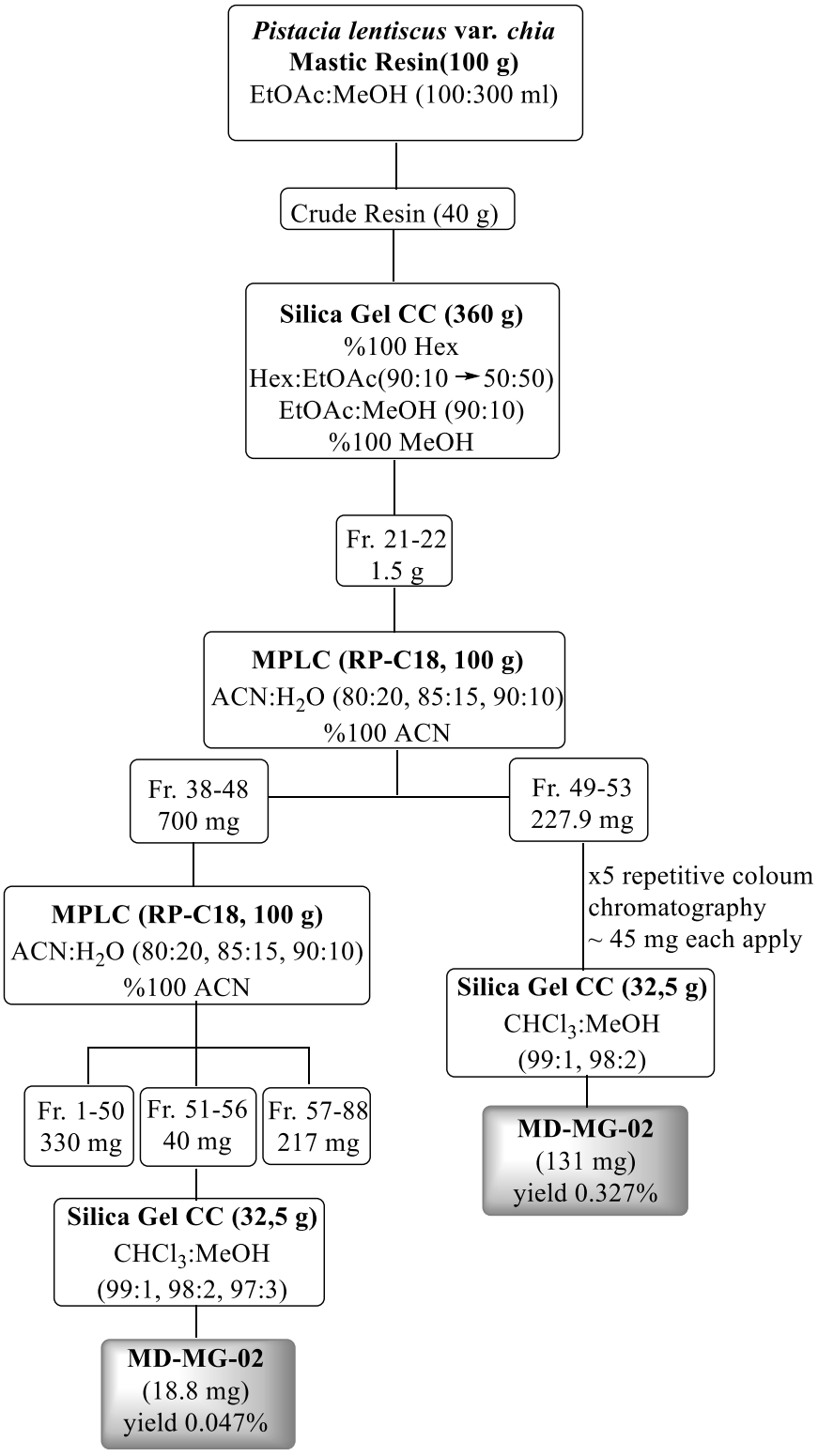

Figure 11. Isolation scheme of main fraction 21-22

(cont. on next page)

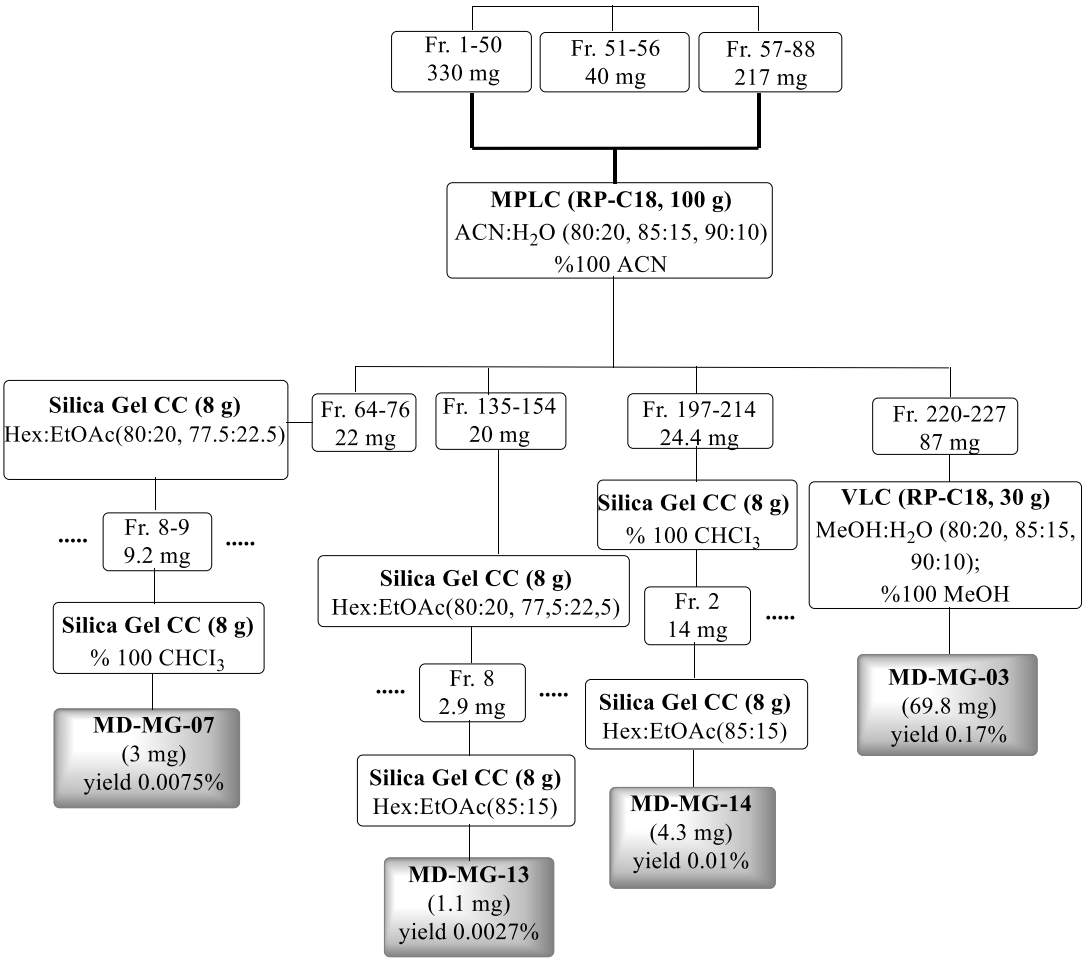

Figure 12. Isolation scheme of main fraction 21-22 (cont)

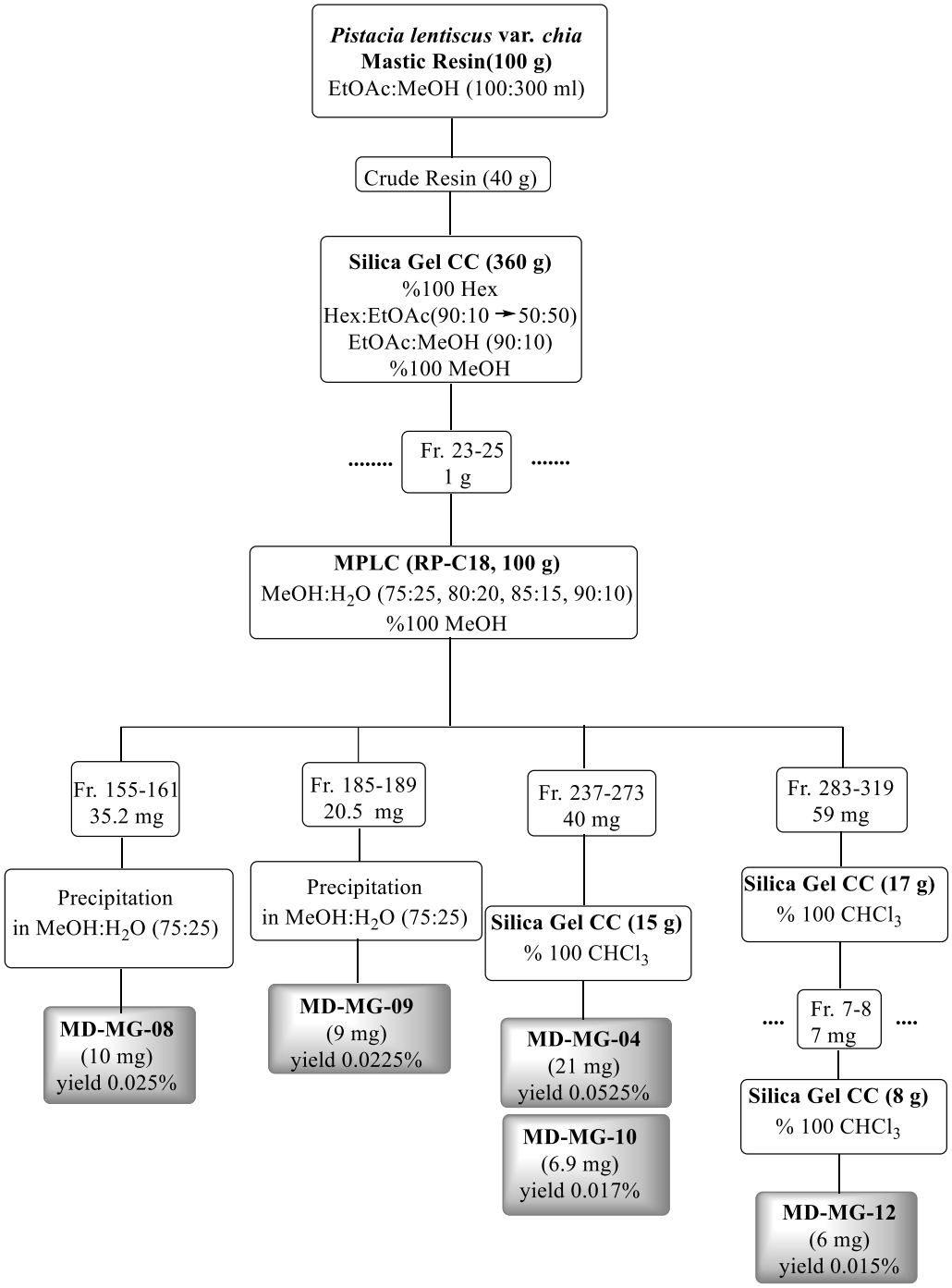

Figure 13. Isolation scheme of main fraction 23-25

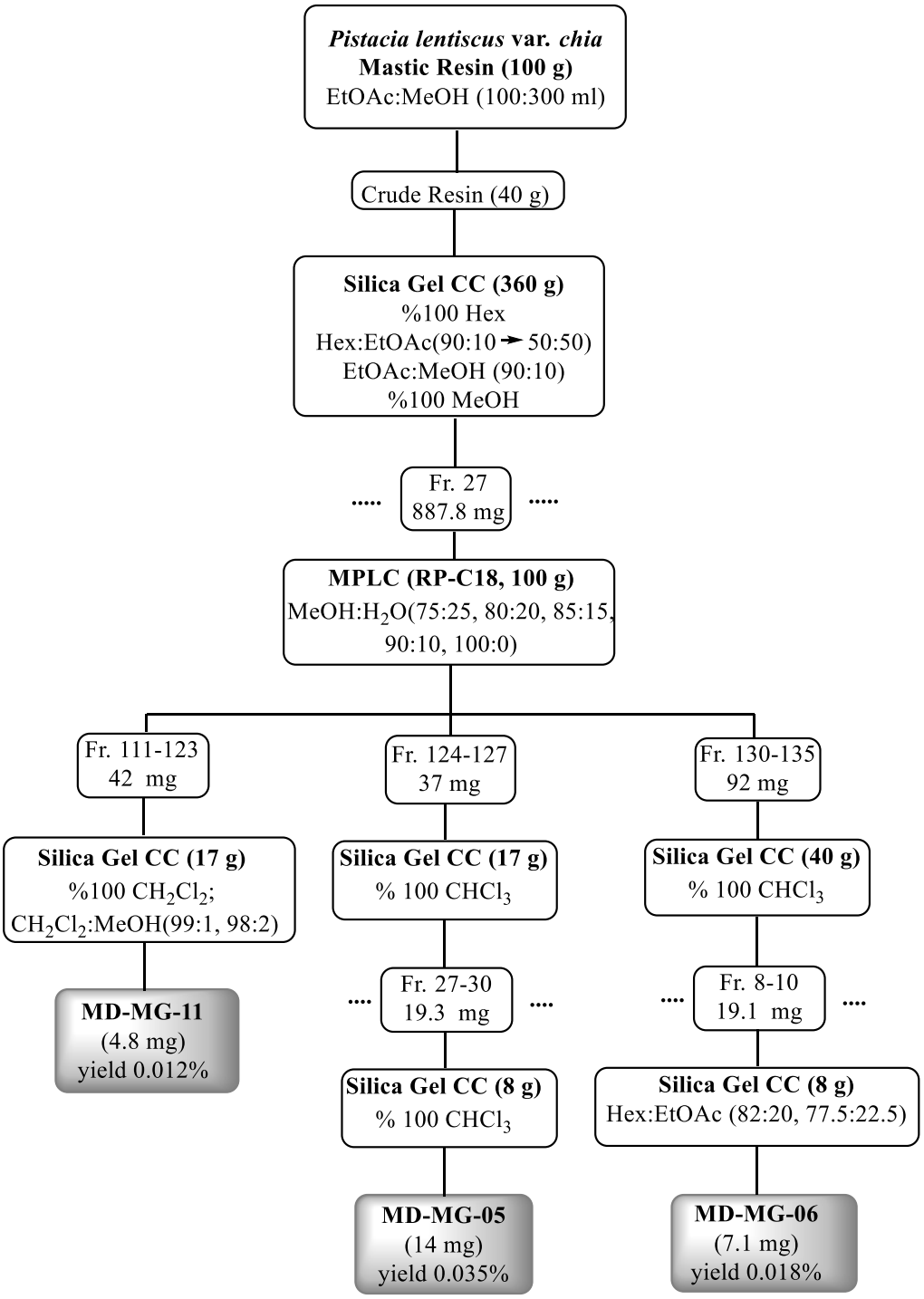

Figure 14. Isolation scheme of main fraction 27

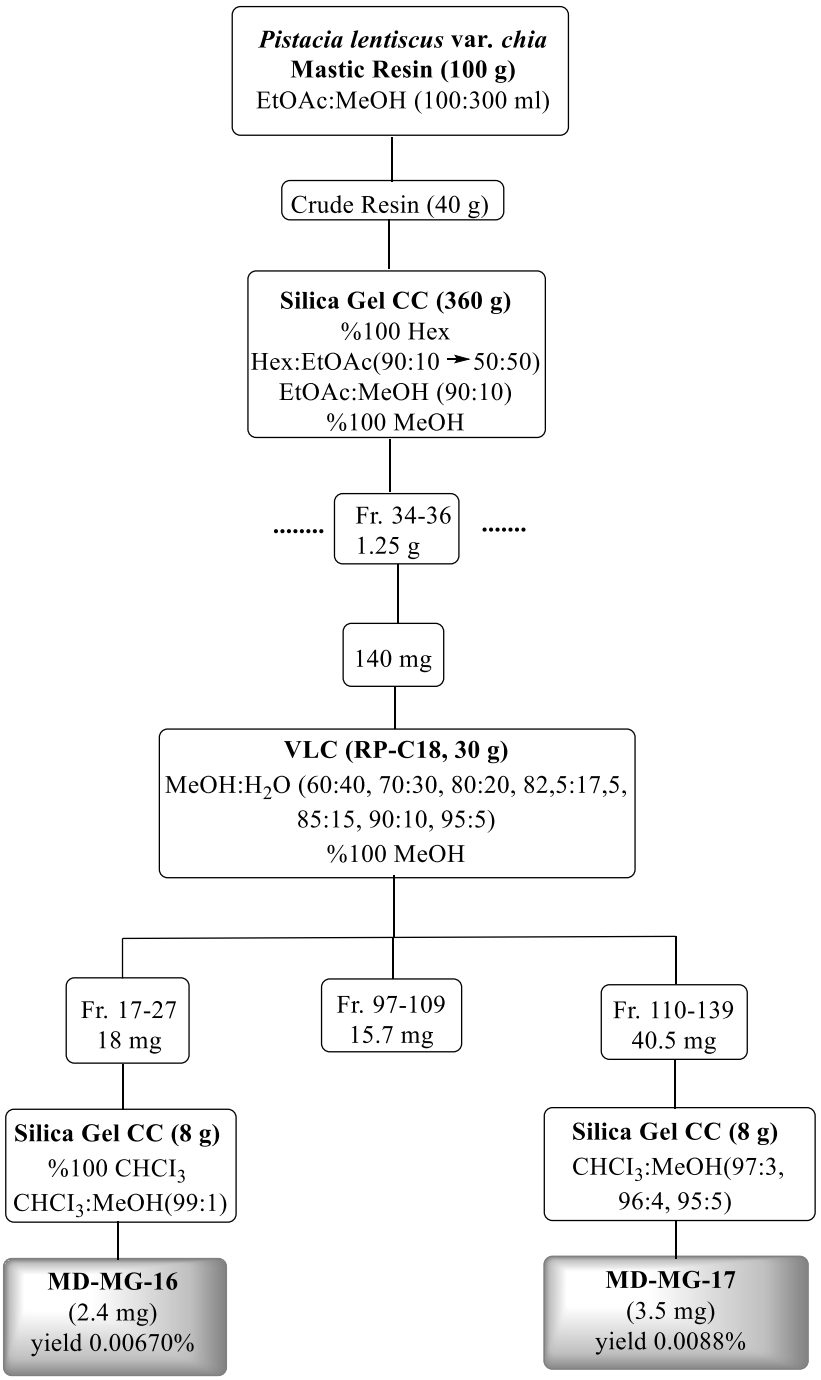

Figure 15. Isolation scheme of main fraction 34-36

Table 2. The isolated compounds, and their codes and amounts

PLANT	THE CODES OF THE COMPOUNDS	THE ISOLATED COMPOUNDS
***Pistacia lentiscus L.* (Mastic gum)**	**MD-MG-01 (45.2 mg)**	**TIRUCALLOL**
	MD-MG-02-09 (158.8 mg)	**OLEANONIC ACID**
	MD-MG-03 (69.8 mg)	**3-O-ACETYL MASTICADIENOLIC ACID**
	MD-MG-04 (21 mg)	**ISOMASTICADIENONIC ACID**
	MD-MG-05 (14 mg)	**OLEANOLIC ACID**
	MD-MG-06-10 (14 mg)	**MYRRHANOL C**
	MD-MG-07-08-11 (17.8 mg)	**MORONIC ACID**
	MD-MG-12 (6 mg)	**DAMMARENEDIOL**
	MD-MG-13-22* (19.1 mg)	**3-OXO-17*β*-HYDROXY-NOROLEAN-12-ENE**
	MD-MG-14 (4.3 mg)	**DIPTEROCARPOL**
	MD-MG-17* (3.5 mg)	**3,4-SECO-TIRUCALLA-8,24-DIEN,26-OIC ACID**
	MD-MG-19 (4 mg)	**28-NORLUP-20(29)-EN-3-ONE-17*β*-HYDROPEROXIDE**
	MD-MG-24, 25	**3-OXO-17-HYDROXY-NOROLEAN-12-ENE**

* New compounds

2.2.3. Bioactivity Studies

The methods applied in the biological studies of the thesis are briefly described in this section.

2.2.3.1. Cell culture conditions

SH-SY5Y cells were maintained with DMEM with 10% FBS in an incubator containing 5% CO2 at 37 °C. When cells reached 70% confluence, the old medium was removed, and the cell surface was washed with 0.05% trypsin. Then, cells were treated with 0.25% trypsin at 37 °C until detaching from the surface. The appropriate amount of cells suspension in a fresh medium was transferred to a new culture dish.

2.2.3.2. Cell differentiation

SH-SY5Y cells were seeded in 100 mm plates. The cells were incubated for 24 h at 5% CO2 at 37 °C incubator. Then, 10 µM retinoic acid (RA) was added to induce differentiation. Every two days, the medium was replaced with fresh medium containing RA (10 μM). On day 6, SH-SY5Y cells (20,000 cells/well) were seeded in 96 well plate. Next day, cells were again treated with 10 μM RA. After 24 h, cells were treated with compounds.

2.2.3.3. Cell viability by MTT assay

Cell viability was determined by the 3-(4,5-dimethylthiazol-2-yl)-2,5-diphenyltetrazolium bromide (MTT) test. Living cells convert MTT to formazan crystals by mitochondrial activity, and colorimetric detection of formazan crystals is used to determine the percentage of living cells.

After differentiated and undifferentiated SH-SY5Y cells (both 20,000 cells/well) were seeded in 96 well plates, cells were pre-treated with three concentrations of molecules that dissolved in DMSO for 1 h. Then H_2O_2 (400 µM differentiated and 100 µM for undifferentiated cells) was added to induce toxicity. Following incubation for 24 h, the whole medium was poured off, and fresh media containing 10% MTT was added to each well. Then plates incubated 4 h in incubator. Again, the whole medium was pulled out and DMSO was added to solve formed formazan crystals. Finally, photometric absorbance was measured at the wavelength of 590/690 nm by using a Varioscan flash spectrophotometer by Thermo Scientific.

CHAPTER 3

RESULTS AND DISCUSSION

The results of phytochemical and bioactivity studies are explained in this section.

3.1. Structural elucidation of isolated molecules

Within the scope of this thesis, a thorough study was performed to obtain triterpenic compounds of mastic gum collected from Karaburun peninsula. Structural elucidation of the isolates was carried out using spectroscopic methods (1D NMR, 2D NMR, MS and X-ray diffraction). As a result of detailed inspection of the obtained spectra, a total of 14 molecules possessing triterpene skeleton were established structurally, two of which were found to be new compounds.

3.1.1. Structural elucidation of MD-MG-01

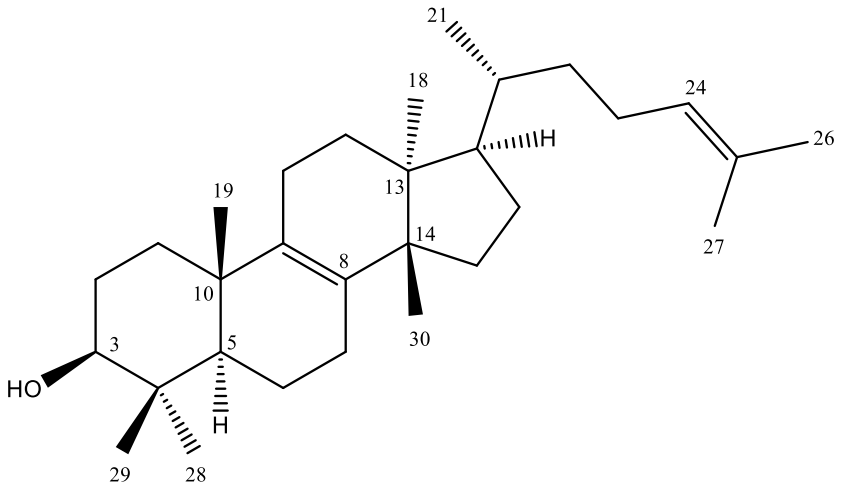

Figure 16**.** Chemical structure of MD-MG-01

The ESI-MS spectrum of MD-MG-01 demonstrated an ion peak for $[M+CH_3OH+H]^+$ at *m/z* 459.4894 (calcd. 459.4197 for $C_{31}H_{55}O_2$), corresponding to the molecular formula of $C_{30}H_{50}O$.

A detailed inspection of the ^{1}H-NMR spectrum of MD-MG-01 exhibited five tertiary and two allylic methyl signals at δ 0.88, 0.96, 1.05, 1.10, 1.28, 1.66 and 1.72 (each

s; respectively H_3-18, H_3-30, H_3-19, H_3-29, H_3-28, H_3-26 and H_3-27) as well as one secondary methyl group at δ 1.01 (3H, d, J=5.8, H-21) (Spectrum 1). Also, an oxymethine proton at δ 3.50 m (H, H-3) in the downfield region was observed. This deduction was supported by the HSQC correlations between H-3 and a hydroxymethine carbon at δ 77.8 (C-3). Hence, the location of the hydroxymethine carbon at C-3 was ascertained by long-range correlations from H-3 to H_3-28 (δ 1.28, s) and H_3-29 (δ 1.10, s). Besides, from the cross-peaks in the COSY spectrum, the oxymethine proton (δ 3.50, m, H-3) showed correlations with vicinal protons (2H, δ 1.90, m, H_2-2)(Table 3).

The ^{13}C-NMR spectrum of MD-MG-01 was low-quality due to its scarce amount; therefore, the carbon data was unambiguously determined by the HSQC and HMBC spectra (Table 3). The ^{13}C-NMR and DEPT-135 spectra showed 30 signals, four of which were in good accordance with the presence of two distinct olefinic systems (δ_C 125.6, d, C-24; δ_C 130.6, s, C-25; δ_C 133.4, s, C-8 and δ_C 134.5, s, C-9). Apart from these signals, the resonances comprised of eight methyl, ten methylene, four methine including one oxygen-bearing (δ_C 77.8, d, C-3) and four quaternary carbons. The 30 resonances of the aglycon moiety were consistent with a $C_{30}H_{50}O$ triterpene framework, indicating the presence of 6 degrees of unsaturation from two double bonds and four ring systems from the tetracyclic framework.

Although four olefinic carbon signals were observed in the ^{13}C-NMR spectrum, the resonance of one olefinic proton at δ 5.27 t (1H, J=6.3, H-24) was apparent in the downfield region of the ^{1}H-NMR spectrum. Based on the HSQC correlations, only one of the four double bond carbons had a cross peak, thus indicating the existence of both a tetrasubstituted and a trisubstituted olefinic systems. Hence, a tetrasubstituted olefinic system was unambiguously ascertained at C-8 by $^{3}J_{C\text{-}H}$ correlations in the HMBC spectrum, which displayed significant cross peaks between both H_3-30 (δ 0.96, s) to C-8 at δ 133.4 and H-19 (δ 1.05, s) to C-9 at δ 134.5. Moreover, the location of a trisubstituted olefinic system was confirmed at C-24 based on the HMBC correlations between allylic methyl signals (δ 1.66, s, 3H, H-26 and δ 1.72, s, 3H, H-27) and olefinic carbons (δ_C 125.6, d, C-24 and δ_C 130.6, s, C-25). Besides, the vicinal correlations of olefinic proton at 5.27 t (H, J=6.3, H-24) was readily deduced from COSY spectrum. Accordingly, olefinic proton was correlated with protons at δ 2.14 m (H, H_2-23) and δ 1.96 m (H, H_2-23) as a part of the spin system involving H_2-15 (δ 1.32, m)/H_2-16 (δ 1.28, m)/H-17 (δ 1.56, m)/H-20 (δ 1.52, m)/H_3-21 (δ 1.01, s)/ H_2-22 (δ 1.55, m), respectively.

Based on this evidence and comparison with the reported data in literature, the framework of MD-MG-01 was established as a tirucallane-type triterpene (tirucallol), a previously identified sapogenol.[18,65]

Table 3. ^{1}H and ^{13}C NMR spectroscopic data of MD-MG-01, [a)] (in C_5D_5N, ^{1}H: 500 MHz, ^{13}C: 125 MHz)

Position	**δ_C (ppm)**	**δ_H (ppm), (J in Hz)**
1	35.6 t	1.74[b)]; 1.26[b)]
2	28.1 t	1.90[b)]
3	77.8 d	3.50 m
4	39.4 s	-
5	51.2 d	1.27[b)]
6	19.1 t	1.76[b)]; 1.46[b)]
7	27.8 t	2.10[b)]; 1.97[b)]
8	133.4 s	-
9	134.5 s	-
10	37.3 s	-
11	21.5 t	2.05[b)]
12	30.9 t	1.75[b)]; 1.25[b)]
13	44.1 s	-
14	50.2 s	-
15	29.5 t	1.32[b)]
16	28.8 t	1.28[b)]
17	49.9 d	1.56[b)]
18	15.5 q	0.88 s
19	20.2 q	1.05 s
20	36.5 d	1.52[b)]
22	36.4 t	1.55[b)]
23	25.1 t	2.14[b)]; 1.96[b)]
24	125.6 d	5.27 t (6.3)
25	130.6 s	-
26	17.8 q	1.66 s
27	25.6 q	1.72 s
28	28.5 q	1.28 s

29	16.3 q	1.10 s
30	24.4 q	0.96 s
3-OH	-	5.93 d (25.9)

a) Assignments were confirmed by 2D-COSY, HSQC and HMBC experiments.

b) Signal pattern was unclear due to overlapping.

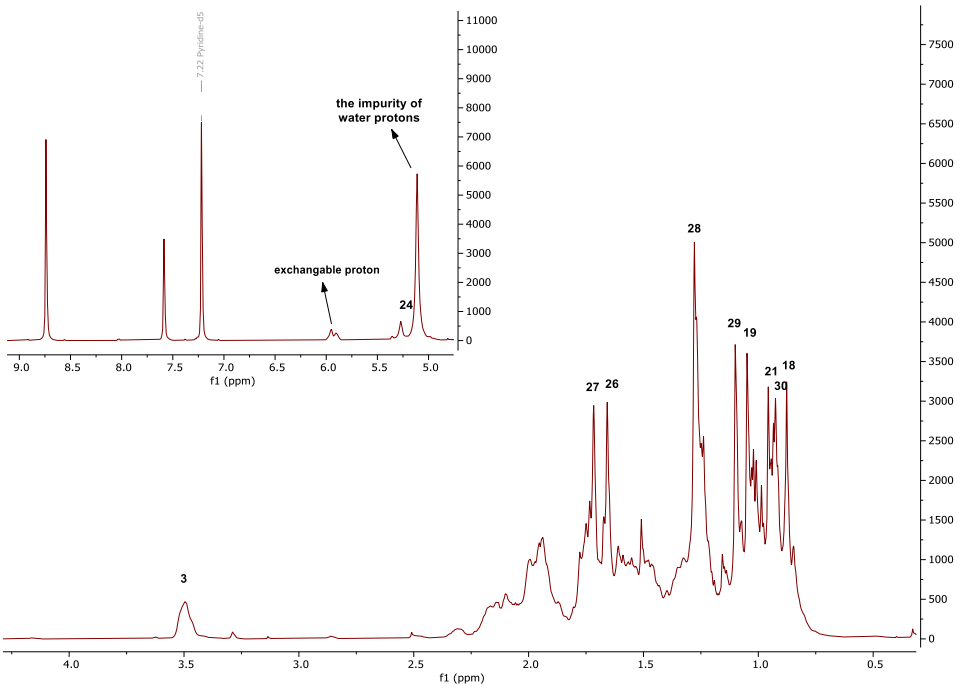

Spectrum 1. ^{1}H-NMR spectrum of MD-MG-01

3.1.2. Structural elucidation of MD-MG-02

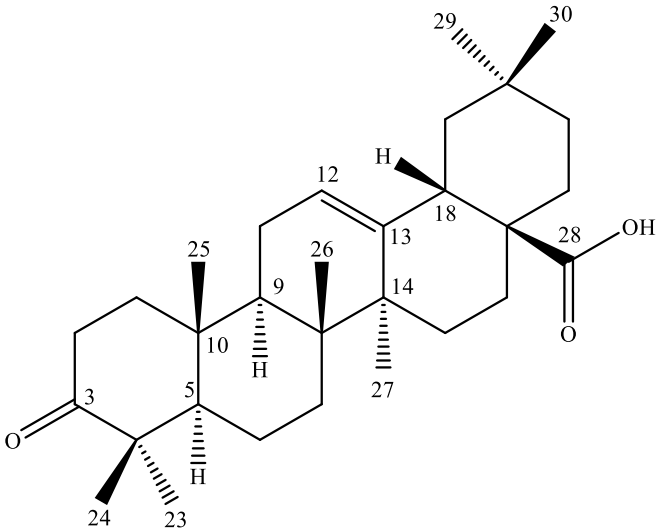

Figure 17. Chemical structure of MD-MG-02, (MD-MG-09)

Based on a major ion peak at *m/z* 453.3372 $[M-H]^-$ in the HR-ESI-MS (negative mode), the molecular formula of MD-MG-02 was suggested to be $C_{30}H_{46}O_3$ (calcd. 453.3369 for $C_{30}H_{45}O_3$) (Spectrum 2), indicating eight degrees of unsaturation. The ^{13}C-NMR (Spectrum 4) and DEPT-135 (Spectrum 48) spectra of MD-MG-02 displayed the presence of 30 carbons, including two carbonyls (δ_C 216.5, s, C-3 and δ_C 180.5, s, C-28), two olefinic (δ_C 122.6, d, C-12 and δ_C 145.1, s, C-13), seven methyl, ten methylene, three methine, six quaternary carbons (Table 4). Two carbonyl carbons and one double bond system accounted for three out of eight degrees of unsaturation. The remaining five degrees of unsaturation were consistent with the molecule containing pentacyclic triterpenoid structure.

The triterpenoid structure of MD-MG-02 was confirmed from the COSY and HMBC spectra (Spectrum 50-51)). The COSY spectrum showed correlations for five major spin systems including H-1/H-2, H-5/H-6/H-7, H-9/H-11/H-12/H-13, H-15/H-16 and H-21/H-22. The HMBC spectra showed cross peaks from the methyl groups (H_3-23, H_3-24, H_3-25, H_3-26, H_3-27, H_3-29, H_3-30) with neighboring carbons supported the presence of oleanane-type pentacyclic triterpenoid.

Also, an olefinic proton at δ 5.48 (t, J=3.8, H-12) was apparent in the ^{1}H-NMR spectrum (Spectrum 3), whereas two olefinic carbon signals were observed in the ^{13}C-NMR spectrum. Thus, a trisubstituted double bond system was deduced. This deduction was justified with the correlation between H-12 and C-12 (δ 122.6) in the HSQC spectrum. The double bond was located between C-12 and C-13 based on the HMBC $^3J_{C-H}$ cross peaks from H_3-30 (δ 1.02, s) to C-13 (δ 145.1), H-9 (δ 1.68, s) to C-12, and H-12 to C-14 (δ 42.5) and C-18 (δ 42.3), while a spin system starting from H-5 (δ 1.32) to H-12 was clearly traced.

Since the lack of any oxymethine proton resonance in the ^{1}H-NMR spectrum and the presence of a carbonyl carbon (δ_C 216.5) in the ^{13}C-NMR spectrum, an oxidation at C-3 was suggested. A detailed inspection of the COSY and HSQC spectra revealed that H_2-2 protons (δ 2.54, ddd, J=15.8, 11.1, 2.7 Hz and 2.38, ddd, J=15.8, 6.9, 3.6 Hz, respectively) undergone a significant down field shift (ca. 0.6 ppm) (Spectrum 49). In addition, the location of ketone was unambiguously ascertained by long-range correlations from H_3-23 (δ 1.15, s)/H_3-24 (δ 1.01, s) to C-3 in the HMBC spectrum.

Besides, another carboxyl group carbon at 180.5 ppm was determined explaining the remaining degree of unsaturation. The position of carboxylic acid was assigned as C-28 based on its HMBC cross-peaks. When the spectroscopic data of MD-MG-02 was

compared with those of previously reported data, the compound was identified as oleanonic acid, a known compound.[66]

Table 4. ^{1}H and ^{13}C NMR spectroscopic data of MD-MG-02, [a] (in C_5D_5N, ^{1}H: 500 MHz, ^{13}C: 125 MHz)

Position	δ_C (ppm)	δ_H (ppm), (J in Hz)
1	39.4 t	1.68[b]; 1.31[b]
2	34.7 t	2.54 ddd (15.8, 11.1, 2.7); 2.38 ddd (15.8, 6.9, 3.6)
3	216.5 s	-
4	47.7 s	-
5	55.6 d	1.32[b]
6	20.1 t	1.39[b]
7	32.9 t	1.46[b]; 1.32[b]
8	39.9 s	-
9	47.5 d	1.68[b]
10	37.2 s	-
11	24.0 t	1.92[b]
12	122.6 d	5.48 t (3.8)
13	145.1 s	-
14	42.5 s	-
15	28.6 t	2.13[b]; 1.20[b]
16	24.1 t	2.13[b]; 1.05[b]
17	47.0 s	-
18	42.3 d	3.30 dd (14.0, 4.6)
19	46.7 t	1.83[b]; 1.32[b]
20	31.3 s	-
21	34.5 t	1.46[b]; 1.20[b]
22	33.4 t	2.04 td (13.9, 4.3); 1.83[b]
23	26.9 q	1.15 s
24	21.9 q	1.01 s
25	15.2 q	0.90 s
26	17.5 q	1.00 s
27	26.3 q	1.25 s
28	180.5 s	-
29	33.6 q	0.96 s
30	24.1 q	1.02 s

a) Assignments were confirmed by 2D-COSY, HSQC and HMBC experiments.

b) Signal pattern was unclear due to overlapping.

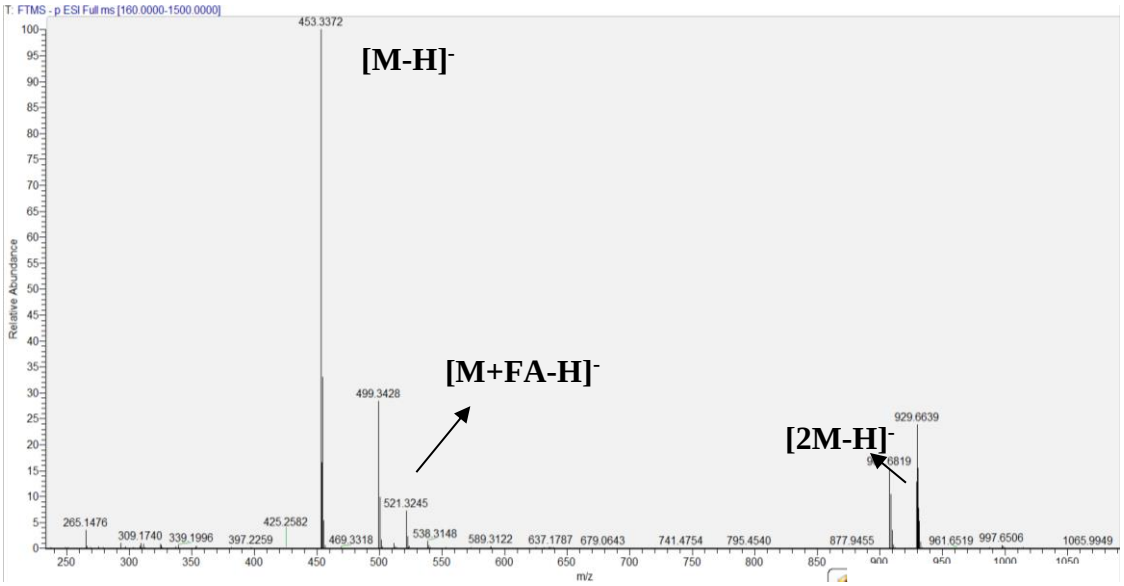

Spectrum 2**.** HR-ESI-MS spectrum of MD-MG-02 (negative mode)

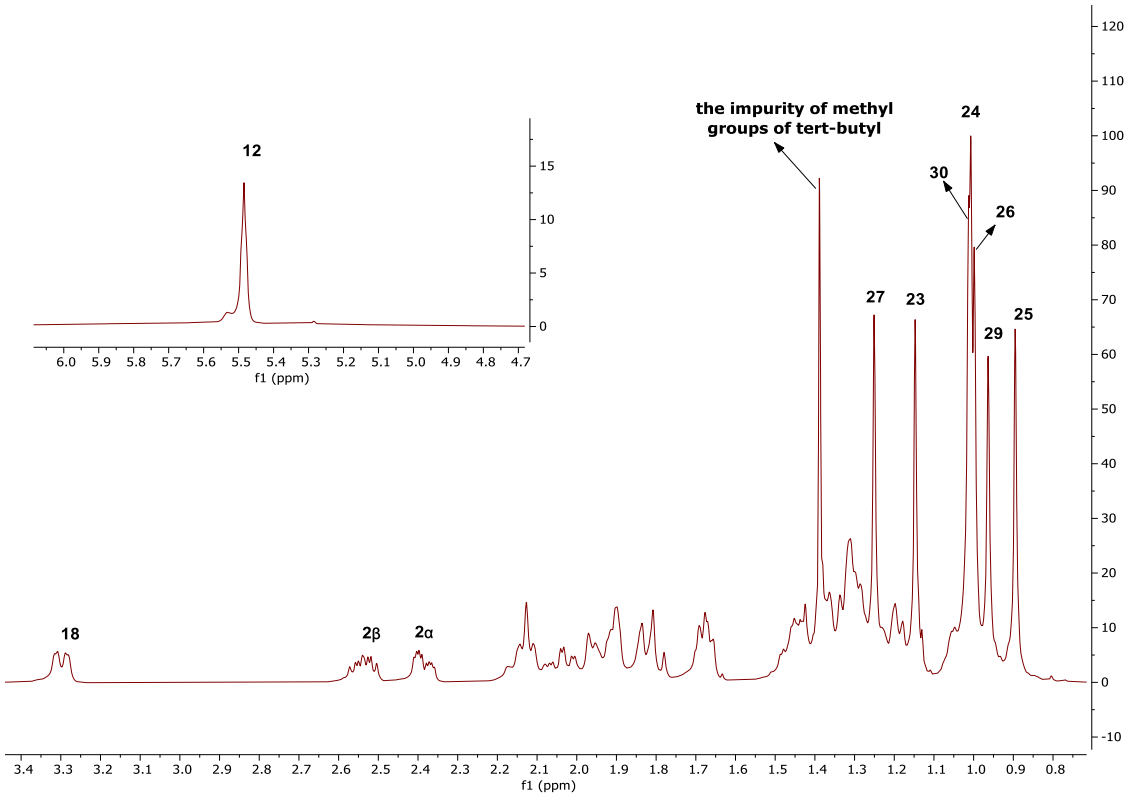

Spectrum 3. ^{1}H-NMR spectrum of MD-MG-02

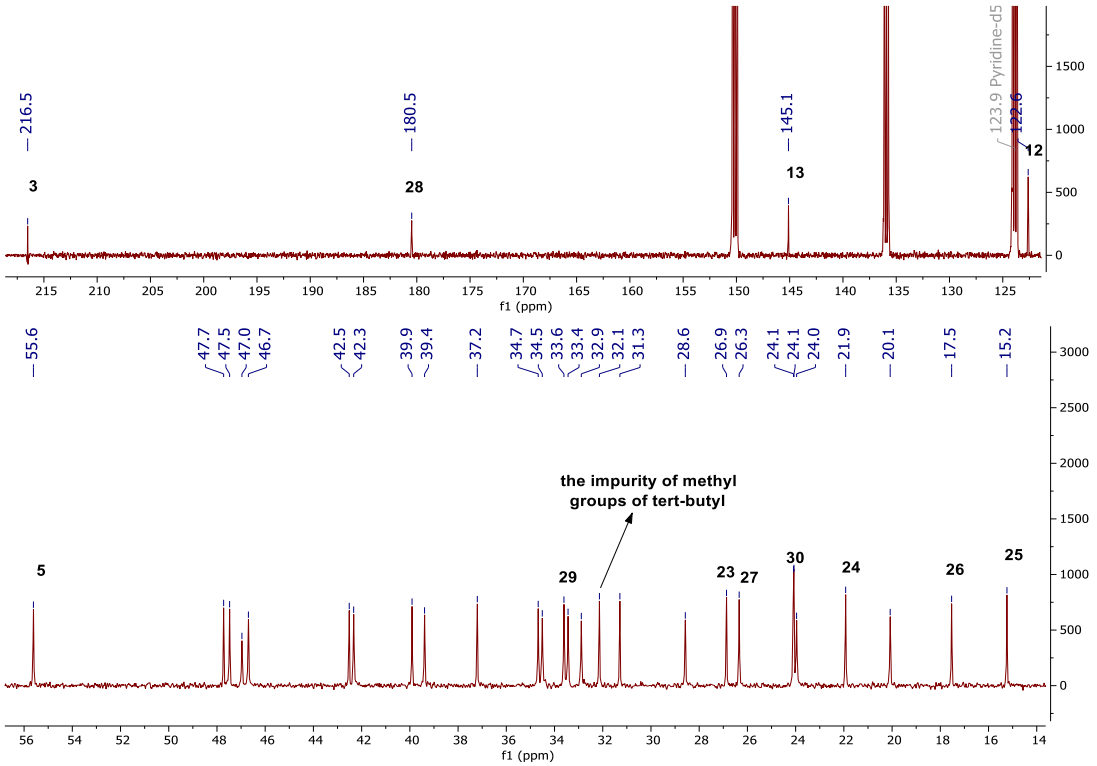

Spectrum 4. ^{13}C-NMR spectrum of MD-MG-02

3.1.3. Structural elucidation of MD-MG-03

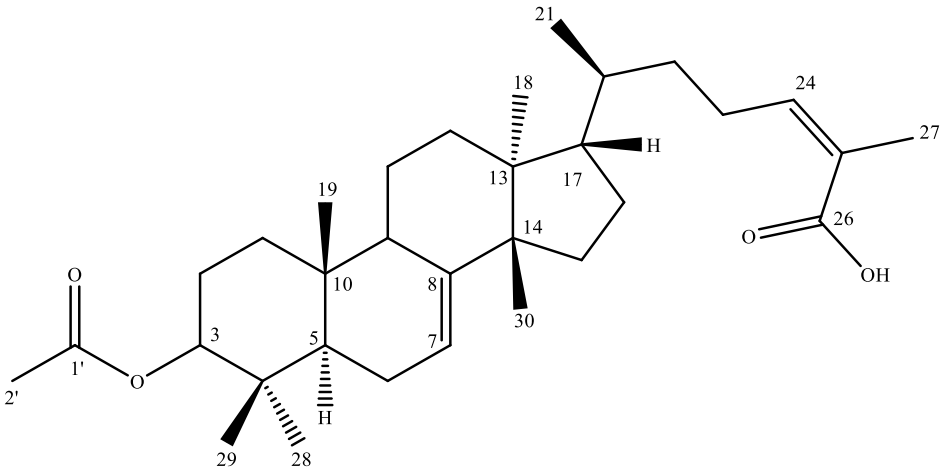

Figure 18. Chemical structure of MD-MG-03

The molecular formula of MD-MG-03 was found to be $C_{32}H_{50}O_4$ based on the HR-ESI-MS analysis (*m/z* 497.3644 $[M-H]^-$, calcd. 497.3631 for $C_{32}H_{49}O_4$). There was a

hydrogen deficiency index of eight in compound MD-MG-03 based on the MS data (Spectrum 5).

The ^{13}C-NMR (Spectrum 7) and DEPT-135 (Spectrum 52) spectra of MD-MG-03 showed 30 signals, assigned to two carbonyls (δ 172.8, s and 179.8, s), four olefinic (δ 118.9, d, 129.1, d, 137.0, s and 147.1, s), one oxygenated methine (δ 82.6, d) carbons, eight methyl, nine methylene, four methine and four quaternary carbons. Four of eight hydrogen deficiency index was regarded as two carbonyl carbons and two double bond systems. The four remaining unsaturation was implied a tetracyclic triterpene framework.

Initial inspection of the ^{1}H-NMR spectrum displayed six tertiary methyl protons at δ 0.72, 0.74, 0.78, 0.88, 0.91 and 1.76, and a secondary methyl group at δ 0.81 (d, J=6.0, H_3-21). Two olefinic signals at 5.06 and 5.19 ppm in the low-field region were readily noticed (Spectrum 6). By the HSQC spectrum, the corresponding protons were determined to be at δ_C 129.1 and 118.9, respectively. Based on the HMBC spectrum, the long-range correlations of these carbons revealed the presence of two distinct trisubstituted olefinic systems.

H_2-6 resonance was shifted to the low-field in the ^{1}H-NMR spectrum. When COSY correlation was traced, the spin system was determined through H-5/H_2-6 and H_2-6/H-7 couplings (Spectrum 54). Besides, C-8 (δ 147.1) was correlated with H_3-30 signal at δ 0.91 in the HMBC spectrum (Spectrum 55). These facts confirmed the position of double bond between C-7 and C-8. On the other hand, the olefinic proton (δ 5.06) was correlated with C-22 (δ 37.3), C-26 (δ 179.8) and C-27 (δ 21.6) in the HMBC spectrum. Also, the vicinal couplings between H_2-23/H-24 signals were noticed as a part of the spin system from H_2-15 to H-24. These findings verified the presence of a double bond at C-24.

Also, the characteristic signals of H-3 at δ 4.41 (dd, J=10.0, 5.5) and C-3 (δ 82.6) were shifted to the low-field in the ^{1}H- and ^{13}C-NMR spectra, besides one tertiary methyl signal at δ 1.95 was correlated with a carbonyl group (δ_C=172.8, s, C-1') on the basis of HMBC cross-peaks. Thus, an O-acetylation was suggested. The location of the acetoxy groups was suggested due to acylation originated shift of H-3 (ca. 2.3 ppm). This assumption was verified by long-range correlations from H-3 to C-1' (acetyl carbonyl), and H_3-28 and H_3-29 to C-3 (Table 5).

As a result, MD-MG-03 was identified as 3-O-acetyl masticadienolic acid, previously reported from mastic gum.[19]

Table 5. ^{1}H and ^{13}C NMR spectroscopic data of MD-MG-03, [a] (in CD_3OD, ^{1}H: 500 MHz, ^{13}C: 125 MHz)

Position	**δ_C (ppm)**	**δ_H (ppm), (J in Hz)**
1	38.0 t	1.62[b]; 1.33[b]
2	25.2 t	1.59[b]
3	82.6 d	4.41 dd (10.0, 5.5)
4	38.9 s	-
5	52.2 d	1.34[b]
6	24.8 t	2.05[b]; 1.90[b]
7	118.9 d	5.19 dd (6.7; 2.9)
8	147.1 s	-
9	50.2 d	2.19[b]
10	35.9 s	-
11	19.3 t	1.47[b]; 0.84[b]
12	35.0 t	1.57[b]; 1.37[b]
13	44.6 s	-
14	52.3 s	-
15	35.1 t	1.73[b]; 1.44[b]
16	29.2 t	1.90[b]; 1.86[b]
17	54.3 d	1.42[b]
18	22.5 q	0.74 s
19	13.7 q	0.72 s
20	37.4 d	1.31[b]
21	18.9 q	0.81 d (6.0)
22	37.3 t	1.45[b]; 1.01[b]
23	27.6 t	2.19[b]; 2.03[b]
24	129.1 d	5.06 t (7.2)
25	137.0 s	-

26	179.8 s	-
27	21.6 q	1.76 s
28	28.1 q	0.78 s
29	16.3 q	0.88 s
30	27.9 q	0.91 s
1’	172.8 s	-
2’	21.2 q	1.95 s

a) Assignments were confirmed by 2D-COSY, HSQC, HMBC experiments.

b) Signal pattern was unclear due to overlapping.

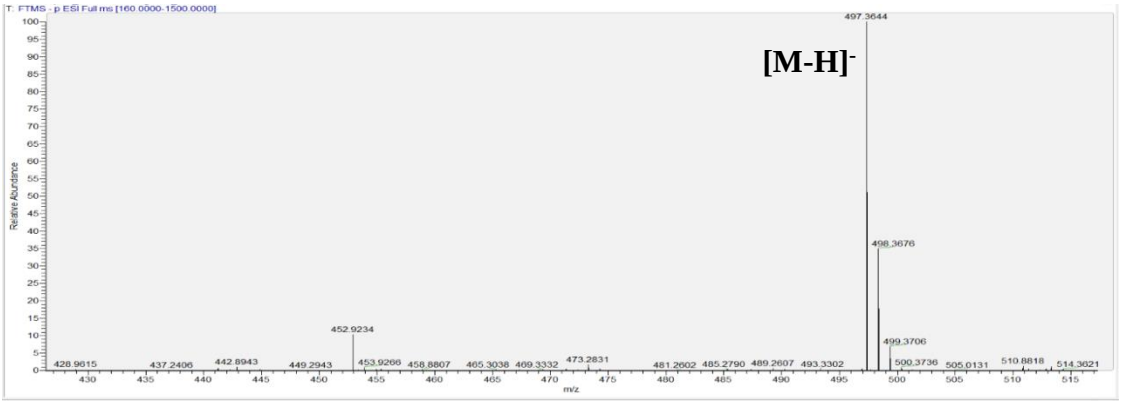

Spectrum 5. HR-ESI-MS spectrum of MD-MG-03 (negative mode)

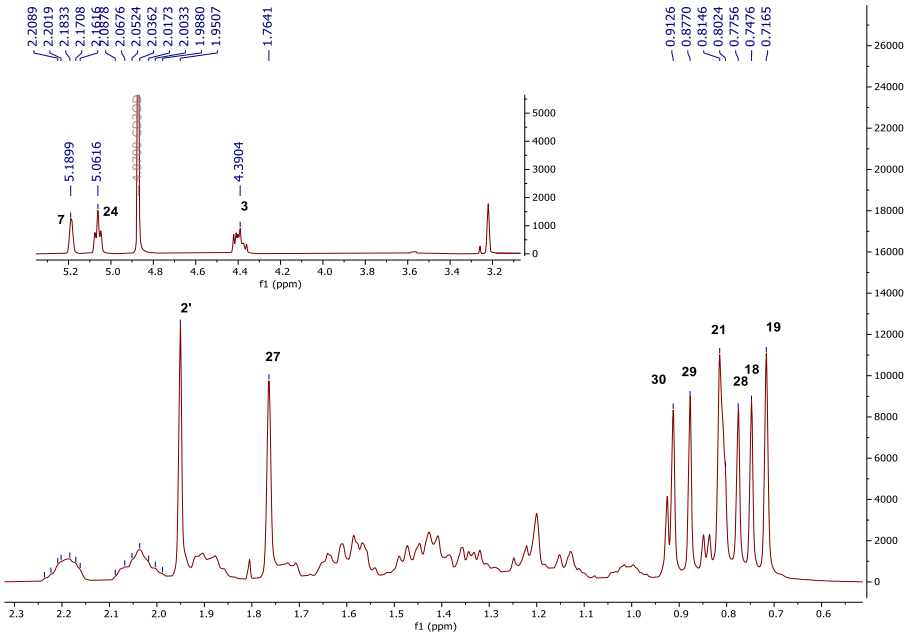

Spectrum 6. ^{1}H-NMR spectrum of MD-MG-03

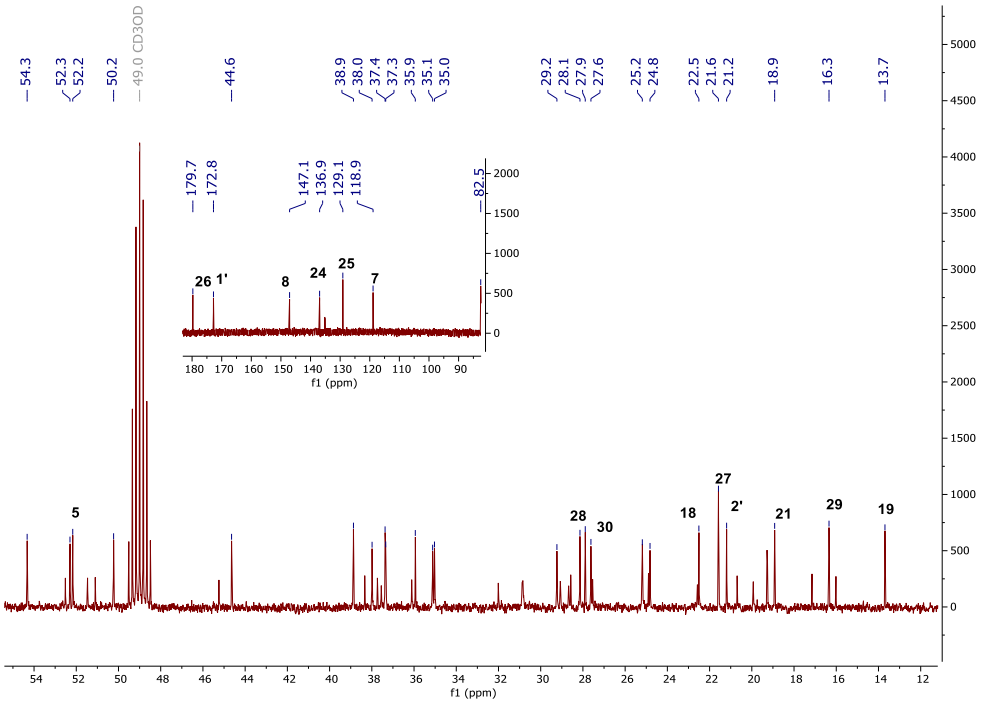

Spectrum 7. ^{13}C-NMR spectrum of MD-MG-03

3.1.4. Structural elucidation of MD-MG-04

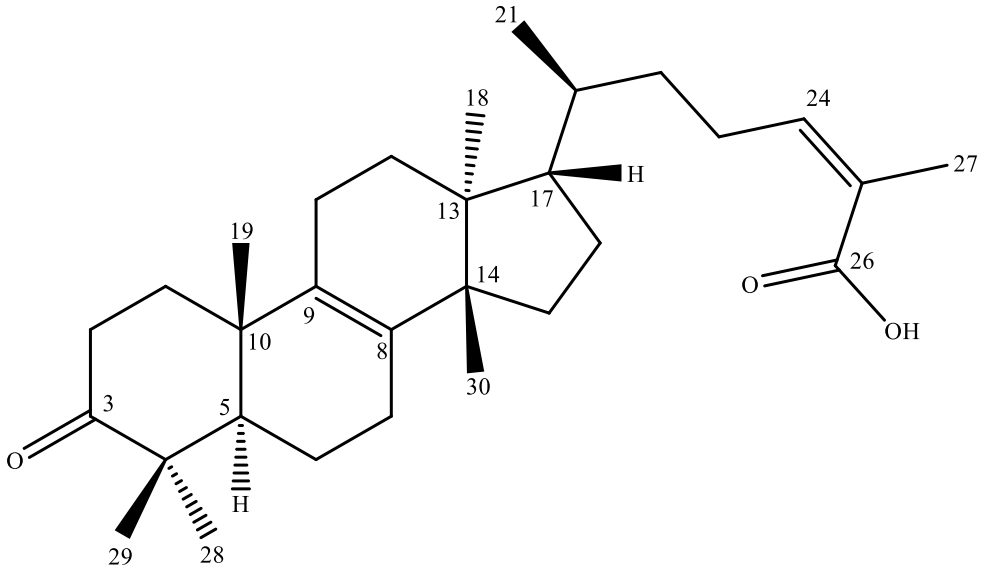

Figure 19. Chemical structure of MD-MG-04

The molecular formula of MD-MG-04 was determined as $C_{30}H_{46}O_3$ based on its

HR-ESI-MS data (*m/z* 453.3373 $[M-H]^-$, calcd. 453.3369 for $C_{30}H_{45}O_3$) (Spectrum 8). Comparison of the 1D-NMR data of MD-MG-04 with those of MD-MG-03 revealed the lack of olefinic H-7 proton as well as the absence of characteristic resonances belonging to H-3. In the ^{13}C-NMR spectrum, the appearance of a carbonyl signal at δ 216.9 indicated oxidation of a secondary alcohol to a ketone (Spectrum 10). Moreover, the existence of a tetrasubstituted double bond system was verified because of the lacking correlation of the double bond carbons (δ_C 135.1, s, C-8 and δ_C 133.3, s, C-9) with no proton in the HSQC spectrum, suggesting an isomeric form of masticadienonic acid (Spectrum 57). Hence, this suggestion was also confirmed via long-range correlations from H_3-30 (δ 0.92, s) to C-8, from H_3-19 (δ 0.98, s) to C-9, from H_3-28 (δ 1.06, s), H_3-29 (δ 1.15, s) and H_2-2 (δ 2.54, m) to C-3 (δ 216.9, s) (Table 6). Therefore, the tetrasubstituted double bond was assigned at C-8, while the ketone group was located at C-3. Consequently, MD-MG-04 was elucidated as isomasticadienonic acid.[18,21]

Table 6. ^{1}H and ^{13}C NMR spectroscopic data of MD-MG-04, [a] (in C_5D_5N, ^{1}H: 500 MHz, ^{13}C: 125 MHz)

Position	**δ_C (ppm)**	**δ_H (ppm), (J in Hz)**
1	36.0 t	1.86[b]; 1.53[b]
2	35.0 t	2.54[b]
3	216.9 s	-
4	47.6 s	-
5	51.7 d	1.70[b]
6	20.7 t	1.53[b]; 1.37[b]
7	28.0 t	2.05[b]
8	135.1 s	-
9	133.3 s	-
10	37.6 s	-
11	28.7 t	1.94[b]; 1.37[b]
12	31.3 t	1.73[b]; 1.37[b]
13	44.7 s	-
14	50.6 s	-
15	30.4 t	1.59[b]; 1.23[b]
16	21.9 t	2.02[b]; 1.86[b]
17	50.7 d	1.55[b]

18	16.1 q	0.80 s
19	19.2 q	0.98 s
20	37.2 d	1.53[b)]
21	20.1 q	1.03 d (6.5)
22	36.8 t	1.70[b)]; 1.30[b)]
23	27.4 t	2.89[b)]; 2.77[b)]
24	143.1 d	6.07 t (7.3)
25	129.0 s	-
26	170.9 s	-
27	21.5 q	2.15 s
28	21.9 q	1.06 s
29	27.2 q	1.15 s
30	24.7 q	0.92 s

a) Assignments were confirmed by 2D-COSY, HSQC, HMBC experiments.

b) Signal pattern was unclear due to overlapping.

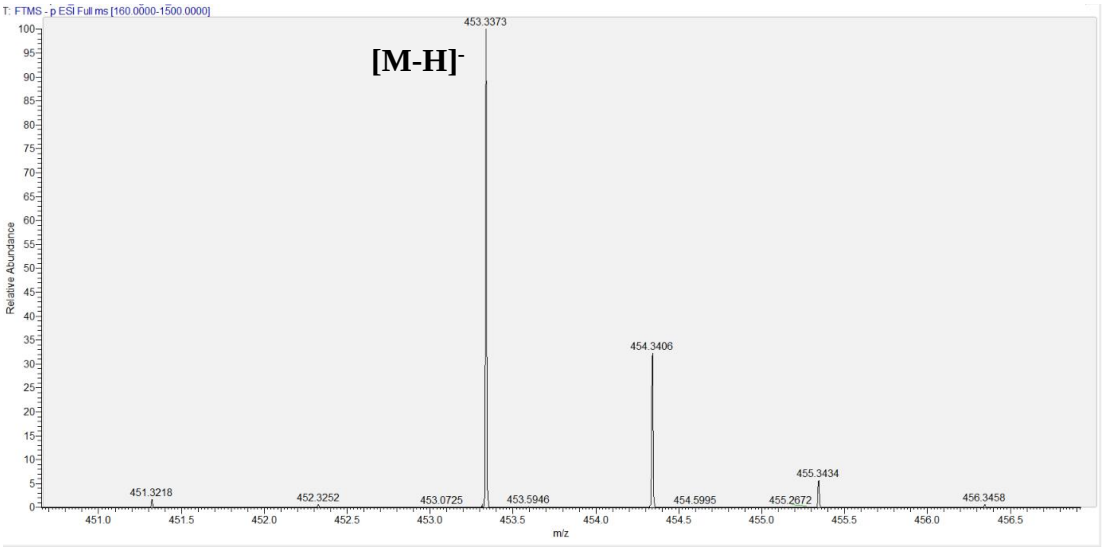

Spectrum 8. HR-ESI-MS spectrum of MD-MG-04 (negative mode)

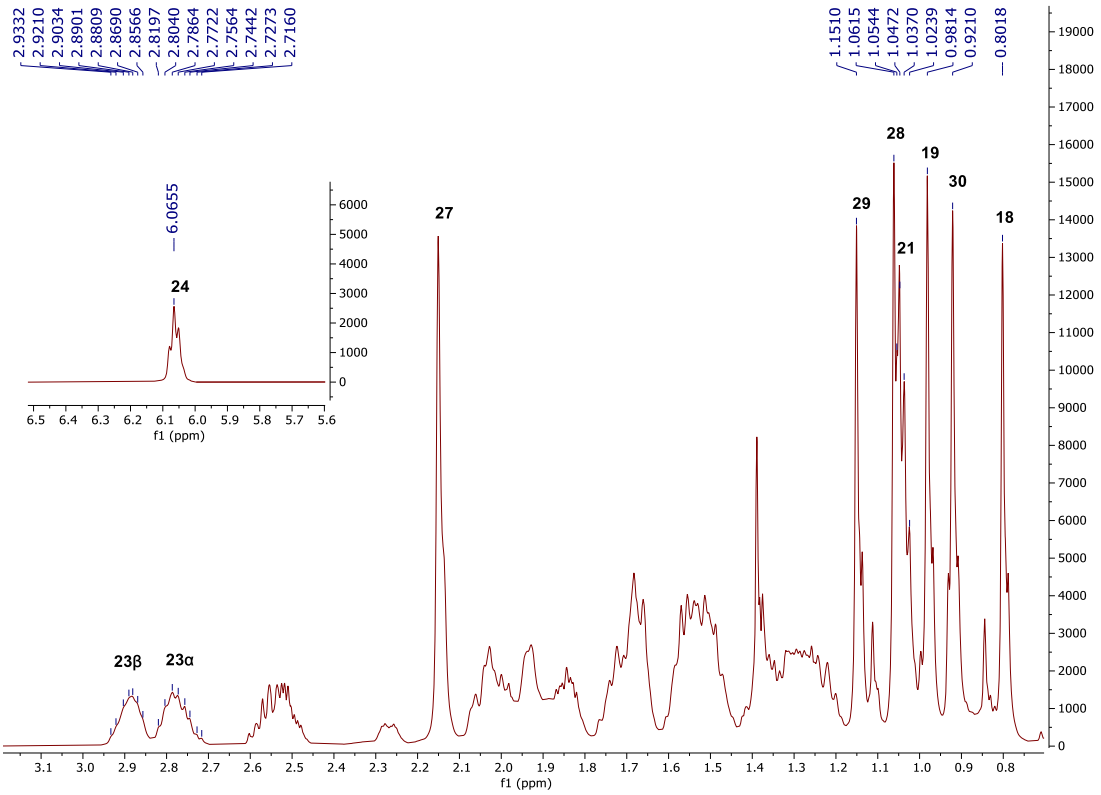

Spectrum 9. ^{1}H-NMR spectrum of MD-MG-04

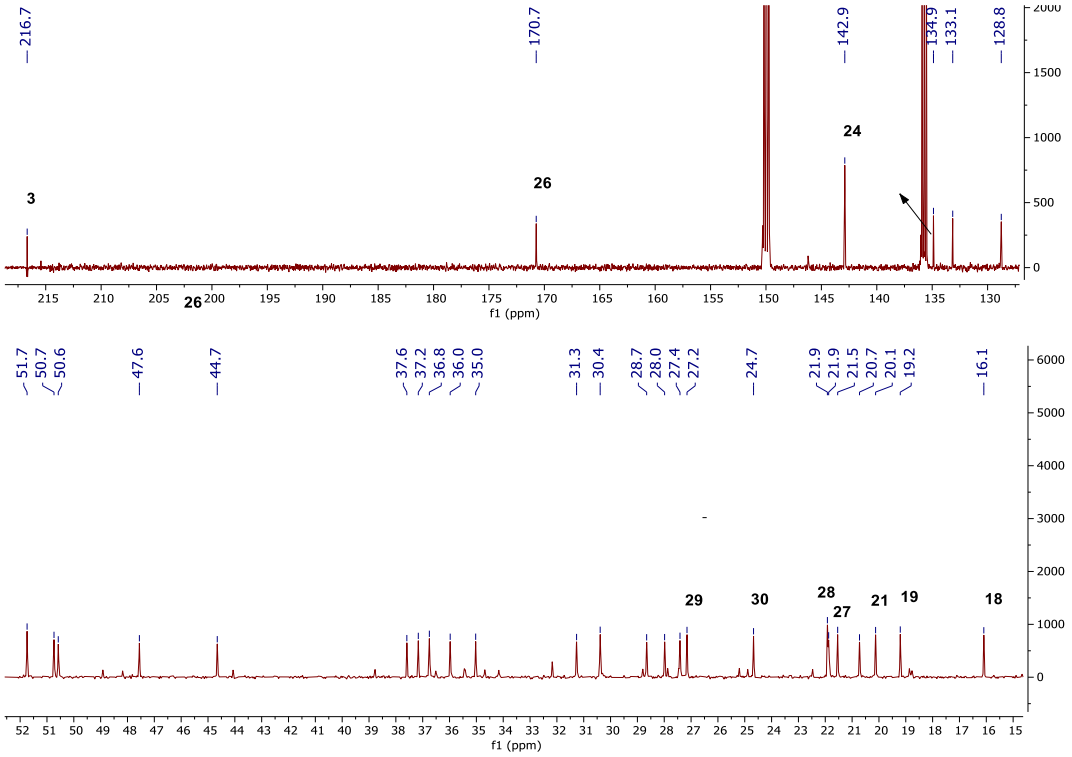

Spectrum 10. ^{13}C-NMR spectrum of MD-MG-04

3.1.5. Structural Elucidation of MD-MG-05

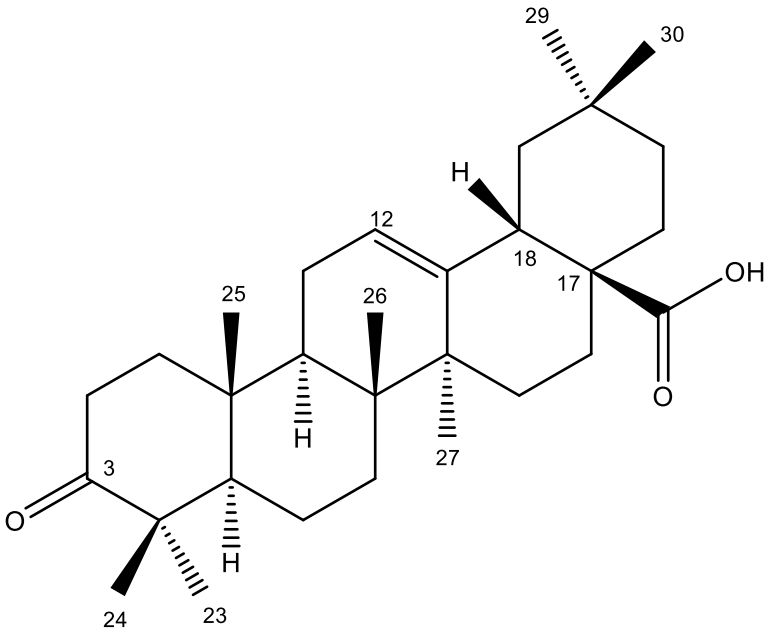

Figure 20. Chemical structure of MD-MG-05

The HR-ESI-MS analysis of MD-MG-05 gave the major ion peak at *m/z* 455.3519 $[M-H]^-$ (calcd 455.3531 for $C_{30}H_{47}0_3$, Spectrum 11), indicating the molecular formula $C_{30}H_{48}O_3$. When the ^{1}H- and ^{13}C-NMR data of MD-MG-05 were compared with MD-MG-02, the presence of a secondary alcohol was suggested (Spectrum 12-13). Because the carbonyl carbon in the ^{13}C-NMR spectrum was missing, whereas an oxo-methine proton signal was apparent in the down-field region of the ^{1}H-NMR spectrum. This proton was also correlated with an oxo-methine carbon at δ 78.6. Moreover, the long-range correlations from H_3-23 (δ 1.25, s) and H_3-24 (δ 1.02, s) protons to the carbon at δ_C 78.6 supported secondary alcohol character of C-3 (Table 7). Additionally, a spin system starting from H_2-1 (δ 1.55, m and δ 1.00, m)/H_2-2 (δ 2.17, m and δ 1.84, m)/H-3 (δ 3.45, m) was clearly traced in the COSY spectrum (Spectrum 62).

The comprehensive inspections of the 1D- and 2D-NMR spectra showed unchanged resonances for the remaining sections of triterpenic skeleton. As a result, MD-MG-05 was identified as oleanolic acid.[67,68]

Table 7. ^{1}H and ^{13}C NMR spectroscopic data of MD-MG-06, [a)] (in C_5D_5N, ^{1}H: 500 MHz, ^{13}C: 125 MHz)

Position	δ_C (ppm)	δ_H (ppm), (J in Hz)
1	39.0 t	1.00, 1.55
2	28.2 t	2.17, 1.84
3	78.6 d	3.45
4	39.9 s	-
5	56.3 d	0.88
6	19.3 t	1.57, 1.37
7	33.4 t	1.53, 1.36
8	39.5 s	-
9	48.6 d	1.70
10	37.5 s	-
11	24.0 t	2.07, 1.98
12	122.9 d	5.50
13	145.2 s	-
14	42.3 s	-
15	28.4 t	1.84, 1.26
16	23.7	2.15, 196
17	47.2 s	-
18	42.1 d	3.32
19	47.0 t	1.83, 1.32
20	31.1 s	-
21	34.7 t	1.48, 1.22
22	33.3 t	2.05, 1.83
23	28.9 q	1.25
24	16.1 q	0.89
25	17.1 q	1.02
26	18.0 q	1.03
27	26.7 q	1.30
28	180.6 s	-
29	33.8 q	0.97
30	24.2 q	1.03

a) Assignments were confirmed by 2D-COSY, HSQC, and HMBCexperiments.

b) Signal pattern was unclear due to overlapping.

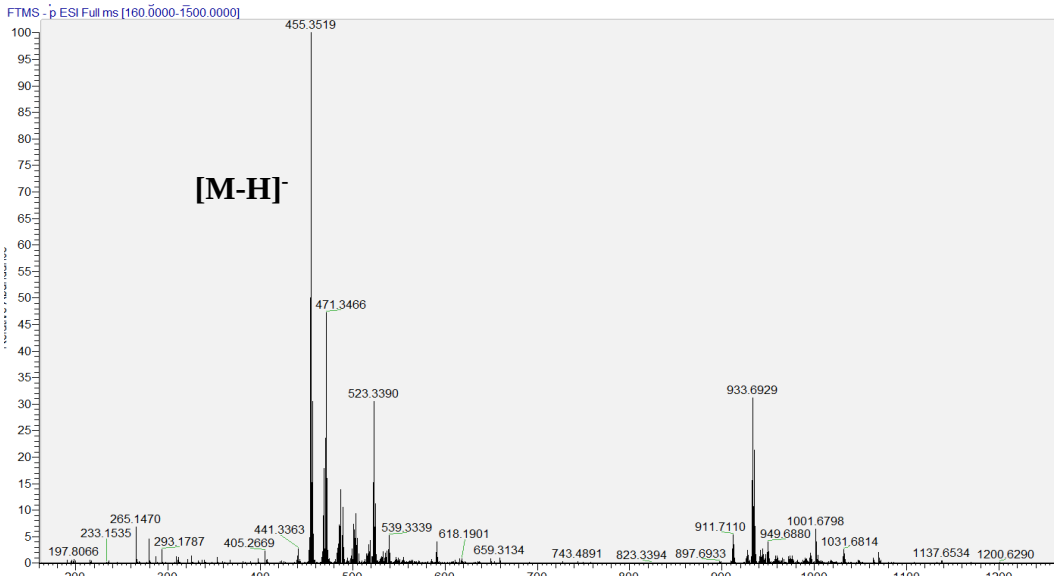

Spectrum 11**.** HR-ESI-MS spectrum of MD-MG-05 (negative mode)

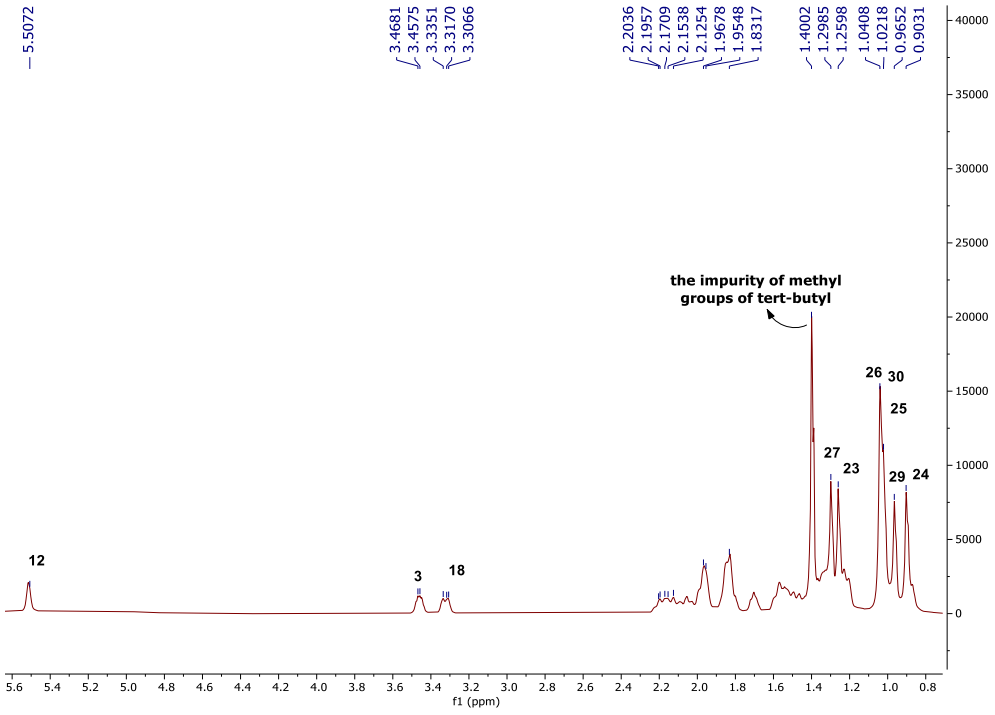

Spectrum 12. ^{1}H-NMR spectrum of MD-MG-05

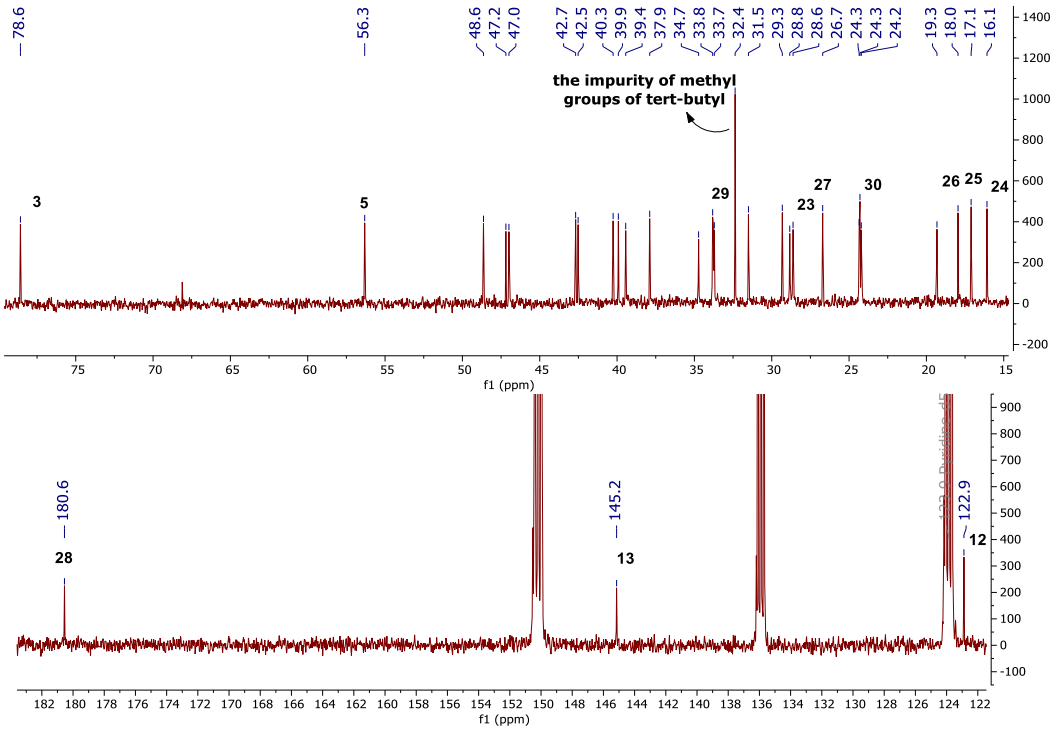

Spectrum 13. ^{13}C-NMR spectrum of MD-MG-05

3.1.6. Structural elucidation of MD-MG-06

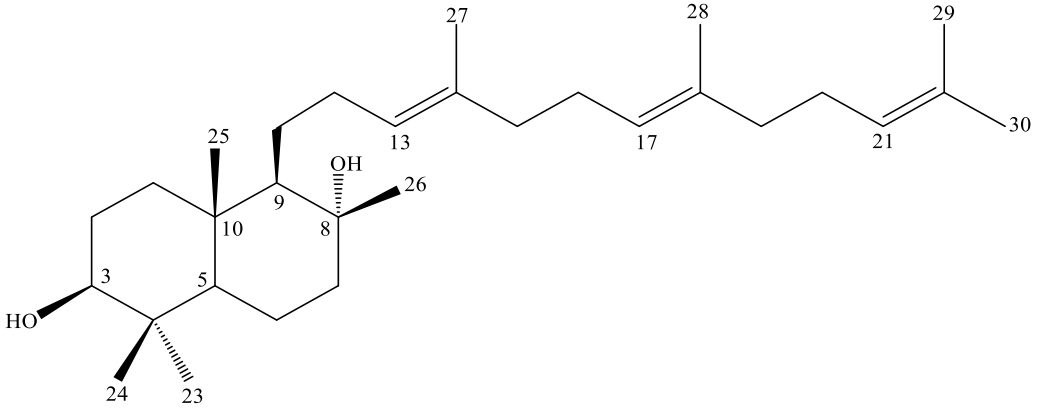

Figure 21. Chemical structure of MD-MG-06, (MD-MG-10)

The ESI-MS spectrum of MD-MG-06 displayed a quasimolecular ion peak at *m/z* 443.3532 $[M-H]^-$ (calcd. 443.3889 for $C_{30}H_{51}O_2$), suggesting a molecular formula of $C_{30}H_{52}O_2$ (Spectrum 14). The ^{1}H- and ^{13}C-NMR showed eight singlet signals of methyl groups at δ 0.91, 1.06, 1.25, 1.37, 1.60, 1.65, 1.68, 1.71, which were attached to non-protonated carbons (Table 8). The presence of methyl signals at about δ 1.6-1.8 indicated

that these methyl groups were adjacent to double bond systems (Spectrum 15-16). Thus, four of the eight methyl groups were described as allylic methyl resonances. Beside one oxymethine signal at δ 3.49 (ddd, J=10.9, 5.5, 4.9, H-3) was evident in ^{1}H-NMR spectrum, correlating with a carbon signal at δ 78.4 (d, C-3) in the HSQC spectrum (Spectrum 65). The HMBC correlations of H-3 with the methyl carbons at δ 16.7 and δ 29.1 and with the methylene carbon at δ 28.5 as well as vicinal coupling with H_2-2 protons at δ 1.93 (m, 2H) and geminal coupling with exchangeable proton at δ 5.92 (d, J=5.5, OH-3) verified the presence of a secondary alcohol at C-3 (Spectrum 67). A tertiary alcohol resonance at δ 73.3 (s, C-8) was noticed via inspection of the ^{13}C-NMR and DEPT-135 spectra (Spectrum 64). Since C-9 (δ 62.4, d) was correlated to two methyl groups at δ 0.91 (s, H_3-25) and δ 1.37 (s, H_3-26), the tertiary alcohol carbon was ascertained at C-8 position. Moreover, the interfragment relationship and substitution patterns of the rings A and B were established by HMBC correlations whilst the spin systems were traced in the COSY spectrum (Spectrum 66).

Also, the inspection of the ^{1}H-NMR spectrum revealed three distinct olefinic proton signals at δ 5.24 dd (J=7.5, 7.0, H-21), δ 5.30 t (J=7.0, H-17) and δ 5.46 t (J=7.2, H-13) whereas six olefinic carbons at δ 125.2 (d, C-21), δ 125.3 (d, C-17), δ 126.6 (d, C-13), δ 131.5 (s, C-22), δ 134.7 (s, C-14) and δ 135.4 (s, C-18) were observed in the ^{13}C-NMR and DEPT-135 spectra. These protons showed correlations with three different carbons in their HSQC spectrum. Also, based on the $^{2}J_{C\text{-}H}$ and $^{3}J_{C\text{-}H}$ correlations of each olefinic systems with both allylic methyl groups and methylene signals in close proximity, the positions of the double bonds were assigned to be C-13, C-17 and C-21.

Consequently, on the basis of the spectral data and their comparison with those of previously published, the framework of MD-MG-06 was found to be a polypodane type bicyclic triterpenoid, and the structure was established as myrrhanol C, a known compound.[35,69]

Table 8. ^{1}H and ^{13}C NMR spectroscopic data of MD-MG-06, [a] (in C_5D_5N, ^{1}H: 500 MHz, ^{13}C: 125 MHz)

Position	δ_C (ppm)	δ_H (ppm), (J in Hz)
1	38.9 t	1.80[b]; 1.24[b]
2	28.5 t	1.93[b]
3	78.4 d	3.49 ddd (10.9, 5.5, 4.9)
4	39.8 s	-

5	56.0 d	1.08[b)]
6	21.2 t	1.74[b)]; 1.44[b)]
7	45.4 t	2.08[b)]; 1.82[b)]
8	73.3 s	-
9	62.4 d	1.42[b)]
10	39.4 s	-
11	26.9 t	1.91[b)]; 1.42[b)]
12	32.8 t	2.57 dq (12.1, 6.3); 2.31 dq (13.1, 6.3)
13	126.6 d	5.46 t (7.2)
14	134.7 s	-
15	40.4 t	2.12[b)]
16	27.4 t	2.21[b)]
17	125.3 d	5.30 t (7.0)
18	135.4 s	-
19	40.4 t	2.08[b)]
20	27.4 t	2.16[b)]
21	125.2 d	5.24 dd (7.5, 7.0)
22	131.5 s	-
23	16.7 q	1.06 s
24	29.1 q	1.25 s
25	16.4 q	0.91 s
26	24.9 q	1.37 s
27	16.7 q	1.71 s
28	16.5 q	1.65 s
29	18.1 q	1.60 s
30	26.2 q	1.68 s
3-OH	-	5.92 d (5.5)
8-OH	-	5.24 s

a) Assignments were confirmed by 2D-COSY, HSQC, and HMBC experiments.

b) Signal pattern was unclear due to overlapping.

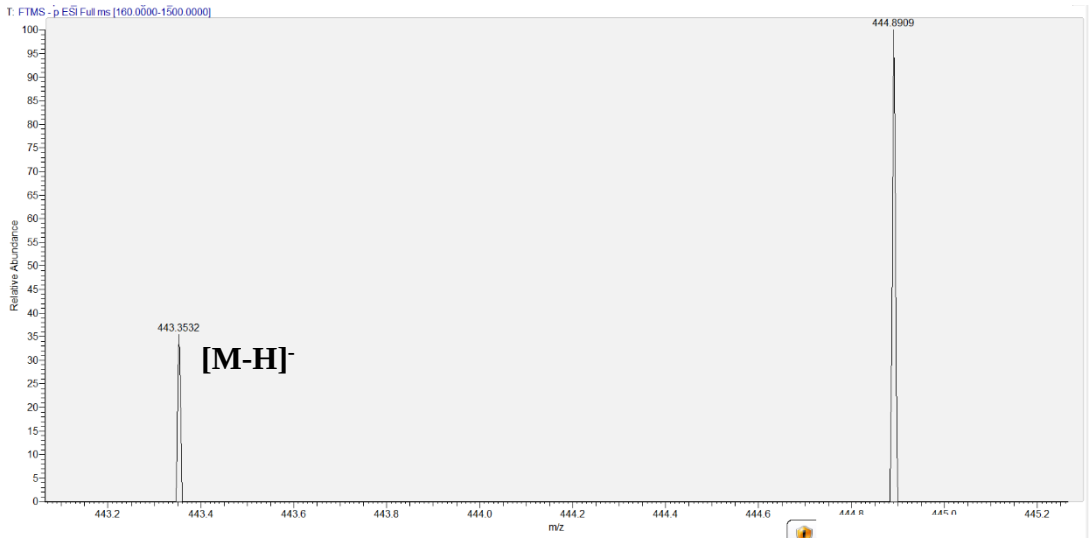

Spectrum 14. HR-ESI-MS spectrum of MD-MG-06 (negative mode)

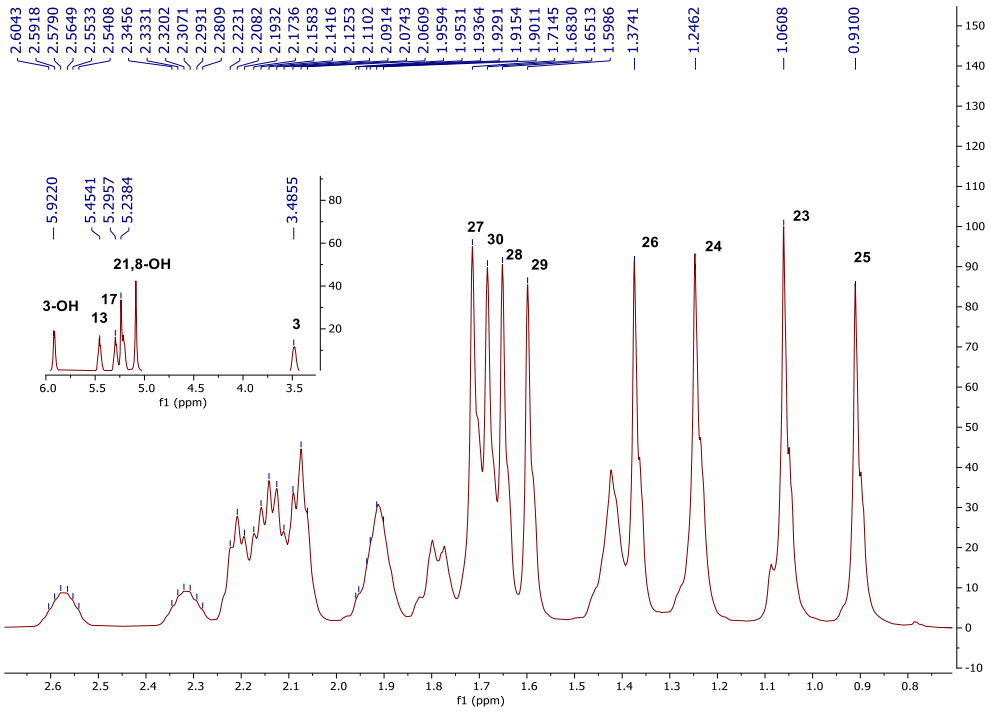

Spectrum 15. ^{1}H-NMR spectrum of MD-MG-06

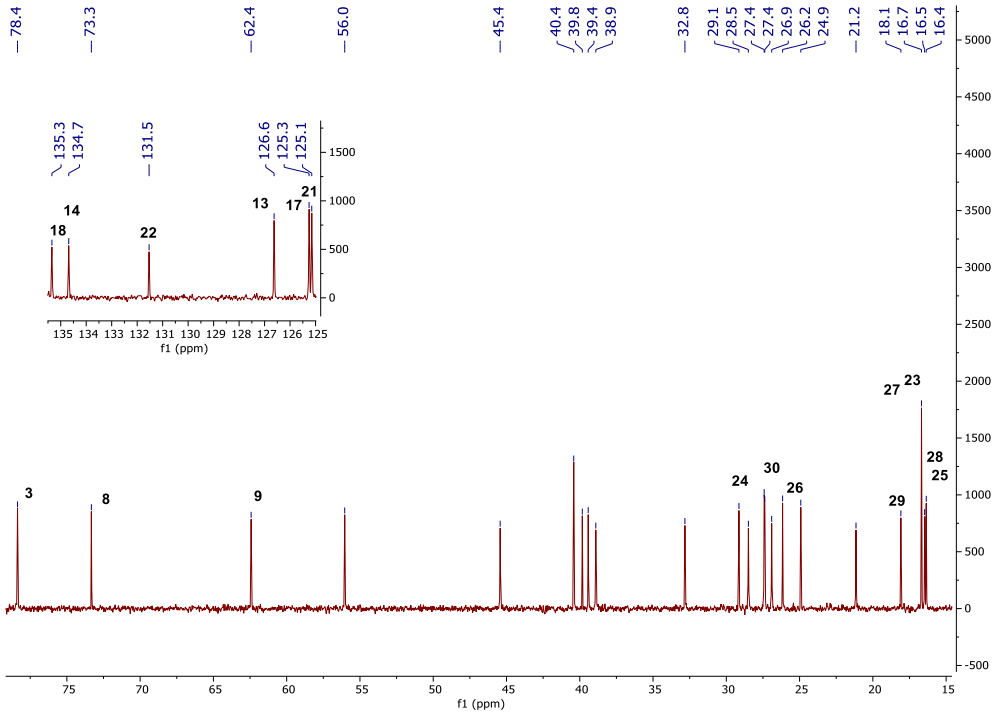

Spectrum 16. ^{13}C-NMR spectrum of MD-MG-06

3.1.7. Structural elucidation of MD-MG-07

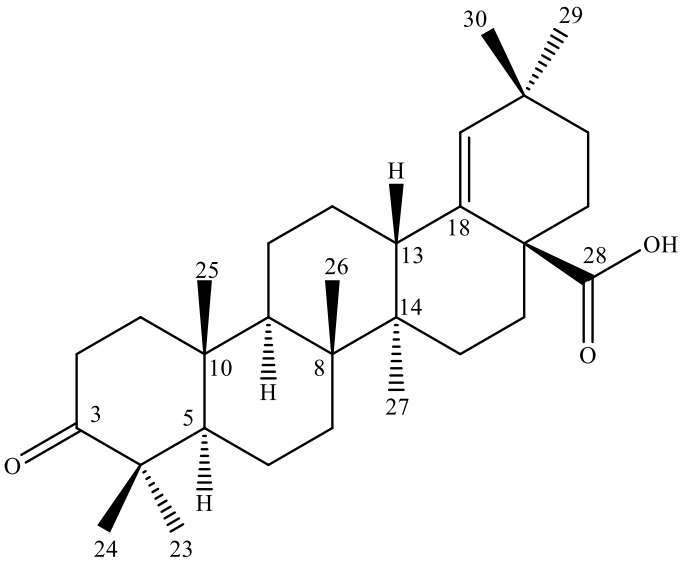

Figure 22. Chemical structure of MD-MG-07 (MD-MG-08 and MD-MG-11)

In the HR-ESI-MS spectrum of MD-MG-07, a base ion peak was observed at *m/z* 453.3372 $[M-H]^-$, proposing a molecular formula of $C_{30}H_{46}O_3$ (calcd. 453.3369 for $C_{30}H_{45}O_3$) (Spectrum 17).

Initial inspection of the ^{1}H- and ^{13}C-NMR spectra (Table 9) showed that MD-MG-07 were similar to MD-MG-02 except for characteristic signal of H-18 (Spectrum 18-19). Besides, a new proton at δ 2.68 dd (J=11.7, 3.0, H-13), which corresponded to a carbon at δ_C 41.5 in the HSQC spectrum, was readily noticed (Spectrum 69). The proton signals, originating from the methylene groups (H_2-11: δ 1.43 and 1.19, m) resonated in the higher field, showed cross peaks with other methylene signals (H_2-12: δ 1.66 and 1.22, m) and subsequently with H-13 in the COSY spectrum (Spectrum 70).

Also, the presence of two olefinic carbons at δ 131.9 (d, C-19) and 138.6 (s, C-18) was observed in the ^{13}C-NMR and DEPT-135 spectra whereas an olefinic proton was evident at δ 5.28 s (H-19) in the down-field region of the ^{1}H-NMR spectrum, indicating the migration of C-12 double bond in the skeleton compared to MD-MG-02. No coupling of H-19 suggested that C-19 was surrounded by two quaternary carbons at α-position. This assumption was also verified with the $^2J_{C-H}$ and $^3J_{C-H}$ long-distance correlations in the HMBC spectrum from H-29/H-30 (each s, δ 1.13 and 1.08, respectively) to C-19; H-13 to C-12 (δ 26.2)/C-18 and H-19 to C-13 (δ 41.5)/C-17 (δ 48.3)/C-20 (δ 32.2). Moreover, H-19 displayed a weak interaction with C-28 (δ 178.8) in long distance. Based on this data, the olefinic bond was undoubtedly located between C-18 and C19 (Spectrum 71).

A comparison of the spectroscopic data of MD-MG-07 with moronic acid revealed that they were identical, consequently, the structure of MD-MG-07 was established as moronic acid.[68,70]

Table 9. ^{1}H and ^{13}C NMR spectroscopic data of MD-MG-07, [a] (in C_5D_5N, ^{1}H: 500 MHz, ^{13}C: 125 MHz)

Position	**δ_C (ppm)**	**δ_H (ppm), (J in Hz)**
1	39.6 t	1.79[b]; 1.35[b]
2	34.0 t	2.53[b]; 2.48[b]
3	216.5 s	-
4	47.0 s	-
5	54.5 d	1.34[b]

6	19.6 t	1.33[b)]
7	*	*
8	40.5 s	-
9	50.4 d	1.36[b)]
10	36.7 s	-
11	21.5 t	1.43[b)]; 1.19[b)]
12	26.2 t	1.66[b)]; 1.22[b)]
13	41.5 d	2.68 dd (11.7, 3.0)
14	42.7 s	-
15	29.7 t	1.98 td (13.5, 4.2); 1.27[b)]
16	33.8 t	2.56[b)]; 1.54[b)]
17	48.3 s	-
18	138.6 s	-
19	131.9 d	5.28 s
20	32.2 s	-
21	*	*
22	*	*
23	20.9 q	1.01 s
24	26.7 q	1.10 s
25	15.8 q	0.99 s
26	16.3 q	0.80 s
27	15.0 q	0.91 s
28	178.8 s	-
29	30.6 q	1.13 s
30	29.1 q	1.08 s

a) Assignments were confirmed by 2D-COSY, HSQC, and HMBC experiments.

b) Signal pattern was unclear due to overlapping.

*) Assignments of proton and carbon data were unsuccessful by overlapping.

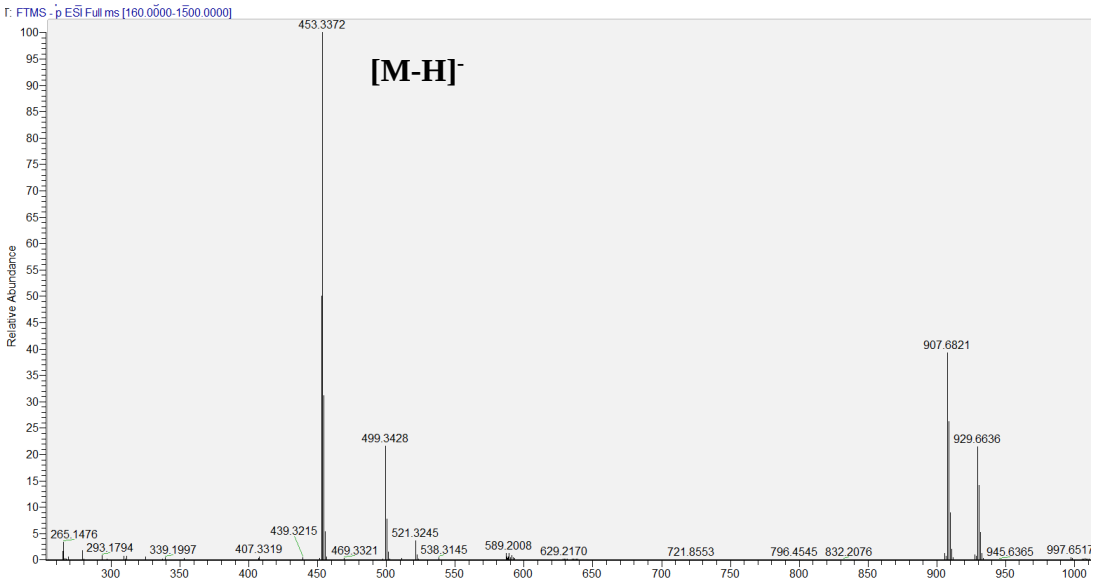

Spectrum 17. HR-ESI-MS spectrum of MD-MG-07 (negative mode)

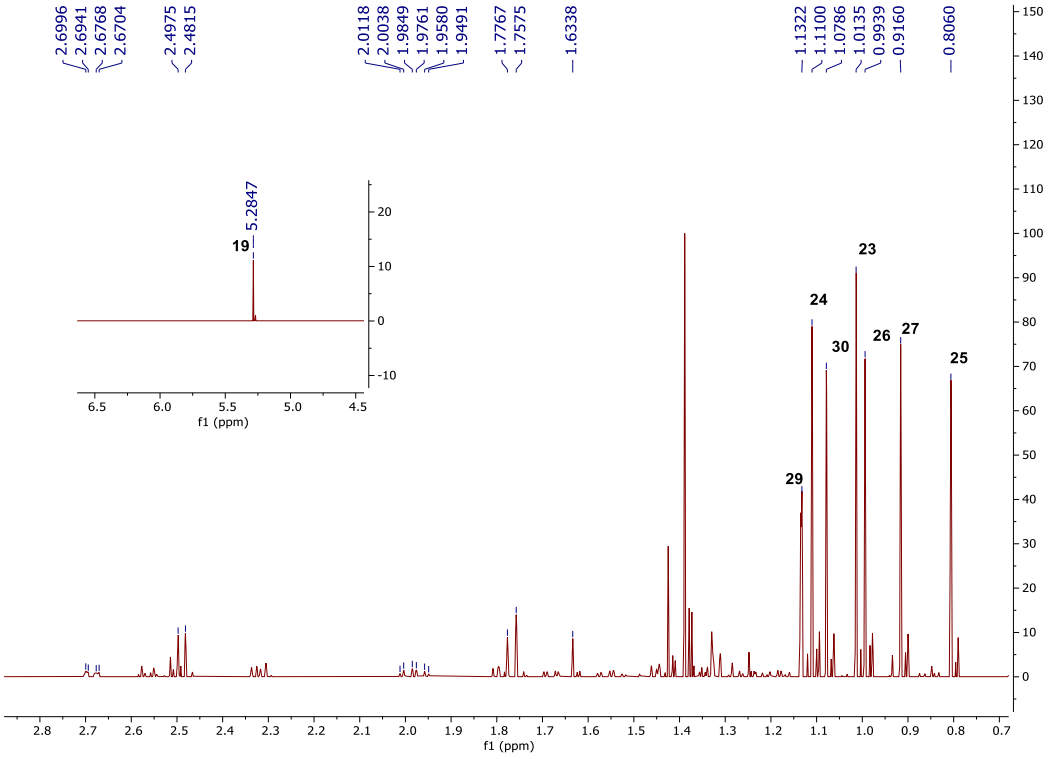

Spectrum 18. ^{1}H-NMR spectrum of MD-MG-07

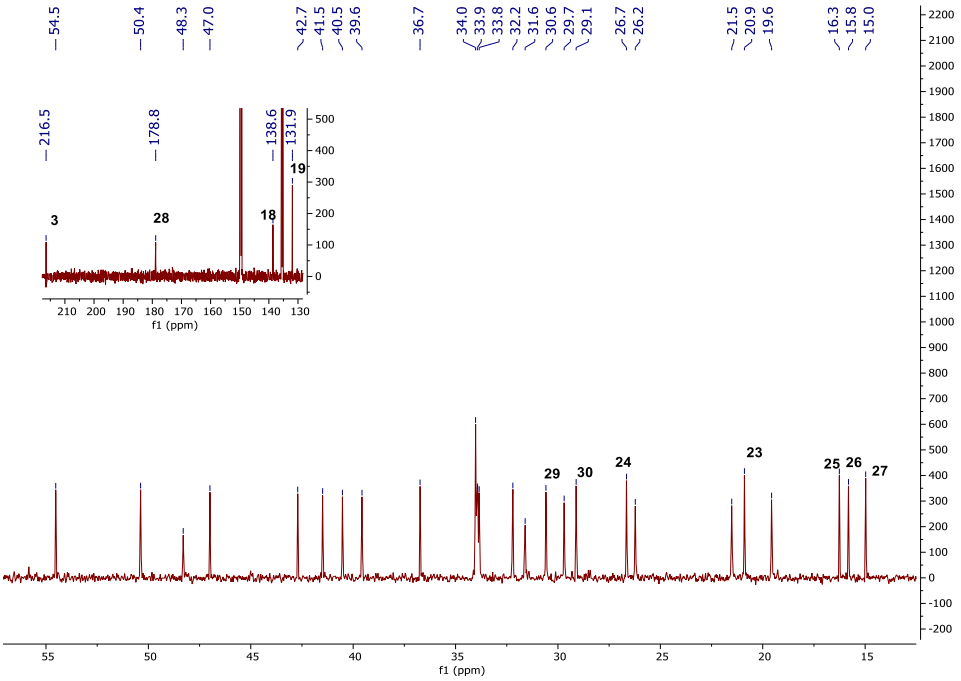

Spectrum 19. ^{13}C-NMR spectrum of MD-MG-07

3.1.8. Structural elucidation of MD-MG-12

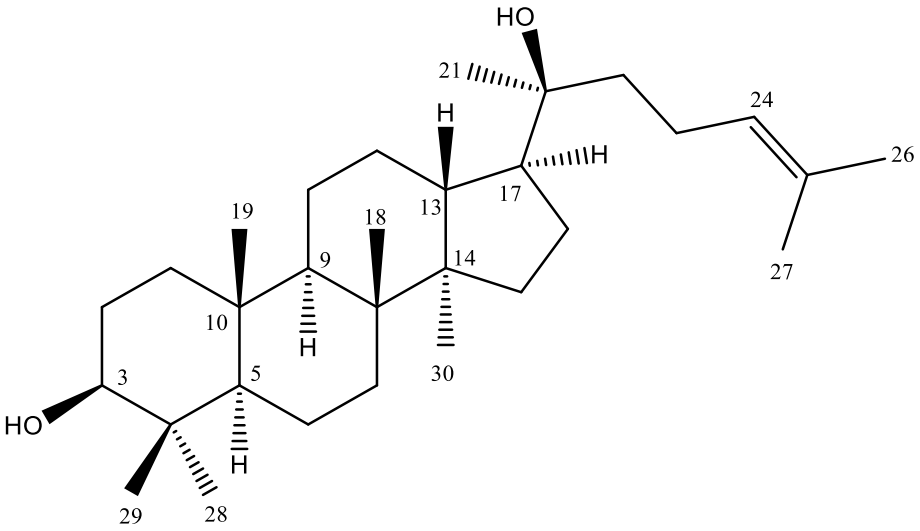

Figure 23. Chemical structure of MD-MG-12

^{1}H-NMR spectrum of MD-MG-12 revealed eight tertiary methyl resonances at δ 0.86, 0.92, 0.94, 1.03, 1.25, 1.44, 1.67 and 1.72 (each s; respectively H_3-30, H_3-19, H_3-29, H_3-18, H_3-21, H_3-27, and H_3-26) (Spectrum 20). Also, an oxymethine proton at δ 3.64 dd (J=4.5, 3.5; H-3) suggested the existence of a hydroxymethine group. This inference

was verified through HSQC cross peaks between H-3 and one hydroxymethine carbon at δ 75.7 (C-3) (Spectrum 73). Thus, the hydroxymethine carbon was determined at C-3 by long-range correlations to H_3-28/H_3-29.

The ^{13}C-NMR and DEPT-135 revealed an olefinic system (δ_C 126.4, d, C-24 and δ_C 131.4, s, C-25) with almost identical spectral data with those of MD-MG-01, establishing the side chain methyl allyl system (Spectrum 21-72). Moreover, the location of this trisubstituted olefinic system at C-24 was confirmed based on the long-range correlations, from H-26/H-27 to C-24/C-25; H-22/H-23 to C-24; H-24 to C-22/C-23/C-26/C-27. Besides, the vicinal couplings of the olefinic proton were immediately deduced from the COSY spectrum. Hence, olefinic proton was correlated with protons at δ 2.44 ddt (J=12.5, 7.4, 5.7; H_2-23), 2.35 ddt (J=12.5, 7.4, 5.9; H_2-23) and allylic methyl signals (Spectrum 74). Apart from these signals, the carbon signals included eight methyl, ten methylene, five methine including one oxygen-bearing (δ_C 75.7, d, C-3) and five quaternary carbons including one tertiary alcohol carbon at δ 74.4 (s, C-20). The 30 resonances of the framework were consistent with a $C_{30}H_{52}O_2$ triterpenic nucleus, indicating the presence of 5 degrees of unsaturation with a double bond and four ring systems (Table 10).

As H_2-15/H_2-16/H-17 spin system was not continuing with the side chain, the second OH substitution was inferred to be at C-20. This suggestion was partly substantiated with the downfield shift of H_3-21 (+0.4 ppm) in the ^{1}H-NMR spectrum, and singlet appearance of the H_3-21 methyl resonance. Based on the HMBC interactions from H-21 to C-17/C-20/C-22, the tertiary alcohol group was unambiguously located at C-20 (Spectrum 75).

A comparison of the spectral data of MD-MG-012 with those of (20S)-dammar-24-ene-3*β*,20-diol (dammarenediol-II)[19,71] revealed that they were superimposable. Consequently, the structure of MD-MG-12 was established as dammarenediol-II.

Table 10. ^{1}H and ^{13}C NMR spectroscopic data of MD-MG-12, [a] (in C_5D_5N, ^{1}H: 500 MHz, ^{13}C: 125 MHz)

Position	δ_C (ppm)	δ_H (ppm), (J in Hz)
1	34.6 t	1.79[b]; 1.47[b]
2	26.9 t	2.05[b]; 1.79[b]
3	75.7 d	3.64 dd (4.5, 3.5)
4	38.5 s	-

5	50.1 d	1.75[b)]
6	19.0 t	1.52[b)]
7	36.0 t	1.63[b)]; 1.27[b)]
8	41.3 s	-
9	51.3 d	1.63[b)]
10	38.0 s	-
11	22.2 t	1.63[b)]; 1.29[b)]
12	25.7 t	1.95[b)]; 1.88[b)]
13	42.8 d	1.97[b)]
14	51.0 s	-
15	32.0 t	1.63[b)]; 1.11 dt (9.2, 5.3)
16	28.5 t	2.11[b)]
17	50.6 d	1.95[b)]
18	16.1 q	1.03 s
19	16.8 q	0.92 s
20	74.4 s	-
21	26.6 q	1.44 s
22	42.2 t	1.84[b)]; 1.78[b)]
23	23.7 t	2.44 ddt (12.5, 7.4, 5.7); 2.35 ddt (12.5, 7.4, 5.9)
24	126.4 d	5.35 t (7.4)
25	131.4 s	-
26	26.2 q	1.72 s
27	18.1 q	1.67 s
28	29.8 q	1.25 s
29	22.9 q	0.94 s
30	17.1 q	0.86 s
3-OH		5.74 d (4.5)
20-OH		5.23 s

a) Assignments were confirmed by 2D-COSY, HSQC, and HMBC experiments.

b) Signal pattern was unclear due to overlapping.

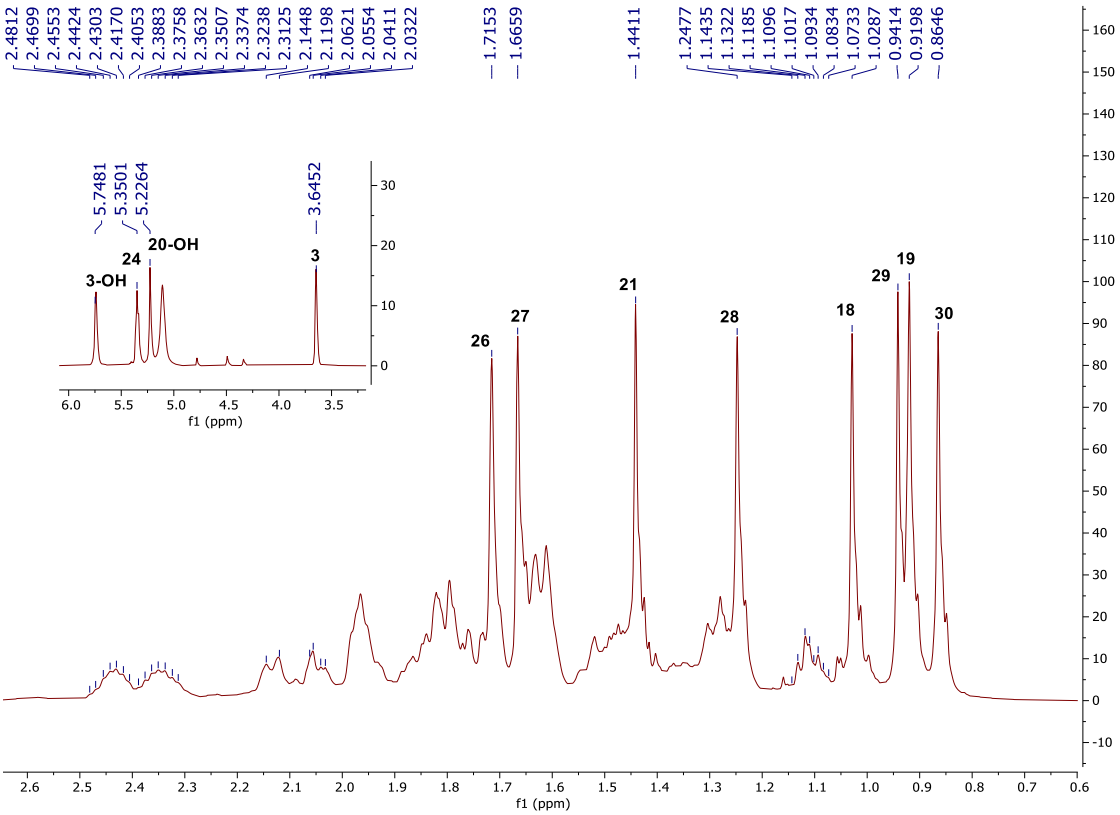

Spectrum 20. ^{1}H-NMR spectrum of MD-MG-12

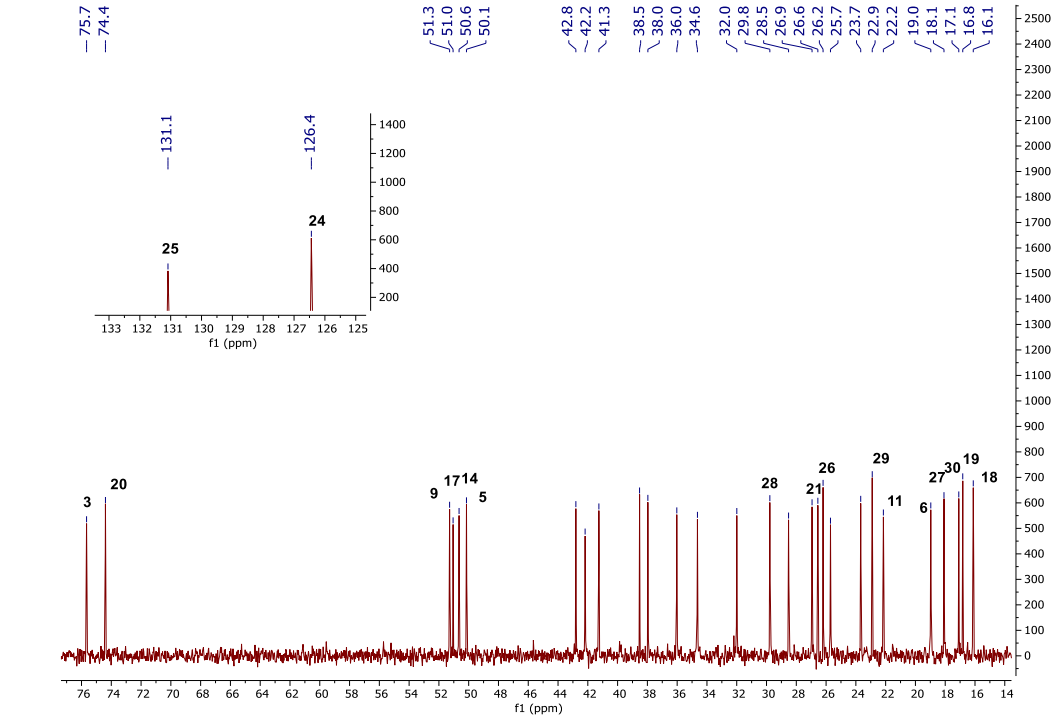

Spectrum 21. ^{13}C-NMR spectrum of MD-MG-12

3.1.9. Structural elucidation of MD-MG-13

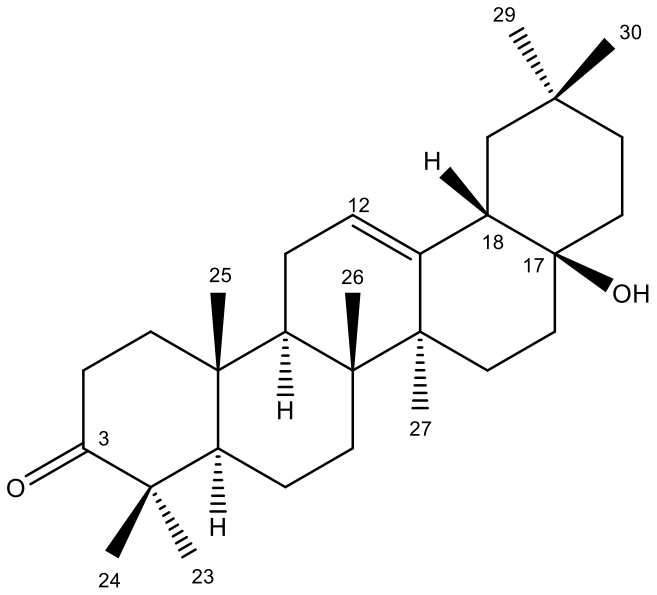

Figure 24. Structure of MD-MG-13, (MD-MG- 22)

The ESI-MS spectrum of MD-MG-13 provided an ion peak at *m/z* 449.31977 $[M+Na]^+$ (positive mode), the molecular formula was suggested as $C_{29}H_{46}O_2$ (calcd. 449.33955 for $C_{29}H_{46}NaO_2$) (Spectrum 22) with seven degrees of unsaturation.

The ^{1}H-NMR spectrum of MD-MG-13 revealed seven tertiary methyl groups at δ 0.94, 0.96, 0.99, 1.05, 1.17, 1.22 and 1.24 (each s, H_3-29, H_3-25, H_3-30, H_3-24, H_3-23, H_3-26 and H_3-27, respectively,) in the up-field region (Spectrum 23). Additionally, an olefinic proton at δ 5.32 (m, H-12) was obvious in the ^{1}H-NMR spectrum while two olefinic carbon resonances were noted in the ^{13}C-NMR spectrum (Spectrum 24). Thus, the presence of a trisubstituted double bond system was evident, which was further corroborated with the HSQC spectrum showing a cross peak between H-12 and C-12 (δ 122.8) (Spectrum 26). The double bond was located between C-12 and C-13 based on $^3J_{C\text{-}H}$ cross peaks from H_3-27 (δ 1.24, s) to C-13, H-9 (δ 1.72, m) to C-12 and also H-12 to C-14 (δ 42.7, s) and C-18 (δ 49.3) (Table 11). Also, apart from these olefinic carbons, 27 carbon signals were identified as seven methyl, ten methylene, three methine and seven non-protonated carbons including a ketone group (δ_C 216.8) and a tertiary alcohol carbon (δc 71.3). Since total of 29 carbon atoms were observed and two out of the seven degrees

of unsaturation were accounted for a carbonyl and a double bond system, the presence of a pentacyclic nor-triterpene skeleton was suggested.

The existence of a pentacyclic skeleton in MD-MG-13 was also substantiated via the HMBC and COSY spectra. When the COSY spectrum was established, the first spin system was traced from H_2-1 protons (δ_H 1.77 and 1.35) to H_2-2 (δ_H 2.55 and δ_H 2.42). Also, the second spin system involved H-5 (δ_H 1.38), H_2-6 (δ_H 1.42) and H_2-7 (δ_H 1.49 and 1.42) (Spectrum 27). Additionally, another spin system was apparent between H-9 (δ_H 1.72) and H_2-11 (δ_H 2.00 and 1.93). Moreover, the spin systems from H_2-15 (δ_H 2.49 and 1.09) to H_2-16 (δ_H 2.17 and 1.43); from H-18 (δ_H 2.58) to H_2-19 (δ_H 1.83 and 1.36) and from H_2-21 (δ_H 1.41 and 1.31) to H_2-22 (δ_H 2.05 and 1.71) were assigned. Besides, the pentacyclic system was unambiguously determined by the HMBC cross-peaks from H_3-25 (δ 0.96) to C-1 (δc 39.6), C-5 (δc 55.9), C-9 (δc 47.8), C-10 (δc 37.5); from H_3-26 (δ_H 1.22) to C-7 (δ_C 33.4), C-8 (δc 40.4), C-9 (δ_C 47.8), C-14 (δc 42.7); from H_3-27 (δ_H 1.24) to C-13 (δ_C 146.3), C-14 (δc 42.7), C-15 (δ_C 26.9) and from H_3-29/H_3-30 (δ_H 0.94 and 0.99, respectively) to the C-19 (δ_C 49.4), C-20 (δ_C 31.7), C-21 (δ_C 37.6) (Spectrum 28).

Since the absence of an oxymethine proton resonance in the ^{1}H-NMR spectrum together with the presence of a carbonyl carbon (δ_C 216.5) in the ^{13}C-NMR spectrum, an oxidation at C-3 was inferred. A detailed inspection of the HMBC spectrum revealed that H_2-2 protons (δ 2.55 and 2.42) showed a strong correlation with ketone carbon whereas this carbon in turn correlated with both H_3-23 (δ 1.17, s) and H_3-24 (δ 1.05, s). Hence, the presence of a ketone functionality at C-3 was proven.

More detailed inspection of the NMR spectral data of MD-MG-13 was consistent with the presence of a 28-nor-oleanane skeleton.[72] Indeed, the abovementioned tertiary alcohol group was proposed to be at C-17. After a thorough literature search, a C-17 hydroxy substituted nor-oleanane triterpenoid was found to be isolated from mastic gum. However, the configuration at C-17 was uncertain, and the reported carbon data for C-17 was about 13 ppm downfield shifted ($\delta_{C\text{-}17}$ 84.2) compared to that of MD-MG-13 ($\delta_{C\text{-}17}$ 71.3).[72] This significant difference prompted us to elucidate the absolute stereochemistry unambiguously. Thus, a single-crystal X-ray diffraction analysis (Figure 25) was performed. When XRD data was inspected, it was clear that both H-18 proton and hydroxy group were at the same plane suggesting a cis junction between D and E rings, as well the absolute configurations of C-17 and C-18 were both S.

Consequently, MD-MG-13 was identified as 17(S)-28-norolean-17-ol-12-ene-3-one, a new compound for nature. Although this compound was reported in the literature the stereochemistry at the junction point of ring D and E was firstly elucidated by means of this study.

Table 11. ^{1}H and ^{13}C NMR spectroscopic data of MD-MG-17, [a] (in C_5D_5N, ^{1}H: 500 MHz, ^{13}C: 125 MHz)

Position	δ_C (ppm)	δ_H (ppm), (J in Hz)
1	39.6 t	1.77[b]; 1.35[b]
2	35.0 t	2.55; 2.42[b]
3	216.8 s	-
4	48.0 s	-
5	55.9 d	1.38[b]
6	20.4 t	1.42[b]
7	33.4 t	1.49[b]; 1.42[b]
8	40.4 s	-
9	47.8 d	1.72[b]
10	37.5 s	-
11	24.5 t	2.00; 1.93
12	122.8 d	5.32
13	146.3 s	-
14	42.7 s	-
15	26.9 t	2.49[b]; 1.09[b]
16	28.5 t	2.17 [b]; 1.43[b]
17	71.3 s	-
18	49.3 d	2.58
19	49.4 t	1.83[b]; 1.36[b]
20	31.7 s	-
21	37.6 t	1.41[b]; 1.31[b]
22	39.3 t	2.05; 1.71
23α	27.2 q	1.17 s
24β	22.2 q	1.05 s
25β	15.4 q	0.96 s
26β	18.2 q	1.22 s
27α	26.2 q	1.24 s
28	-	
29α	33.6 q	0.94 s
30β	24.7 q	0.99 s

a) Assignments were confirmed by 2D-COSY, HSQC, HMBC experiments.

b) Signal pattern was unclear due to overlapping.

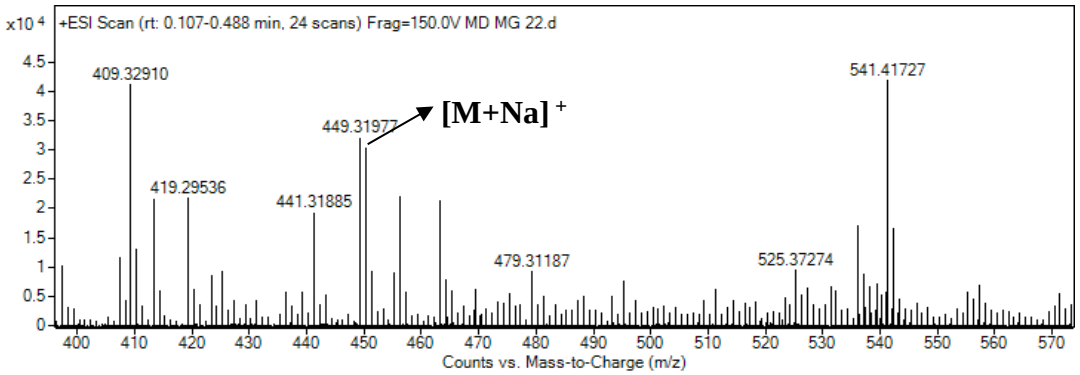

Spectrum 22. HR-ESI-MS spectrum of MD-MG-13 (positive mode)

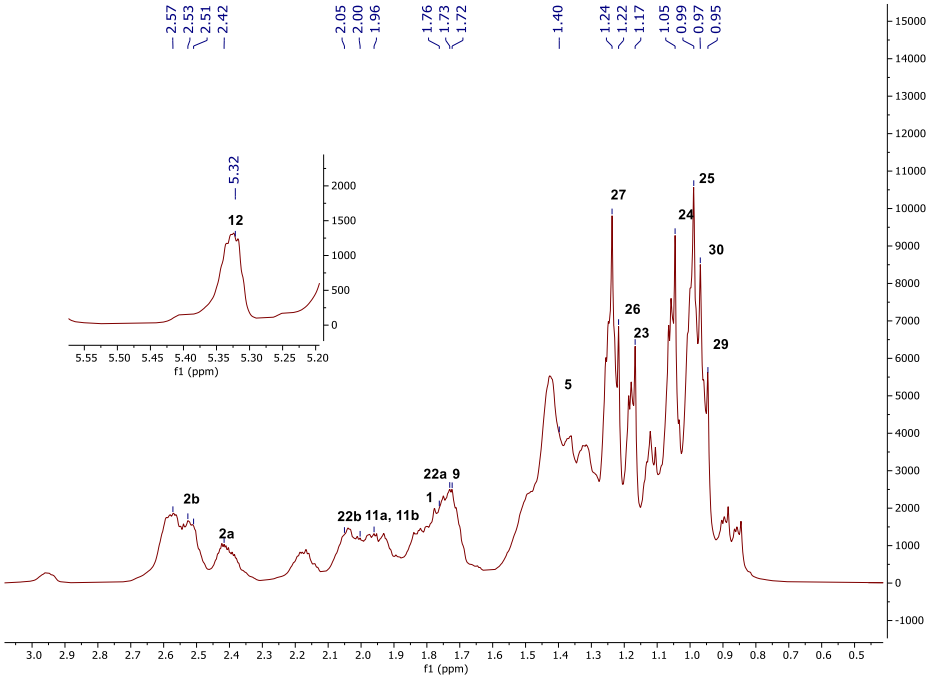

Spectrum 23. ^{1}H-NMR spectrum of MD-MG-13

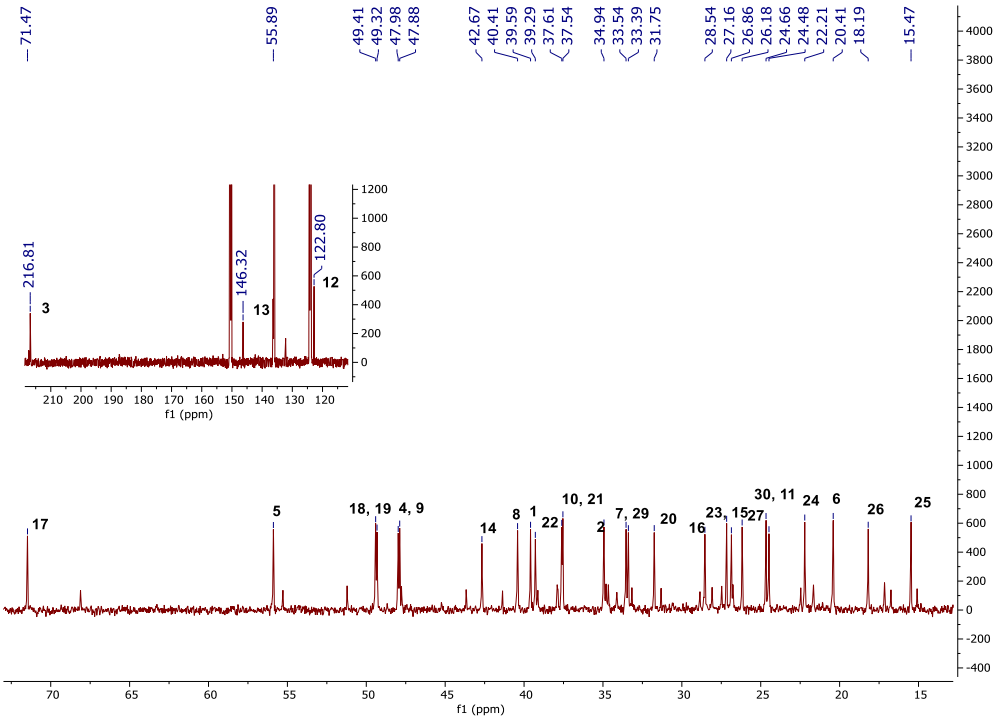

Spectrum 24. ^{13}C-NMR spectrum of MD-MG-13

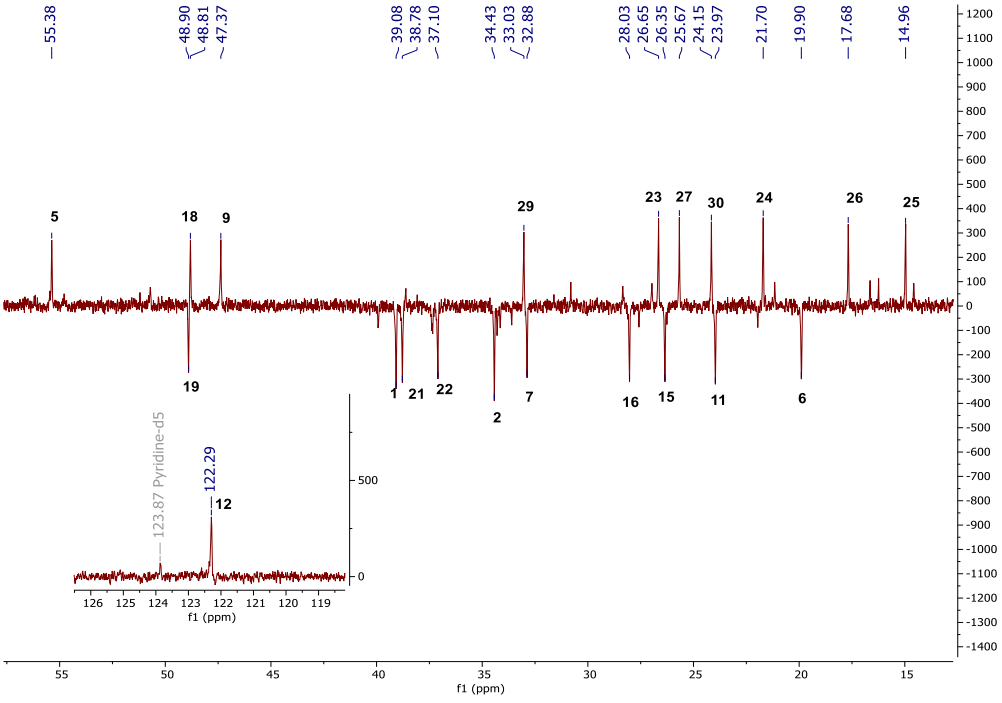

Spectrum 25. DEPT-135 spectrum of MD-MG-13

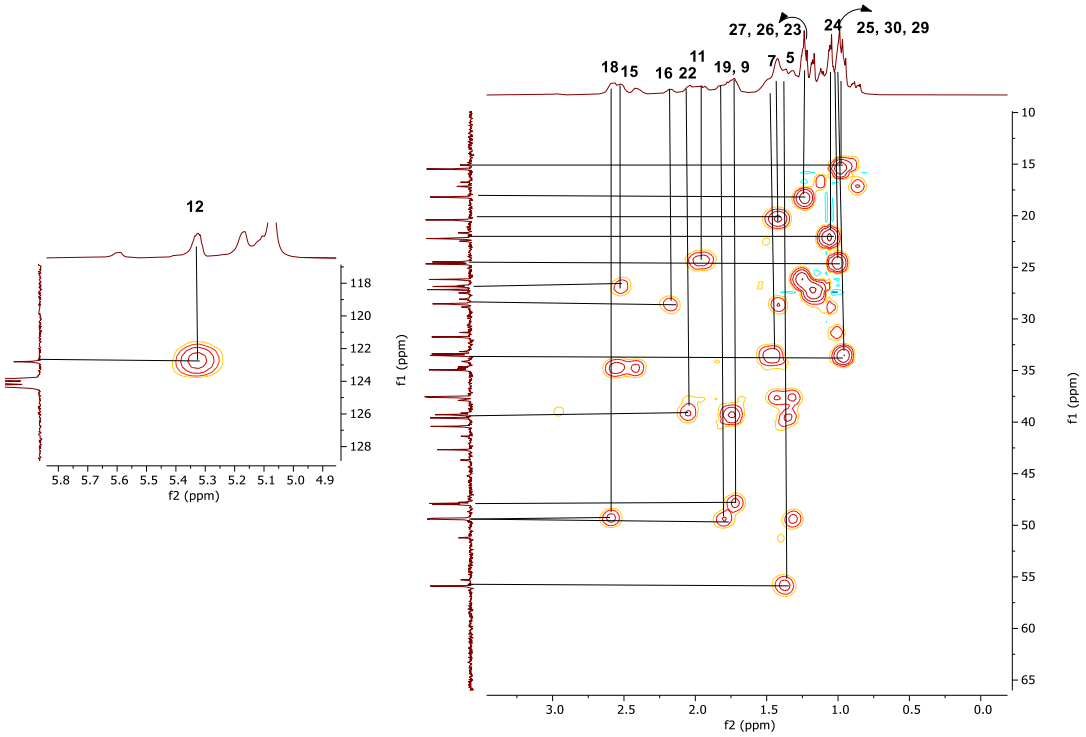

Spectrum 26. HSQC spectrum of MD-MG-13

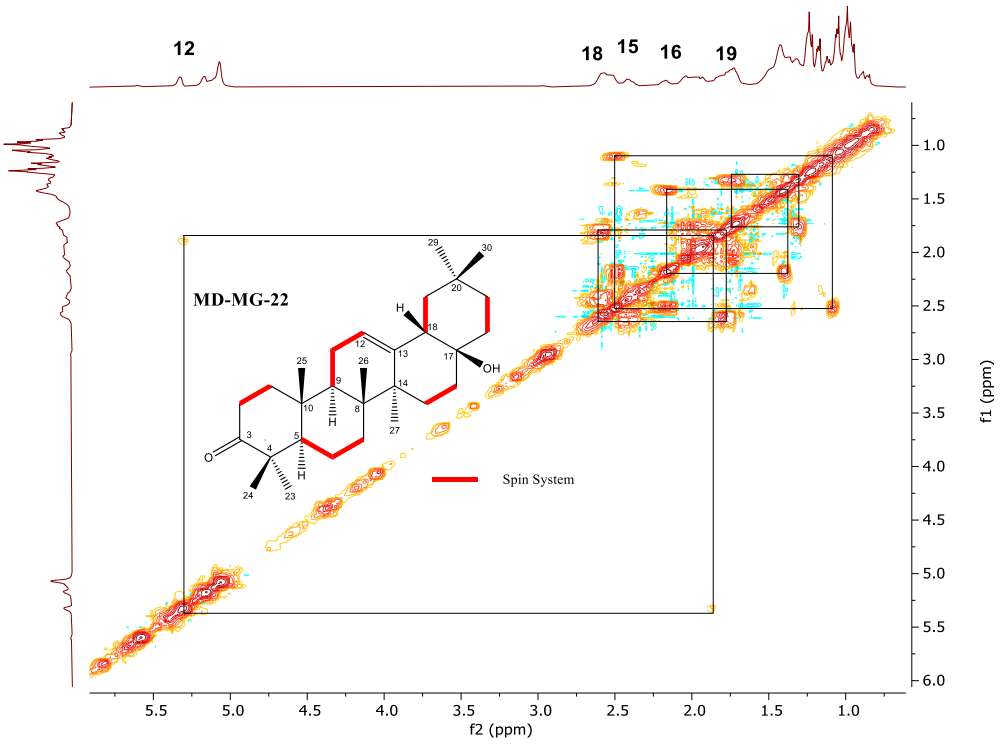

Spectrum 27. COSY spectrum of MD-MG-13

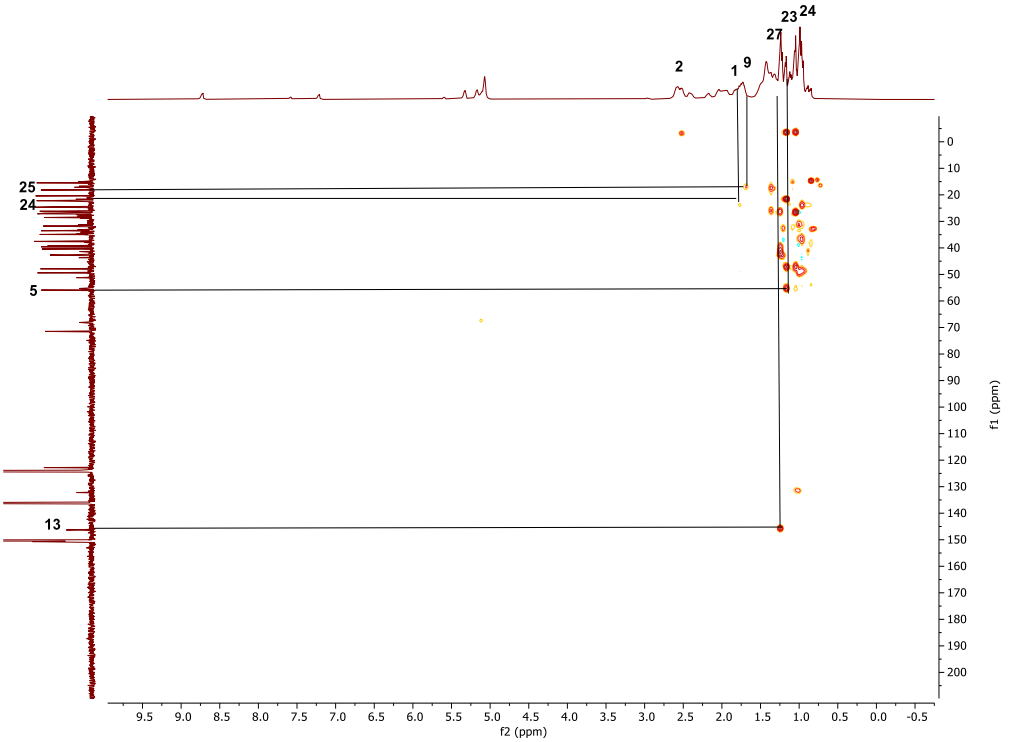

Spectrum 28. HMBC spectrum of MD-MG-13

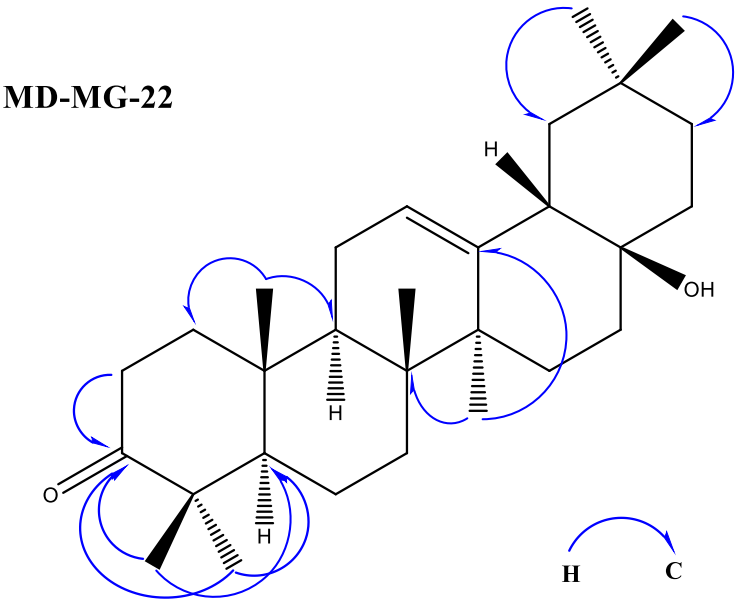

Figure 25. Key HMBC's of MD-MG-13, (MD-MG-22)

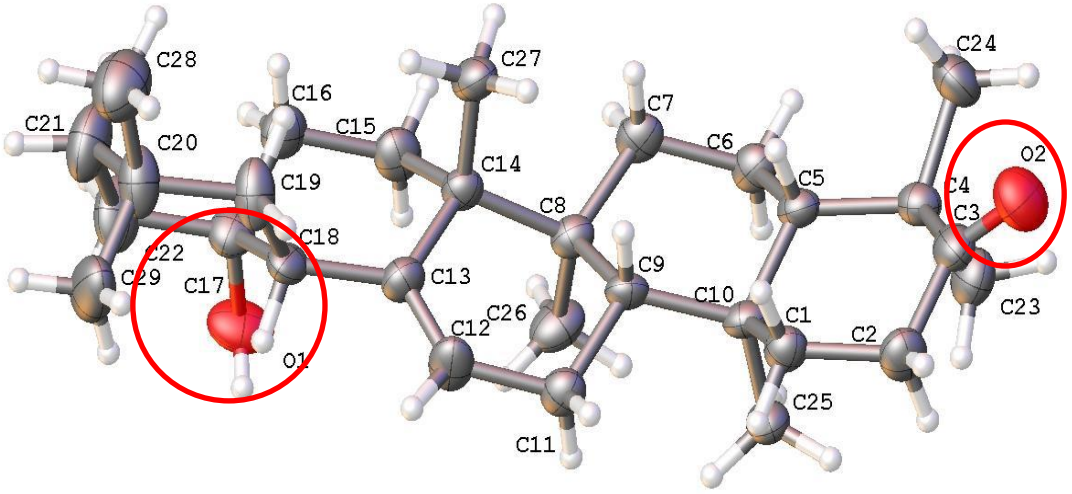

Figure 26. X-ray-derived structure of MD-MG-13

3.1.10. Structural elucidation of MD-MG-14

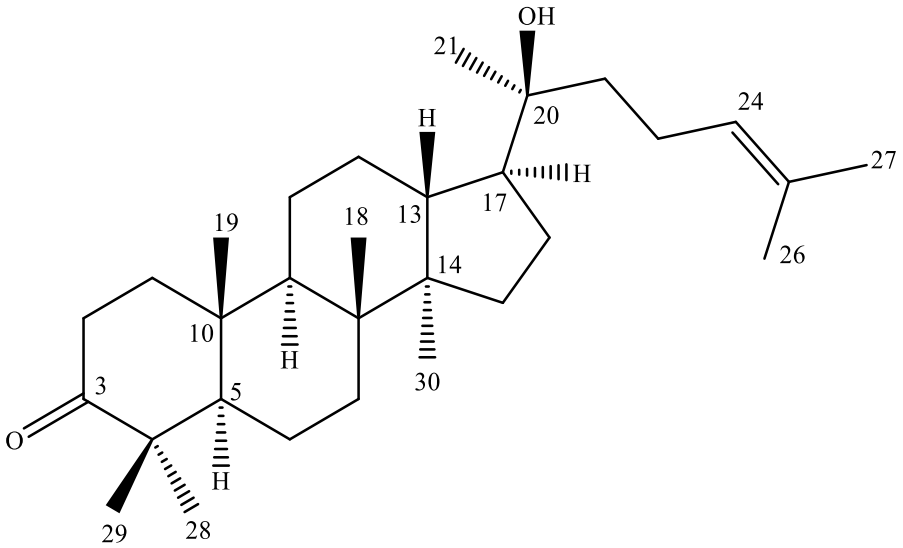

Figure 27. Chemical structure of MD-MG-14

MD-MG-14 was obtained as a colorless amorphous solid. The molecular formula of MD-MG-14 was defined as $C_{30}H_{52}O_2$ based on its HR-ESI-MS data (*m/z* 481.34399 $[M+K]^+$, calcd. 481.34479 for $C_{30}H_{52}O_2K$) (Spectrum 29). When the 1D- and 2D-NMR was compared with the MD-MG-12, a few differences were noticed (Table 12). Comparison of the ^{1}H-NMR data of MD-MG-14 with those of MD-MG-12 revealed the

lack of oxo-methine proton (H-3) whereas low field shifts for two protons, which were assigned to H_2-2 (Spectrum 30), were. In the ^{13}C-NMR spectrum, the appearance of a new carbonyl signal at δ 216.8 together with the absence of an oxo-methine carbon signal implied the oxidation of the secondary alcohol to a ketone (Spectrum 31). Hence, this inference was also corroborated by means of long-range correlations from H_3-28 (δ 1.15, s)/ H_3-29 (δ 1.06, s)/H_2-2 (δ 2.49, m, 2H)/δ 1.73 (one of the protons of H-1) to C-3 (δ 216.8, s) in the HMBC spectrum (Spectrum 79). Therefore, the ketone group was located at C-3. As a result, the structure of MD-MG-14 was identified as 20-hydroxy-24-dammarene-3-one (dipterocarpol), a known compound previously isolated from mastic gum.[19,73]

Table 12. ^{1}H and ^{13}C NMR spectroscopic data of MD-MG-14, [a)] (in C_5D_5N, ^{1}H: 500 MHz, ^{13}C: 125 MHz)

Position	**δ_C (ppm)**	**δ_H (ppm), (J in Hz)**
1	40.4 t	1.73[b)]; 1.29[b)]
2	34.8 t	2.49[b)]
3	216.8 s	-
4	47.9 s	-
5	55.8 d	1.37[b)]
6	20.4 t	1.48[b)]; 1.38[b)]
7	35.3 t	1.51[b)]; 1.24[b)]
8	41.0 s	-
9	50.9 d	1.43[b)]
10	37.4 s	-
11	22.8 t	1.41[b)]; 1.22[b)]
12	25.9 t	1.95[b)]; 1.88[b)]
13	43.0 d	1.97[b)]
14	51.1 s	-
15	32.1 t	1.60 m; 1.12[b]
16	28.5 t	2.32 m; 2.12 m
17	50.9 d	1.99[b)]
18	15.8 q	0.96 s
19	16.6 q	0.85 s
20	74.6 s	-
21	26.8 q	1.44 s
22	42.3 t	1.81[b)]
23	23.9 t	2.44[b)]; 2.37[b)]
24	126.5 d	5.36 dd (8.0, 7.5)

25	131.3 s	-
26	26.4 q	1.71 s
27	18.3 q	1.67 s
28	27.3 q	1.15 s
29	21.7 q	1.06 s
30	17.1 q	0.95 s
20-OH		5.28 s

a) Assignments were confirmed by 2D-COSY, HSQC, and HMBC experiments.

b) Signal pattern was unclear due to overlapping

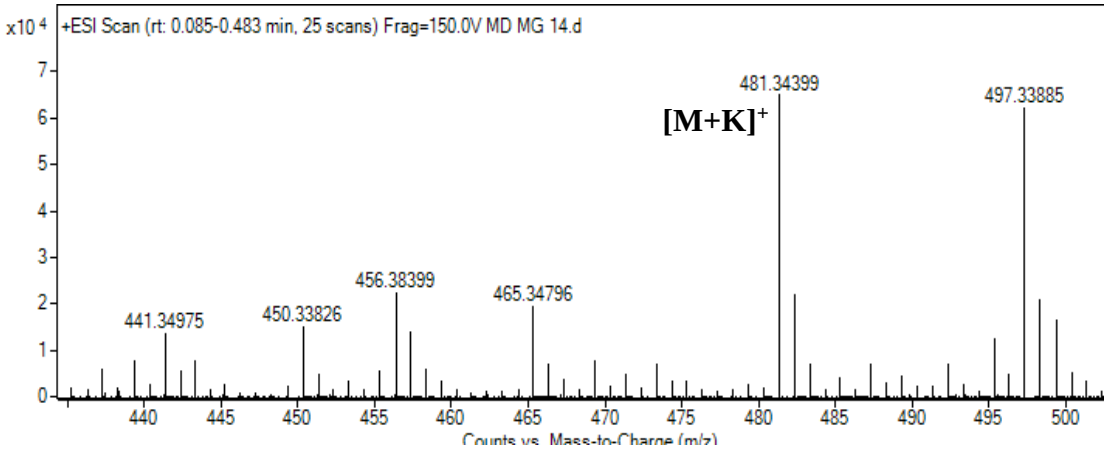

Spectrum 29. HR-ESI-MS spectrum of MD-MG-14 (positive mode)

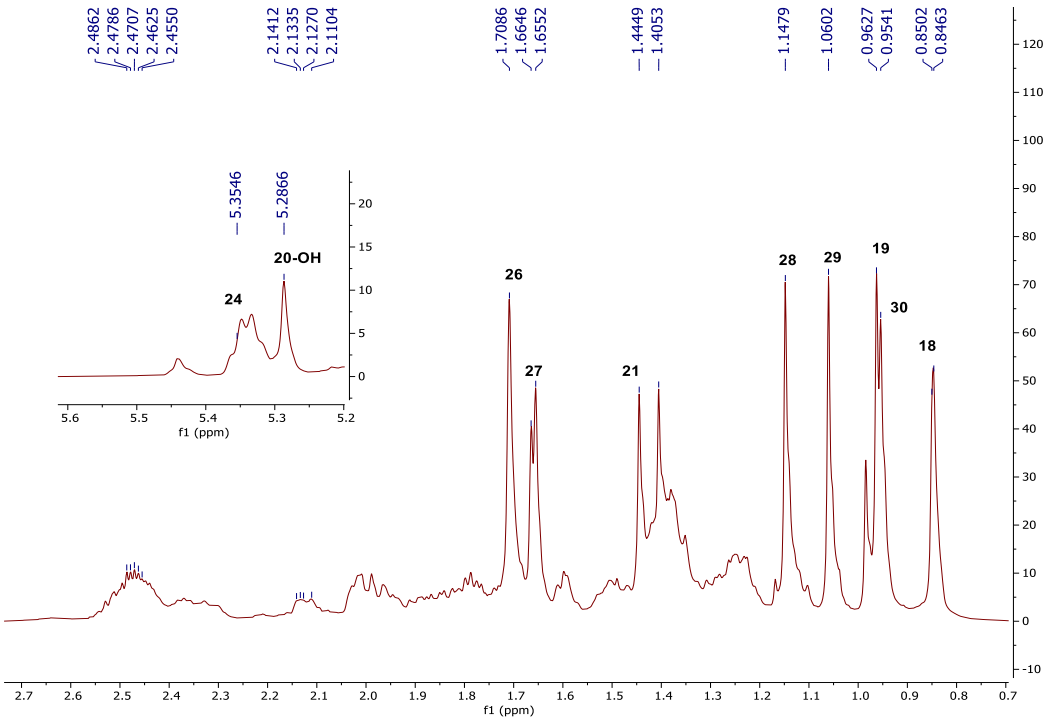

Spectrum 30. [1]H-NMR spectrum of MD-MG-14

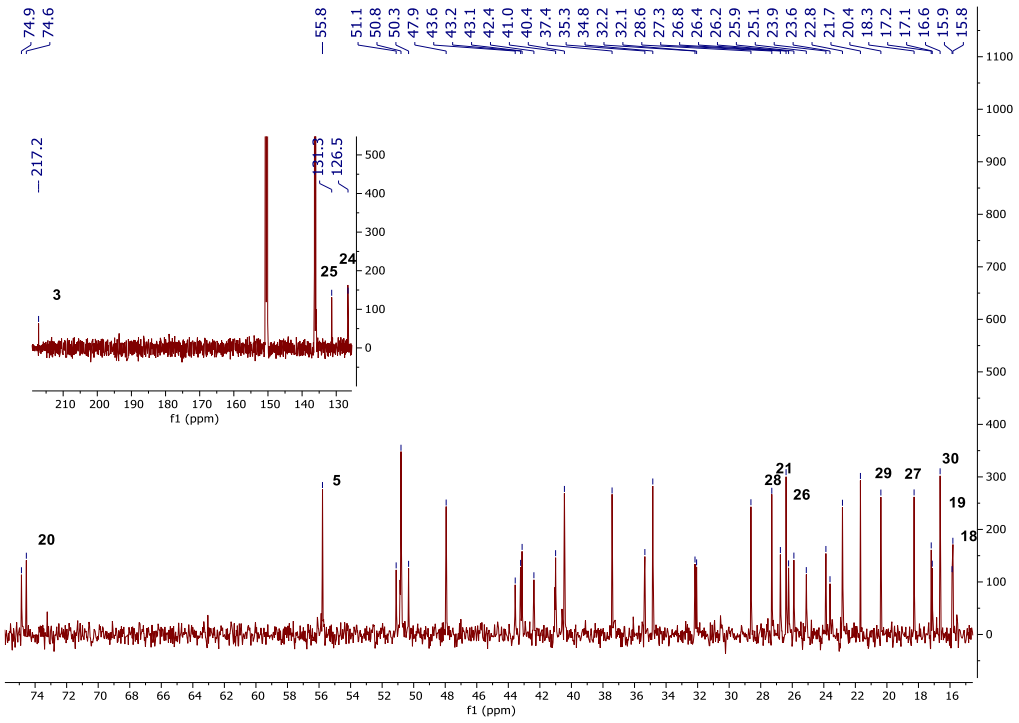

Spectrum 31. ^{13}C-NMR spectrum of MD-MG-14

3.1.11. Structural elucidation of MD-MG-17

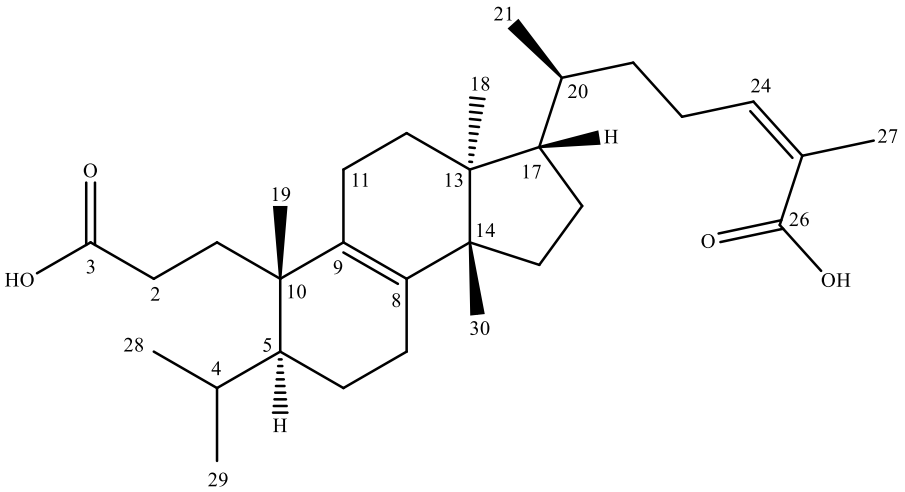

Figure 28. Chemical structure of MD-MG-17

MD-MG-17 gave a major ion peak at *m/z* 471.3473 $[M-H]^-$ in the HR-ESI-MS (negative mode), indicating a molecular formula of $C_{30}H_{48}O_4$ (calcd. 471.3474 for $C_{30}H_{47}O_4$) (Spectrum 32) with seven degrees of unsaturation.

The ^{1}H-NMR spectrum of MD-MG-17 showed signals for four tertiary methyl protons at δ 0.88, 0.91, 0.93 and 2.14 (each s, H_3-18, H_3-30, H_3-19 and H_3-27, respectively) and three secondary methyl groups at δ 0.80 (d J=6.8 Hz, H_3-28), at δ 0.96 (d J=6.8 Hz, H_3-29) and δ 1.01 (d J=6.0 Hz, H_3-21) (Spectrum 33). Also, an olefinic proton was observed at δ 6.06 (t J=7.0 Hz, H-24) which was correlating with a carbon at 143.2 ppm in the HSQC spectrum (Spectrum 36). Through interpreting the ^{13}C NMR and DEPT-135 spectra, the presence of two olefinic systems was evident (δ_C 129.2, s, C-25; δ_C 130.8, s, C-9; δ_C 139.0, s, C-8 and δ_C 143.2, d, C-24) (Spectra 34 and 35). Hence, the presence of a trisubstituted and tetrasubstituted olefinic system was deduced. Moreover, apart from these olefinic carbons, 26 carbon signals were classified as seven methyl, ten methylene, four methine and five non-protonated carbons including two carbonyl carbons (δ_C 171.2 and 177.2) (Table 13). Four out of the seven degrees of unsaturation were established based on the presence of two carbonyl and two double bond systems. The remaining hydrogen deficiency index suggested a tricyclic skeleton.

The tricyclic system was successfully established via interpretation of the 2D NMR spectra. The combined use of COSY, TOCSY and HSQC spectra allowed the assignment of four major spin systems. The first spin system was traced from H_2-15 protons (δ_H 1.57, m and 1.27, m) [H_2-15/H_2-16 (δ_H 2.01, m and 1.38, m)/H-17 (δ_H 1.57, m)/H-20 (δ_H 1.53, m)/H_3-21 (δ_H 1.01, d, J=6.0 Hz)/H_2-22 (δ_H 1.68 and 1.27, m)/H_2-23 (δ_H 2.87 and 2.76, m)] to the olefinic resonance at δ 6.06. Additionally, $^{3}J_{H\text{-}C}$ correlations from the latter aromatic proton to a carboxyl carbon (δ_C 171.2, s, C-26) and one allylic methyl (δ_H 2.14, s, H_3-27) were apparent in the HMBC spectrum, indicating that the side chain of MD-MG-17 was identical to those of MD-MG-03 and MD-MG-04. Moreover, the HMBC correlations from H-27 to C-24/C-25/C-26 and H_3-21 to C-17/C-20/C-22 substantiated the side chain framework extending from C-17. The configuration of $\Delta^{24(25)}$ double bond was assigned as "Z" via the NOESY correlation between H-24 and H-27.

The second spin system commenced with a methine proton (δ_H 1.96, m) coupling with two methyl groups (H_3-28: δ_H 0.80, d, J=6.8 Hz; C-28: δ 19.5 q, H_3-29: δ_H 0.96, d, J=6.8 Hz; C-29: δ 25.0 q) and a methine proton (δ_H 1.38, m, C-5: δ 44.8 d). The latter showed a cross peak with a methylene system (H_2-6: δ_H 1.49 and 1.26, each m; C-6: δ 20.0 t), which, in turn, coupled with another methylene group protons (H_2-7: δ_H 1.97 and 1.80, each m; C-7: δ 28.0 t). Consecutively, the third spin system could be traced between the resonances of two methylene groups: (δ_H 2.09 (H_2-11) and δ_H 1.70 (H_2-12); C-2: δ

31.5 t). The fourth spin system also involved two methylene groups coupling with each other: δ_H 2.12 and 2.02 (H_2-1, each m) → δ_H 2.54 (ddd, J= 16.7, 10.7 and 6.4 Hz) and 2.30 (ddd, J= 15.6, 10.7 and 4.7 Hz) (H_2-2). The low-field shift of the latter methylene group implied that it was in proximity of an electron withdrawing group. Indeed, the carboxyl group at δ 177.2 correlated with δ 2.51 and 2.30 signals in the HMBC spectrum. Based on the abovementioned findings including an isopropyl group (C-4, C-28 and C-29) and propanoic acid (C-1 → C-3), it was suggested that a cleavage reaction in the A-ring of MD-MG-17 took place via Norrish I pathway[74], resulting in a 3,4-seco triterpenoid.

By detailed inspection of the HMBC spectrum non-protonated carbons and methyl groups were connected with the spin systems mentioned above, providing fully established tricyclic skeleton and seco framework [i.e. from H_3-19 (δ 0.93) to C-1 (δc 32.4), C-5 (δc 44.8), C-9 (δc 130.8) and C-10 (δc 42.3); from H_3-18 (δ_H 0.88) to C-12 (δ_C 31.7), C-13 (δ_C 44.7), C-14 (δc 51.7) and C-17 (δ_C 51.0); from H-30 (δ_H 0.91) to C-8 (δ_C 139.0), C-13 (δ_C 44.7), C-14 (δ_C 51.7) and C-15 (δ_C 30.5)] (Figure 29). Additionally, the proton resonances assigned to H_3-28 and H_3-29 displayed cross peaks with C-4 and C5, whereas H-4 correlated with C-5 (δ_C 44.8), C-6 (δ_C 20.0), and C-10 (δ_C 42.3), verifying that the isopropyl unit was extending from C-5. Also, the low field shift of the methylene signals belonging to H_2-11 and H_2-7 together with the long-distance correlations from C-8 (δ_C 130.8) to H_3-30 and from C-9 (δ_C 139.0) to H_3-19 verified the position of the tetrasubstituted double bond system at C-8(C-9).

After establishing the 2D structure of MD-MG-17, the complete structural elucidation required assessment of the stereochemistry. Both lanostane and tirucallane skeletons had same two-dimensional constitution, the differences lie between the configurations at C-13 (δ_C 44.7), C-14 (δ_C 51.7). C-17 (δ_C 51.0) and C-20 (δ_C 37.3). The 2D-NOESY or 2D-ROESY data was not informative to deduce the abovementioned configurations (Spectrum 81-82). Moreover, the reported proton and carbon data for similar lanostane and tirucallane derivatives were not helpful to deduce the stereochemistry. However, based on biogenetic understanding, as no lanostane-type triterpenoid has been reported from mastic gum, we are in favour of a tirucallane skeleton. Further studies including derivatization, CD and/or X-ray diffraction are required to fully elucidate the structure of MD-MG-17.

Consequently, MD-MG-17 was identified as 3,4-seco-tirucalla-8,24-dien,3,26-dioic acid. For this compound we propose the trivial name of 3,4-seco isomasticadienonic acid. This compound thus represented the first 3,4-seco structure isolated from the mastic gum.

Table 13. ^{1}H and ^{13}C NMR spectroscopic data of MD-MG-17, [a] (in C_5D_5N, ^{1}H: 500 MHz, ^{13}C: 125 MHz)

Position	δ_C (ppm)	δ_H (ppm), (J in Hz)
1	32.4 t	2.12[b]; 2.02[b]
2	31.5 t	2.54 ddd (16.7, 10.7, 6.4); 2.30 ddd (15.6, 10.7, 4.7)
3	177.2 s	-
4	26.2 d	1.96[b]
5	44.8 d	1.40[b]
6	20.0 t	1.49[b]; 1.26[b]
7	28.0 t	1.80[b]; 0.99[b]
8	130.8 s	-
9	139.0 s	-
10	42.3 s	-
11	28.8 t	2.01[b]; 1.38[b]
12	31.7 t	1.70[b]; 1.24[b]
13	44.7 s	-
14	51.7 s	-
15	30.5 t	1.58[b]; 1.28[b]
16	22.7 t	1.99[b]
17	51.0 d	1.57[b]
18	17.0 q	0.88 s
19	25.4 q	0.91 s
20	37.3 d	1.50[b]
21	19.3 q	1.01 d (6.4)
22	36.9 t	1.69[b]; 1.25[b]
23	27.5 t	2.89 m; 2.77 m
24	143.2 d	6.06 dd (7.0, 6.7)
25	129.2 s	-
26	171.2 s	-
27	22.1 q	2.15 s
28	19.5 q	0.81 d (6.6)
29	25.0 q	0.81 d (6.6)
30	23.7 q	0.94 s

a) Assignments were confirmed by 2D-COSY, HSQC,HMBC and NOESY experiments.

b) Signal pattern was unclear due to overlapping.

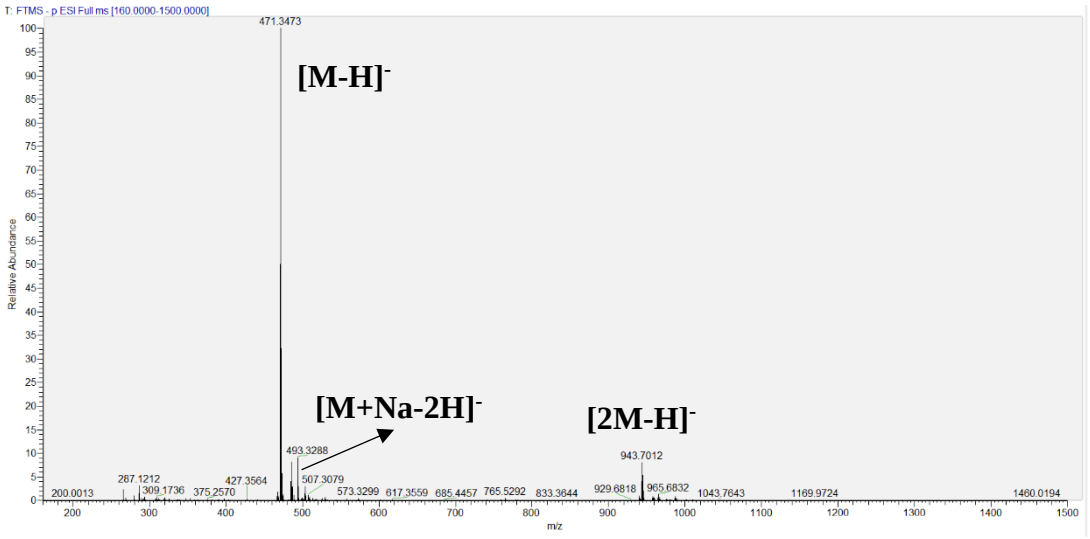

Spectrum 32. HR-ESI-MS spectrum of MD-MG-17 (negative mode)

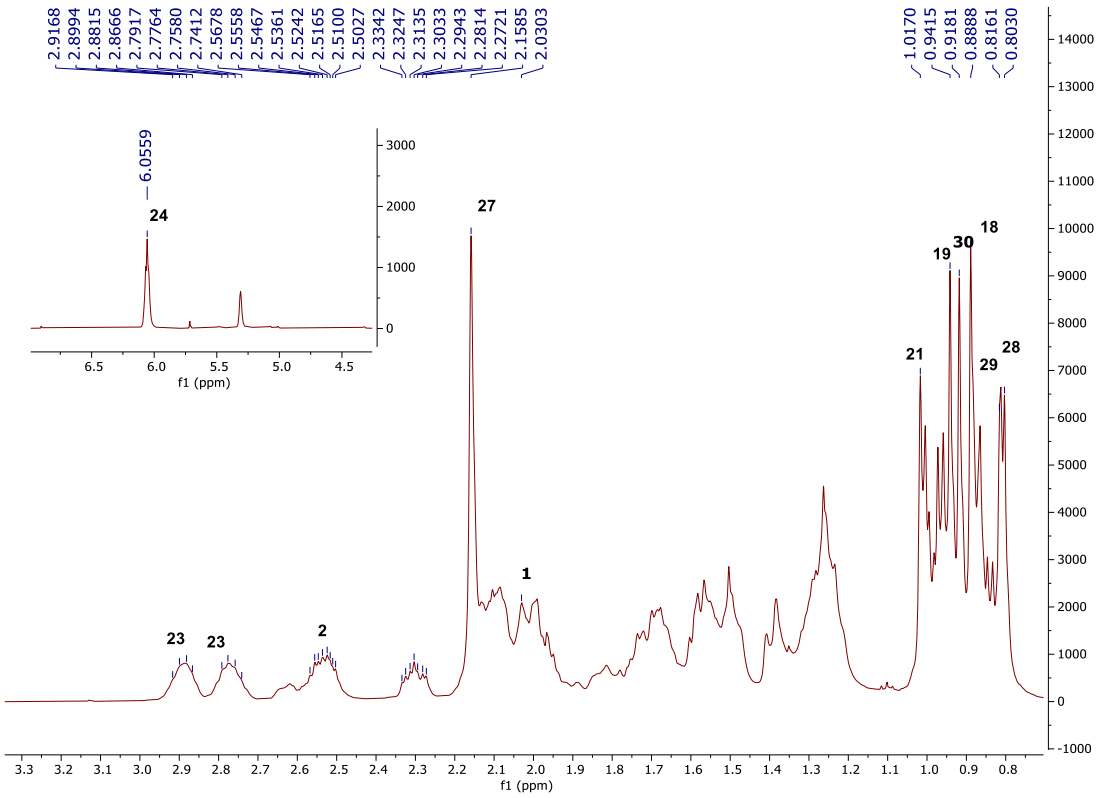

Spectrum 33. ^{1}H-NMR spectrum of MD-MG-17

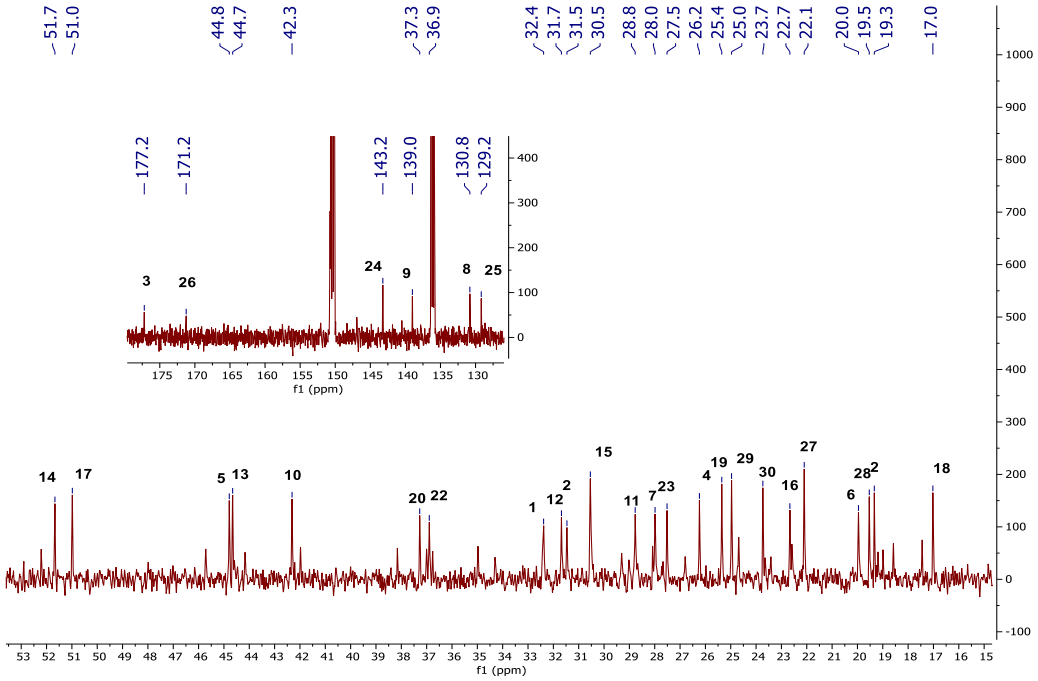

Spectrum 34. ^{13}C-NMR spectrum of MD-MG-17

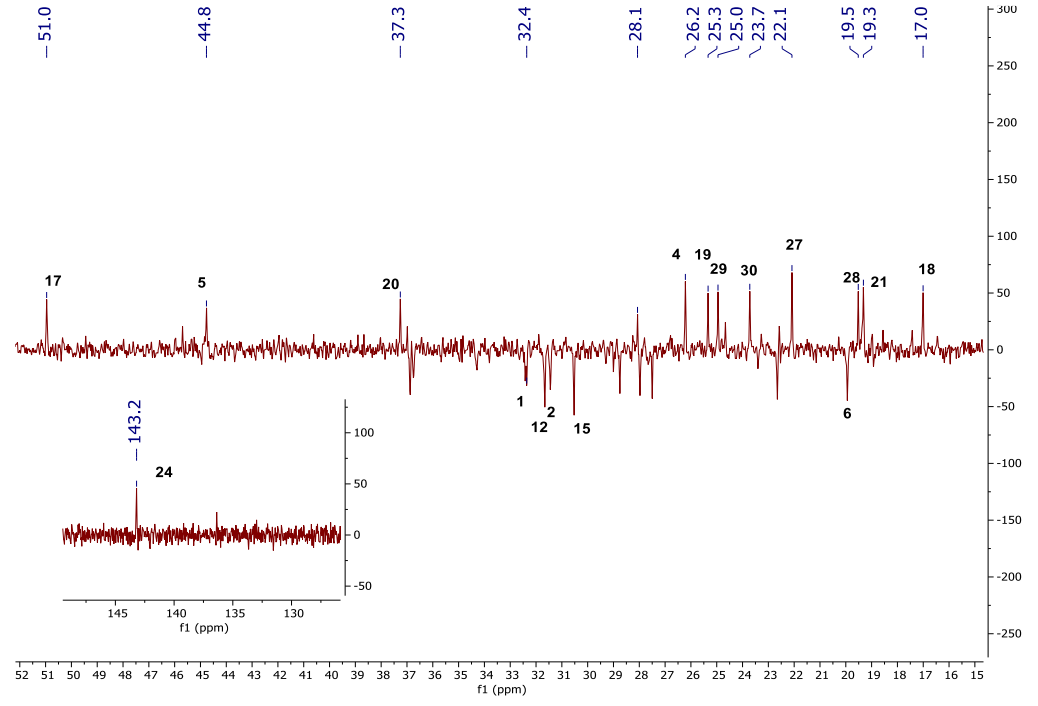

Spectrum 35. DEPT-135 spectrum of MD-MG-17

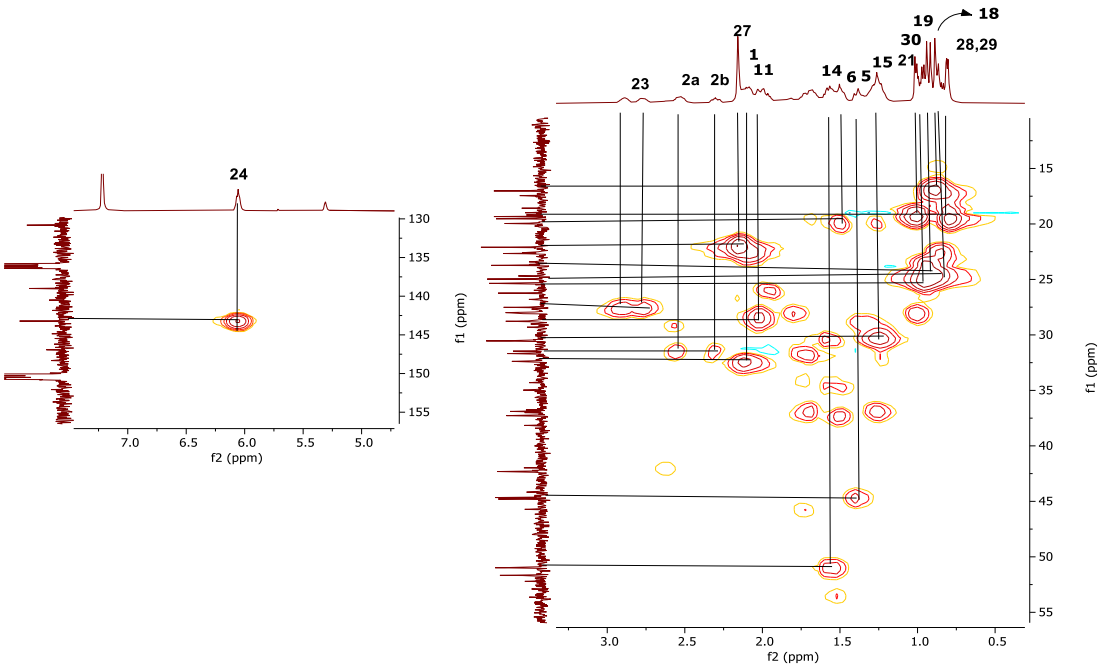

Spectrum 36. HSQC spectrum of MD-MG-17

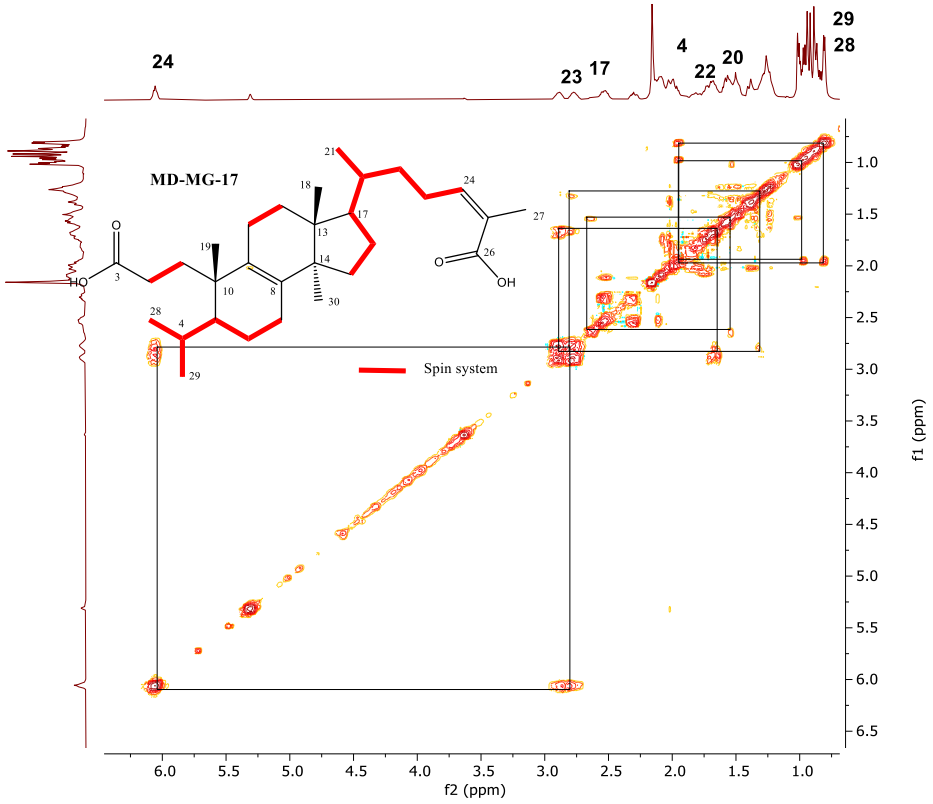

Spectrum 37. COSY spectrum of MD-MG-17

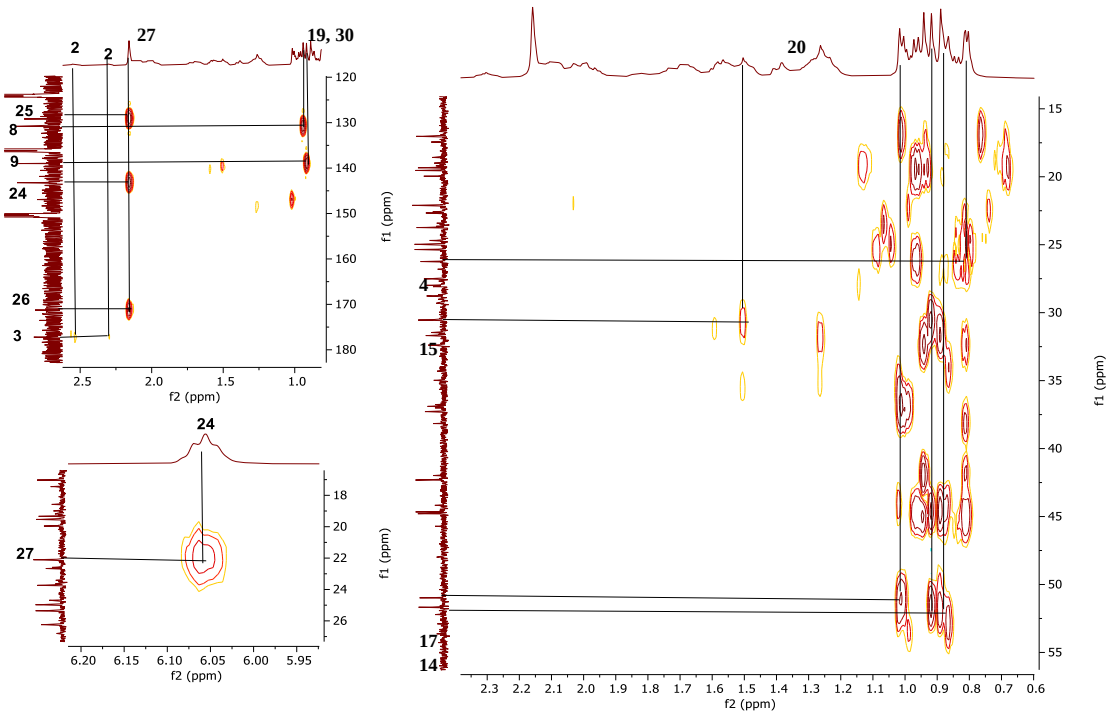

Spectrum 38. HMBC spectrum of MD-MG-17

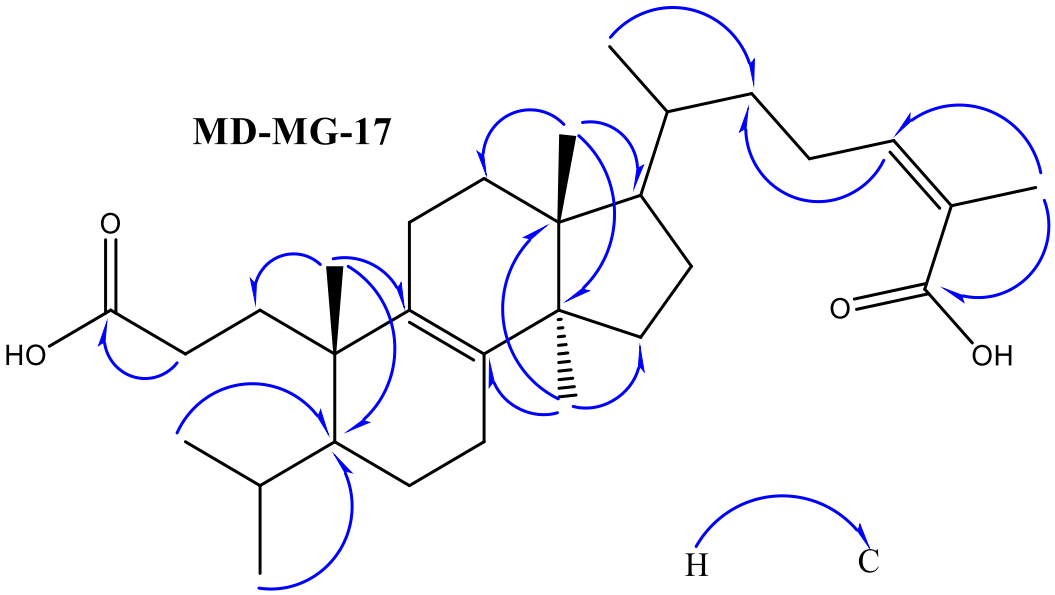

Figure 29. Key HMBC's of MD-MG-17

3.1.12. Structural Elucidation of MD-MG-19

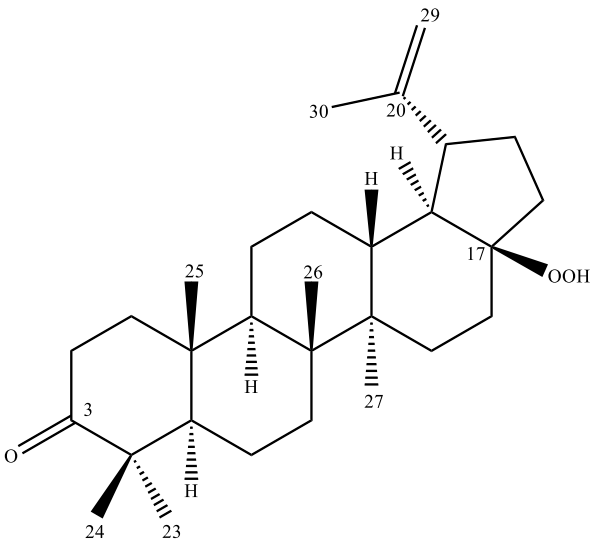

Figure 30. Chemical structure of MD-MG-19

The ESI-MS spectrum of MD-MG-19 demonstrated an ion peak for $[M+C_3H_7OH+Na+H]^+$ at m/z 509.39310 (calcd. 509.39707 for $C_{32}H_{54}NaO_3^-$), which is correspond to the molecular formula of $C_{29}H_{45}O_2^-$ (Spectrum 39). There was a hydrogen deficiency index seven in compound based on the MS data.

The detailed inspection of ^{1}H-NMR spectrum of MD-MG-19 revealed five tertiary and one allylic methyl signal at δ 0.82, 1.02, 1.03, 1.04, 1.15 and 1.77 (each s; respectively H_3-25, H_3-27, H_3-26, H_3-23, H_3-24, and H_3-30) (Spectrum 40). Also, it was easily notice one proton at δ 2.99 dt (J=11.0, 5.2, H-19), correlating a methine carbon at δ 49.3 (C-19) in HSQC spectrum (Spectrum 81). Moreover, two olefinic protons were apparent at δ 4.90 d (J=7.4 Hz, H_2-29) and 4.77 d (J=7.4 Hz, H_2-29) that are correlated with the same carbon at δ 110.7 (t, C-29). As two olefinic carbon resonances were noted at δ 110.7, d and δ 151.3, s via the inspection of ^{13}C-NMR and DEPT-135 spectra, it was obvious that an exocyclic methylene containing double bond system was present in the skeleton (Spectrum 41-80). The presence of this system was confirmed based on long-range correlations from H_3-30 to C-19/C-20/C-29; from H_2-29 to C-19/C-30 and from H-19 to C-18/C-20/C-29/C-30.

The ^{13}C-NMR and DEPT-135 spectra of MD-MG-19 showed 29 signals containing six methyl, eleven methylene, five methine and seven non-protonated carbons involving one ketone (δ 217.2) group. Two out of hydrogen deficiency index of seven

were regarded as a carbonyl carbon and a double bond system containing exocyclic methylene which indicated the presence of lupane-type triterpenoid framework. Major spin systems were traced from H_1-2 to H_2-2, from H-5 to H_2-6 which showed cross-peak with H_2-7 as well as starting from H-9 to H_2-22 including H_2-11/H_2-12/H-13/ H-18/H-19/H_2-21 together with from H_2-15 to H_2-16 in the COSY spectrum (Spectrum 82). These spin systems were connected via long range correlations in HMBC spectrum. When HMBC correlations was determined, it was seen that H_2-2 (δ 2.50, m) was correlated to the ketone group whereas H_3-23 (δ 1.04, s) and H_3-24 (δ 1.15, s) showed strong interactions with the ketone groups. Hence, the ketone group was located at C-3 (Spectrum 83).

When comparing with identified molecule betulin[75], the shifting of C-17 resonances toward lower field (ca. +43.1 ppm) and the lack of primary alcohol proton (δ 3.79 (1H, d, J =10.8, H-28b), 3.33 (1H, d, J = 10.8, H-28a)) and carbon signals (δ 60.6, t, C-28) in the ^{1}H- and ^{13}C-NMR spectra suggested the presence of 28-nor structure (Table 14). The non-protonated carbon at δ 90.8 was apparent in ^{13}C-NMR and DEPT-135. After the literature search, this chemical shift value was encountered at the substitution of *β*-hydroperoxide at C-17 position although +2 ppm shifting was observed at the substitution of α-hydroperoxide.[75] Therefore, the presence of the substitution of *β*-hydroperoxide was thought at C-17 based on the chemical shift value of C-17. However, the existence of superoxide ion rather than hydroperoxide was indicated by MS data. In fact, hydroperoxide was a good leaving group but in MS analysis, the cleavage of hydroperoxide to superoxide ion could be occurred to obtain an ionic compound.

As a result, MD-MG-19 was identified as 28-norlup-20(29)-en-3-one-17β-hydroperoxide.[75]

Table 14. ^{1}H and ^{13}C NMR spectroscopic data of MD-MG-19, [a] (in C_5D_5N, ^{1}H: 500 MHz, ^{13}C: 125 MHz)

Position	**δ_C (ppm)**	**δ_H (ppm), (J in Hz)**
1	40.3 t	1.77[b]; 1.34[b]
2	34.8 t	2.50[b]
3	217.2 s	-
4	47.8 s	-
5	55.3 d	1.34[b]
6	20.4 t	1.35[b]
7	34.5 t	1.39[b]
8	41.5 s	-
9	50.6 d	1.37[b]

10	37.5 s	-
11	22.2 t	1.31[b]; 1.17[b]
12	26.2 t	1.81[b]; 1.07[b]
13	37.5 d	2.22[b]
14	42.9 s	-
15	27.9 t	2.16[b], 1.10[b]
16	28.5 t	2.67[b]; 1.48[b]
17	90.8 s	-
18	49.9 d	1.82[b]
19	49.3 d	2.99 tq (11.0,6.2)
20	151.3 s	-
21	30.7 t	2.25[b]; 1.51[b]
22	33.4 t	2.65[b]; 1.41[b]
23	21.7 q	1.04 s
24	27.3 q	1.15 s
25	16.1 q	0.82 s
26	16.1 q	1.03 s
27	14.2 q	1.02 s
28	-	
29	110.7 t	4.90 d (7.4); 4.77 d (7.4)
30	19.7 q	1.77 s

a) Assignments were confirmed by 2D-COSY, HSQC, and HMBC experiments.

b) Signal pattern was unclear due to overlapping.

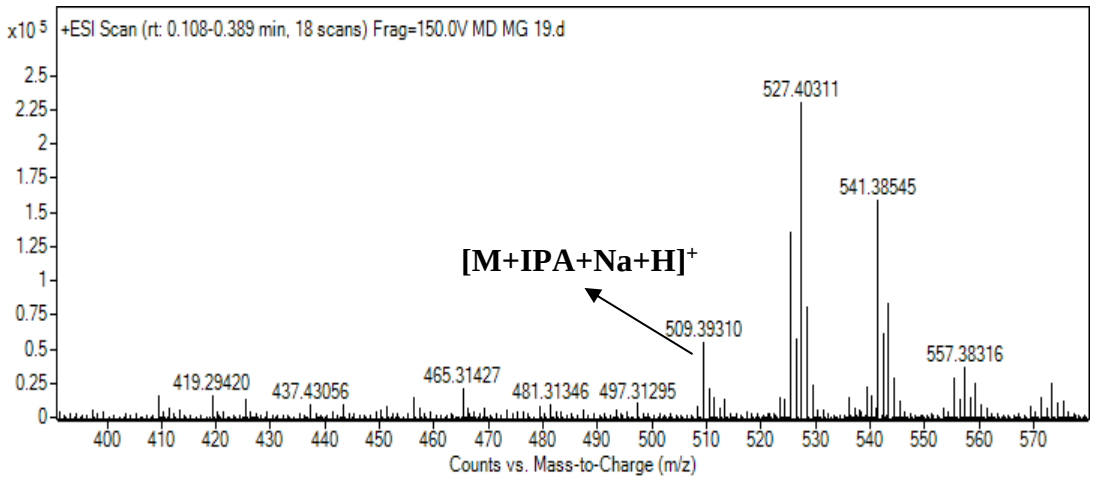

Spectrum 39. HR-ESI-MS spectrum of MD-MG-19 (positive mode).

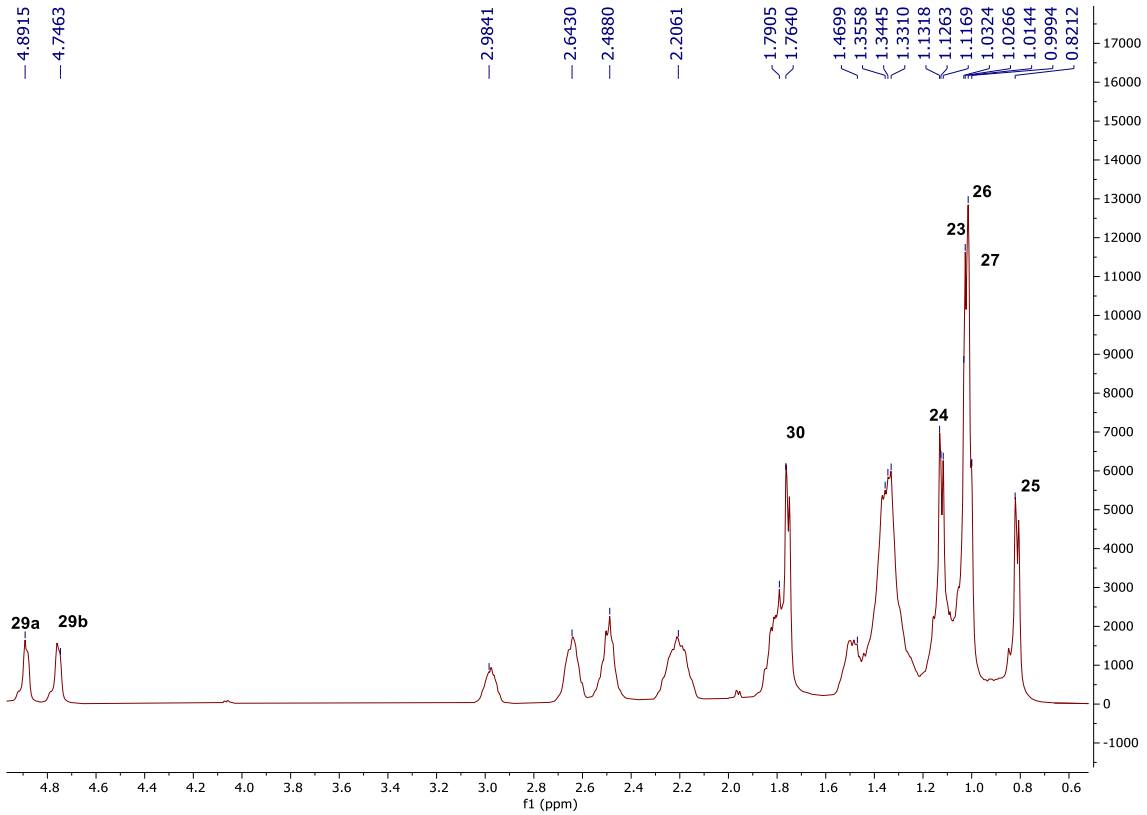

Spectrum 40. ^{1}H-NMR spectrum of MD-MG-19

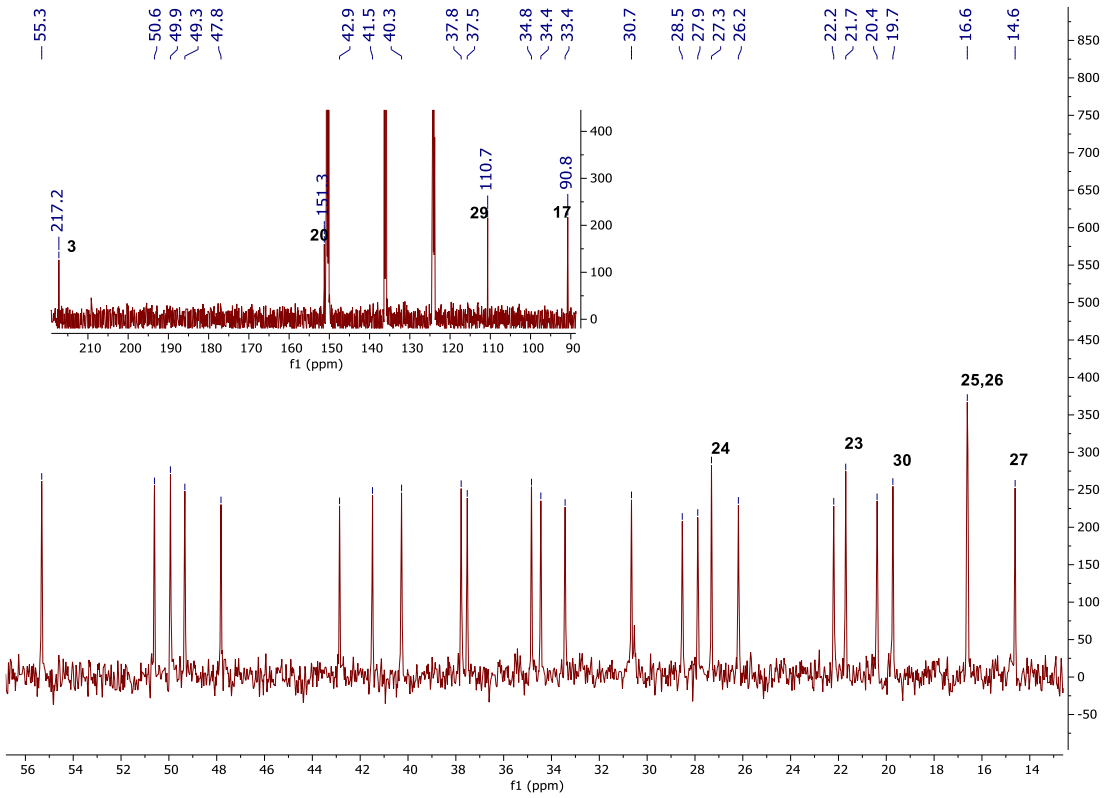

Spectrum 41. ^{13}C-NMR spectrum of MD-MG-19

3.1.13. Structural elucidation of MD-MG-24

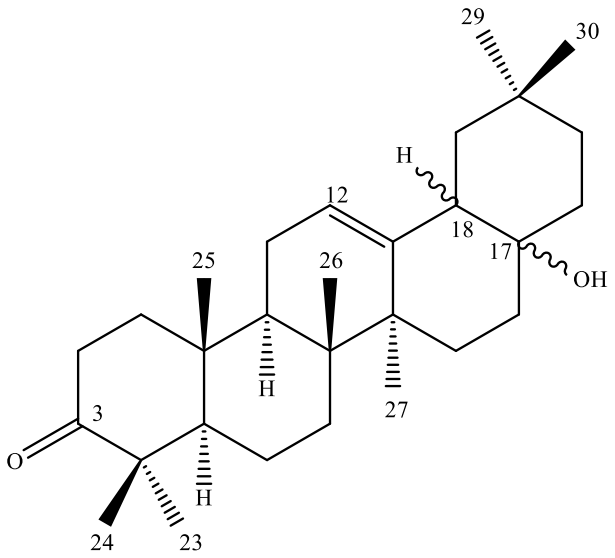

Figure 31. Chemical structure of MD-MG-24

The molecular formula of MD-MG-24 was described as $C_{29}H_{46}O_2$ relying on its ESI-MS data (*m/z* 449.32041 $[M+Na]^+$, calcd. 449.33955 for $C_{30}H_{52}NaO_2$) (Spectrum 42). When the 1D- and 2D-NMR was compared with the MD-MG-13, a few differences was obviously deduced whereas both were similar for the spectroscopic data of ring A, B and C.

Comparison of the ^{1}H-NMR data of MD-MG-24 with those of MD-MG-13 revealed the shifting of H-18 (δ 2.38) toward the higher field (ca. -0.2 ppm) (Spectrum 43) while the olefinic carbons (δ 118.7 and δ 142.6) was resonated with the higher energy resulted in appearance of their signals in the higher field in the ^{13}C-NMR spectrum (ca. -4 ppm) (Spectrum 44). Additionally, the resonances belonging to adjacent protons or carbons of C-17 and C-18 at junction point of ring D and E shifted either lower field or higher field. This fact proposed that the absolute stereochemistry of C-17 and H-18 could be different compared with MD-MG-13.

Table 15. ^{1}H and ^{13}C NMR spectroscopic data of MD-MG-24, a) (in C_5D_5N, ^{1}H: 500 MHz, ^{13}C: 125 MHz)

Position	δ_C (ppm)	δ_H (ppm), (J in Hz)
1	39.9 t	1.81[b]; 1.40 [b]
2	34.7 t	2.52 [b]
3	216.9 s	-
4	47.6 s	-
5	55.4 d	1.40[b]
6	20.2 t	1.38[b]
7	34.4 t	1.53[b]
8	40.0 s	-
9	47.1 d	1.55[b]
10	37.0 s	-
11	24.2 t	2.00[b]; 1.91[b]
12	118.7 d	5.42 d (5.5)
13	142.6 s	-
14	44.2 s	-
15	26.8 t	2.45[b]; 1.17[b]
16	37.2 t	1.74[b]
17	70.5 s	-
18	40.8 d	2.38 dd (12.4, 2.8)
19	38.2 t	1.75[b]; 1.39[b]
20	31.4 s	-
21	34.6 t	1.97[b]; 1.22[b]
22	36.9 t	1.74[b]
23	27.3 q	1.17 s
24	22.0 q	1.07 s
25	16.0 q	0.97 s
26	18.5 q	1.14 s
27	22.8 q	1.20 s
28	-	
29	34.2 q	1.04 s
30	25.1 q	1.01 s

a) Assignments were confirmed by 2D-COSY, HSQC and HMBC experiments.
b) Signal pattern was unclear due to overlapping.

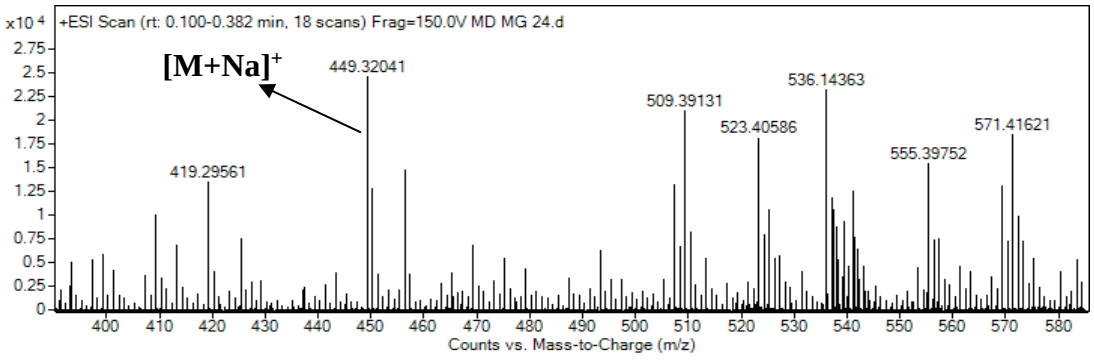

Spectrum 42. HR-ESI-MS spectrum of MD-MG-24 (positive mode)

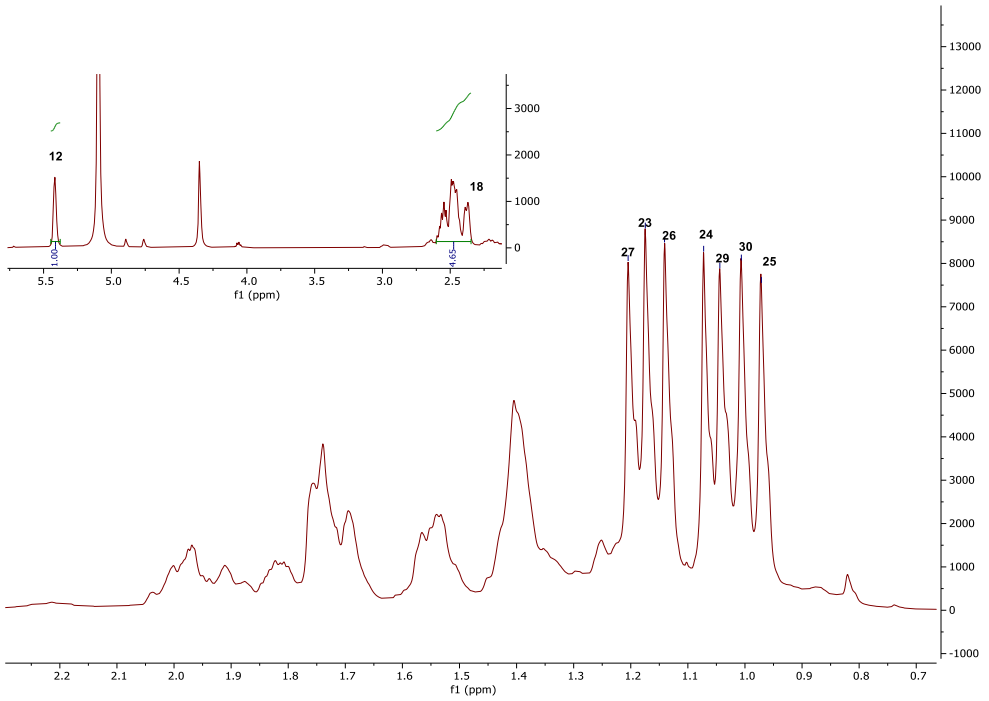

Spectrum 43. ^{1}H-NMR spectrum of MD-MG-24

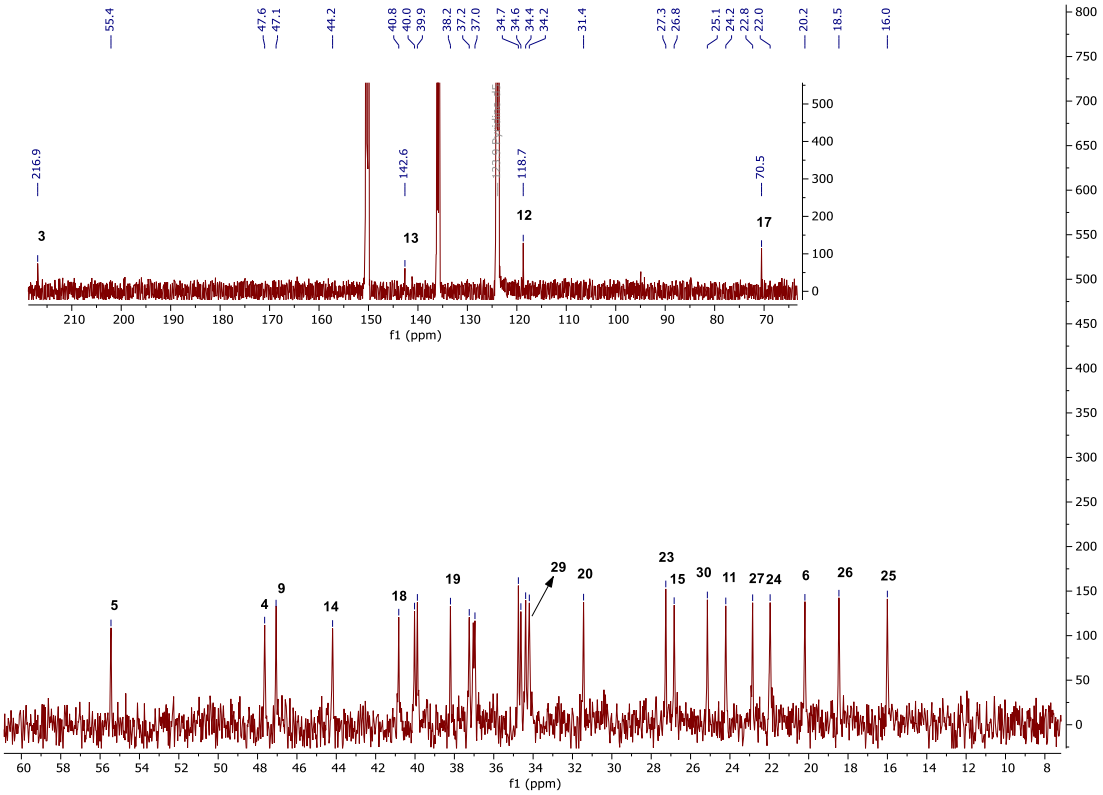

Spectrum 44. ^{13}C-NMR spectrum of MD-MG-24

3.1.14. Structural Elucidation of MD-MG-25

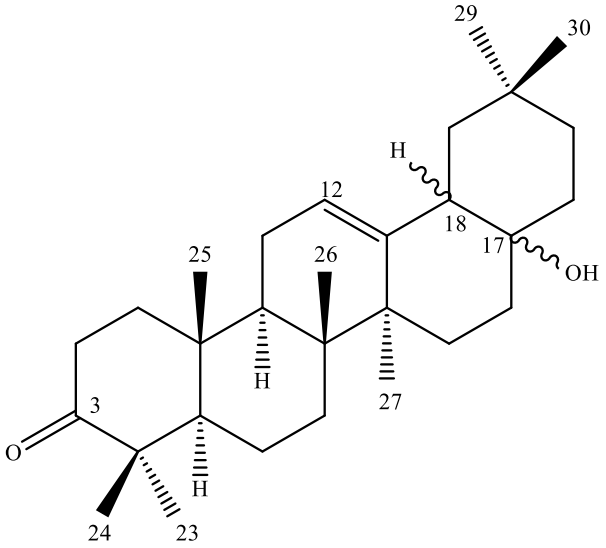

Figure 32. Chemical structure of MD-MG-25

ESI-MS spectrum gave a major peak at *m/z* 505.30572 $[M+Br]^-$, calcd. 505.26812 for $C_{29}H_{46}BrO_2$), suggesting the molecular formula of MD-MG-25 as $C_{29}H_{46}O_2$ (Spectrum 45). Also, the comparison of 1D- and 2D-NMR spectra between MD-MG-25 and MD-MG-13 revealed a few differences on spectroscopic data at junction point of ring D and E.

Comparison of the ^{1}H-NMR data of MD-MG-25 with those of MD-MG-13 revealed the shifting of H-18 (δ 2.68) toward the lower field (ca. -0.1 ppm) (Spectrum 46) while the non-protonated carbon (δ 83.3) was resonated in the lower field in the ^{13}C-NMR spectrum (ca. +12 ppm) (Spectrum 47). Additionally, the resonances belonging to adjacent protons or carbons of C-17 and C-18 at junction point of ring D and E shifted either lower field or higher field. This fact proposed that the absolute stereochemistry of C-17 and H-18 could be different compared with MD-MG-13 and MD-MG-25.

Table 16. ^{1}H and ^{13}C NMR spectroscopic data of MD-MG-25, a) (in C_5D_5N, ^{1}H: 500 MHz, ^{13}C: 125 MHz)

Position	δ_C (ppm)	δ_H (ppm), (J in Hz)
1	39.5 t	1.70[b]; 1.33[b]
2	34.9 t	2.56 ddd (15.8, 11.3, 7.3); 2.40[b]
3	216.8 s	-
4	48.5 s	-
5	55.9 d	1.35[b]

6	20.3 t	1.33[b)]
7	33.4 t	1.43[b)]
8	40.3 s	-
9	47.8 d	1.69[b)]
10	37.5 s	-
11	24.4 t	1.90[b)]
12	122.8 d	5.28 dd (4.0, 3.0)
13	145.2 s	-
14	42.7 s	-
15	26.5 t	2.40[b)]; 1.09[b)]
16	24.5 t	1.97[b)]
17	83.3 s	-
18	44.3 d	2.68 dd (13.8, 4.7)
19	49.3 t	1.83[b)]; 1.36[b)]
20	31.7 s	-
21	36.9 t	1.36[b)]
22	33.0 t	2.22 td (12.8, 6.6); 2.08[b)]
23	27.1 q	1.16 s
24	22.2 q	1.03 s
25	15.4 q	0.93 s
26	18.1 q	1.10 s
27	26.0 q	1.23 s
28	-	
29	33.3 q	0.95 s
30	24.6 q	1.01 s

a) Assignments were confirmed by 2D-COSY, HSQC, and HMBC experiments.
b) Signal pattern was unclear due to overlapping.

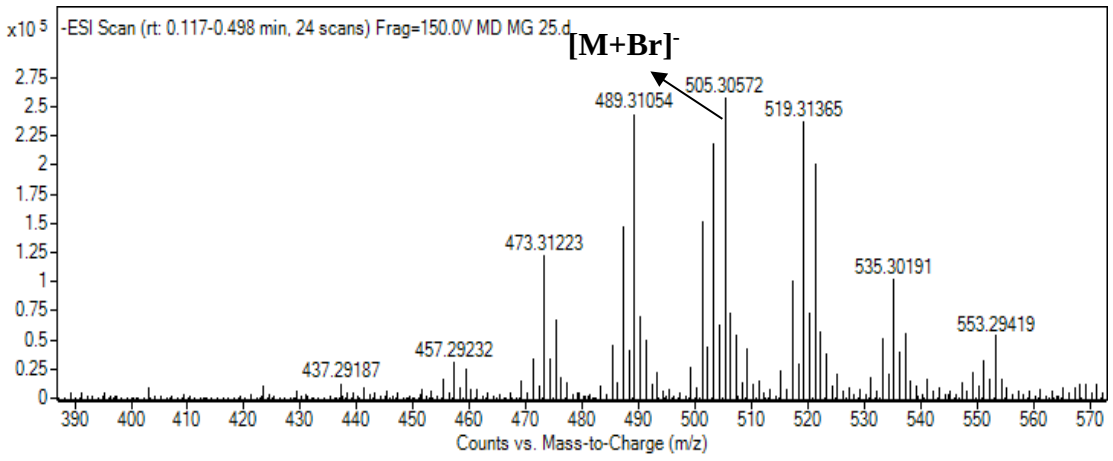

Spectrum 45. HR-ESI-MS spectrum of MD-MG-25 (negative mode)

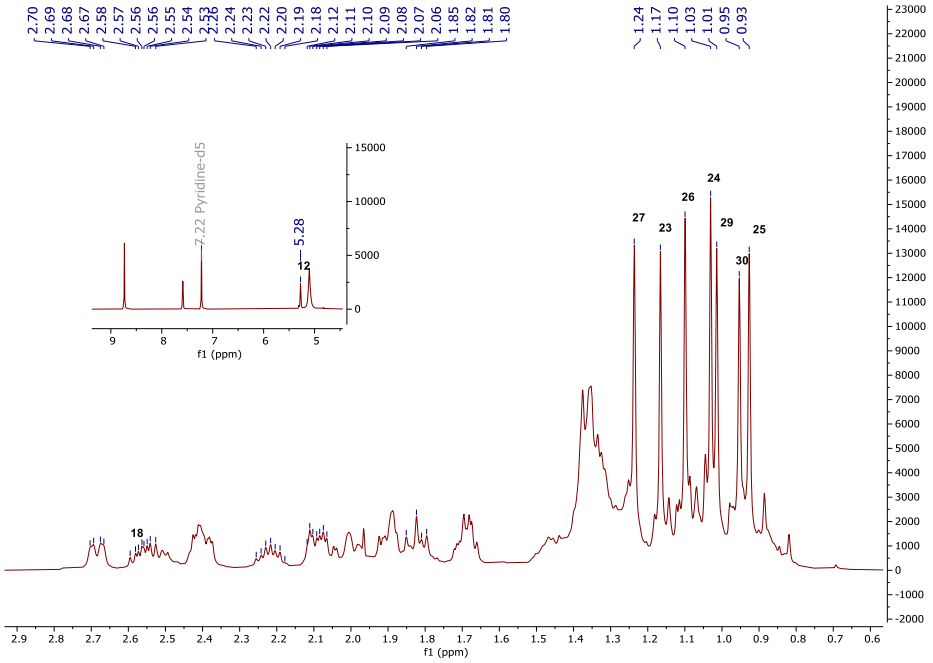

Spectrum 46. ^{1}H-NMR spectrum of MD-MG-25

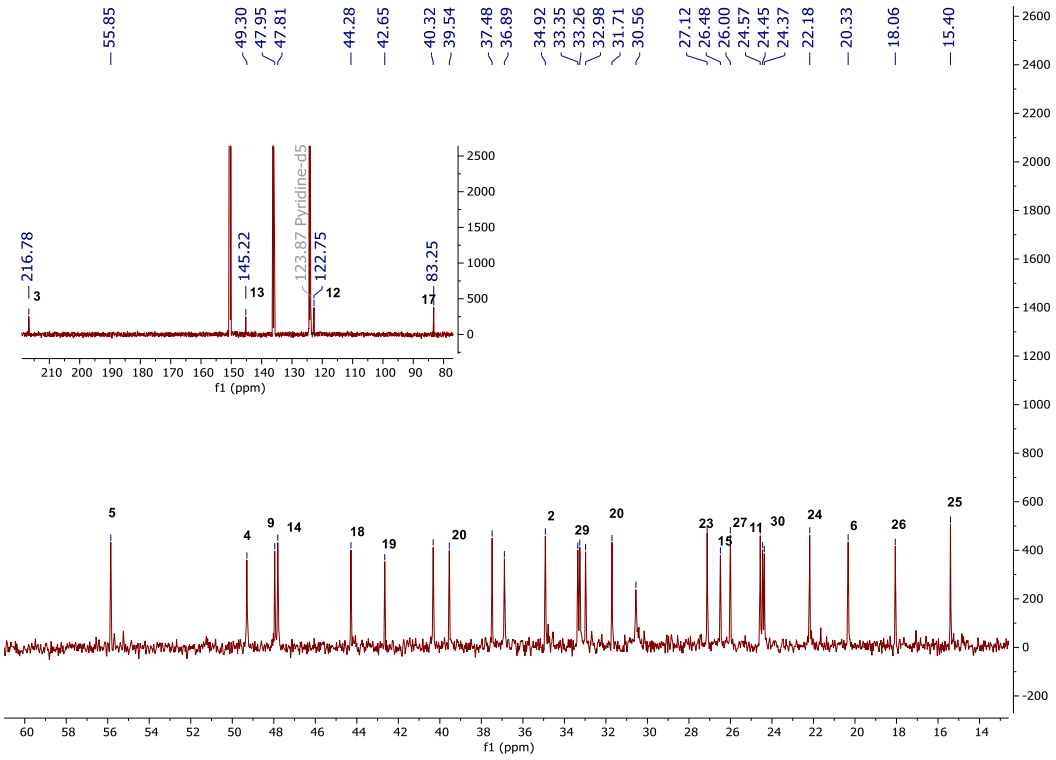

Spectrum 47. ^{13}C-NMR spectrum of MD-MG-25

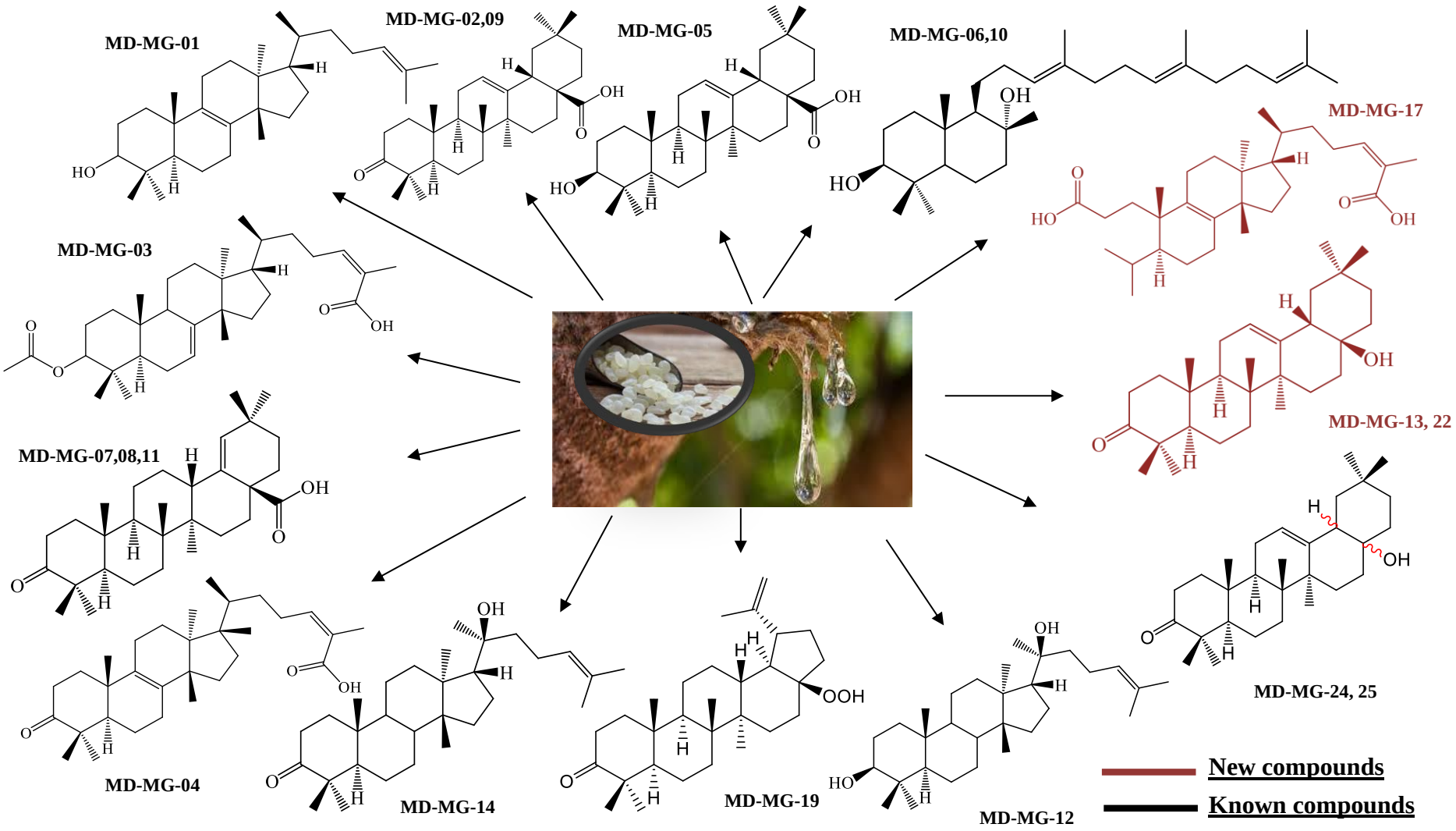

Figure 33. All purified compounds from mastic gum

3.2. Biological activity of selected compounds

Eleven compounds, structures of which were fully established, were selected for bioactivity studies. However, only nine compounds were screened in neuroprotective activity studies due to solubility issues or insufficient quantity for repetitive experiments (**MD-MG-08** and **MD-MG-17**).

3.2.1. Neuroprotective activity

SH-SY5Y cells have been used as an in vitro model for neurotoxicity experiments. Generally, several agents are used to differentiate SH-SY5Y cells into neuron-like differentiated state, although undifferentiated state have also been used. Oxidative stress occurs when ROS is over produced and accumulated, which in turn leads to the progression of neuronal degeneration.[60] Hence, H_2O_2 (hydrogen peroxide) induced damage in SH-SY5Y cells are widely used to model neurotoxicity.[76] In this thesis, the selected compounds were investigated for their neuroprotective effects against H_2O_2 induced oxidative stress of SH-SY5Y cells differentiated with retinoic acid (RA). Additionally, compounds were screened on undifferentiated SH-SY5Y cells as RA could affect several important cell signaling pathways, affecting the results of neuroprotective potential of compounds.[77,78]

Firstly, we determined the difference between undifferentiated cells and retinoic acid-differentiated cells. In the previous study, the differentiation of SH-SY5Y cells was stimulated by retinoic acid at a concentration of 10 μM. Cells were treated for 7 days. SH-SY5Y cells were successfully differentiated into neuronal phenotype (Figure 34).

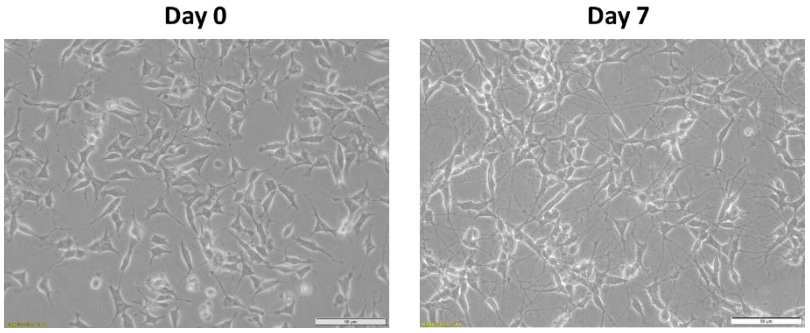

Figure 34.The morphologic difference between undifferentiated SH-SY5Y cells and retinoic acid-differentiated SH-SY5Y cells.

While **MD-MG-05** (**Oleanolic acid, OA**) showed neuroprotective effects against H_2O_2-induced cell death on undifferentiated SH-SY5Y cells, it was not able to protect retinoic acid-differentiated SH-SY5Y cells against H_2O_2 toxicity (Figure 35). After thorough consideration, it was hypothesized that this negative result could be deriving from inhibitory action of retinoic acid on telomerase enzyme[79] since OA was reported as a telomerase activator.[80] Thus, if telomerase activation plays a role in the neuroprotective effect of **MD-MG-05**, retinoic acid differentiation may be affecting the activity of the compound. In parallel, **MD-MG-13**, possessing a similar skeleton with **MD-MG-05** (oleanane-type), reduced H_2O_2 toxicity in undifferentiated SH-SY5Y cells (Figure 36), implying importance of the structural features. However, before reaching to conclusion, neuroprotective effects of **MD-MG-13** must be investigated with retinoic acid-differentiated SH-SY5Y cells, which will take place in due course. Additionally, the activity of **MD-MG-05** and **MD-MG-13** seems to lose their activity at higher concentrations. The solubility problem of both compounds is thought to be the overriding basis for such activity decrease.

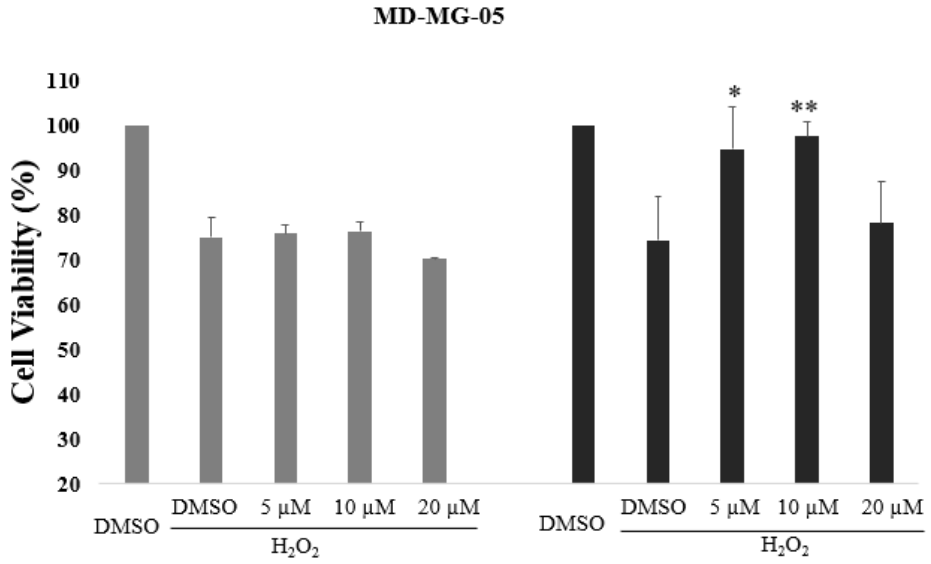

Figure 35. Neuroprotective effects of **MD-MG-05** on retinoic acid-differentiated (left) and undifferentiated (right) SH-SY5Y cells against H_2O_2 toxicity

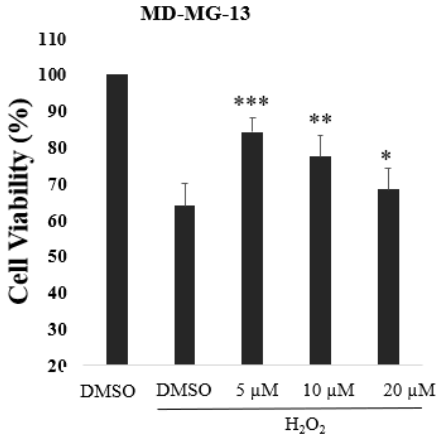

Figure 36. Neuroprotective effects of **MD-MG-13** on undifferentiated SH-SY5Y cells against H_2O_2 toxicity

MD-MG-19 slightly prevented H_2O_2 toxicity at a concentration of 20 µM in both undifferentiated and retinoic acid-differentiated SH-SY5Y cells; however, it showed a cytotoxic effect on cells at a concentration of 40 µM (Figure 37). Although these results indicate that **MD-MG-19** has neuroprotective activity, a low therapeutic index critically reduces the potential of the molecule. Additionally, similar results in both undifferentiated and retinoic acid-differentiated SH-SY5Y cells indicated that **MD-MG-19**, having a different triterpenic framework (lupane), probably exerted neuroprotective activity through a separate pathway than **MD-MG-05**.

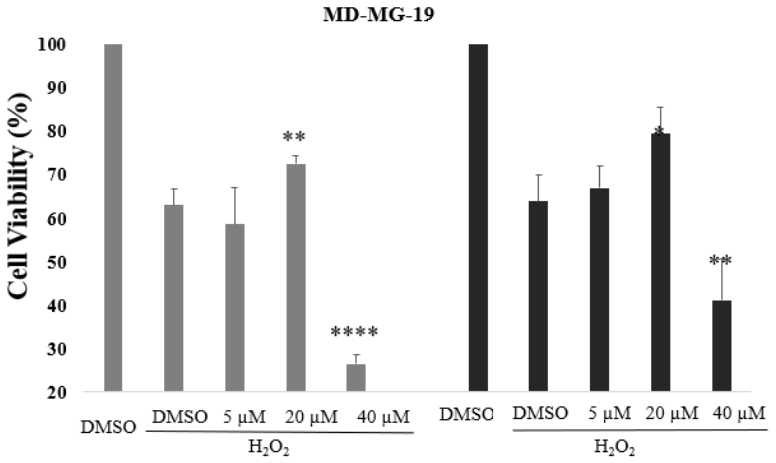

Figure 37. Neuroprotective effects of **MD-MG-19** on retinoic acid-differentiated (left) and undifferentiated (right) SH-SY5Y cells against H_2O_2 toxicity.

Moreover, **MD-MG-02**, **14** and **04** did not exhibit neuroprotective effect on both retinoic acid-differentiated and undifferentiated SH-SY5Y cells after H_2O_2 treatment (Figure 38). Interestingly, the oxidation of C-3(OH) to carbonyl in oleanane skeleton as in **MD-MG-02** seems to be reducing the neuroprotective effect.

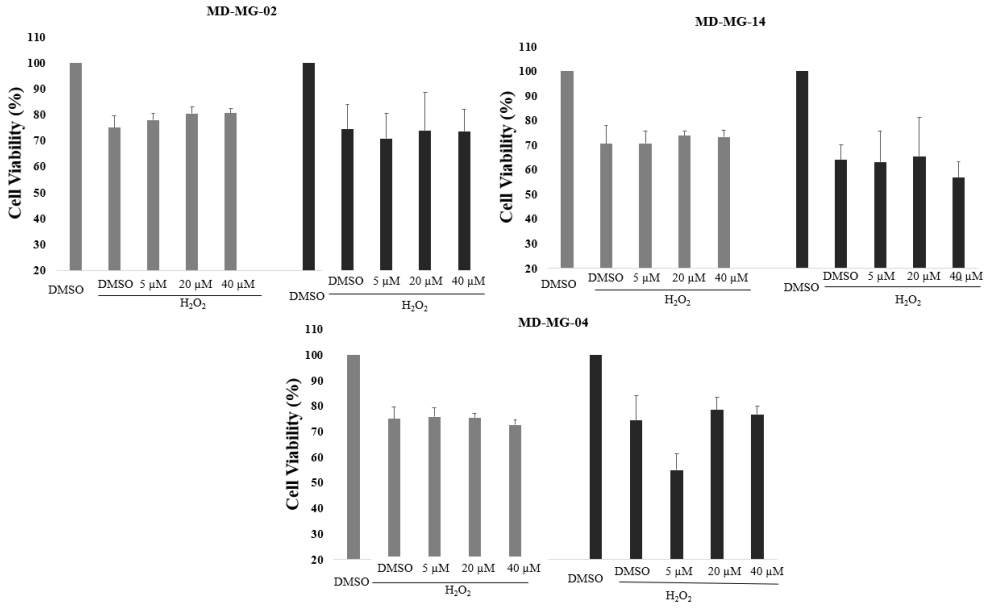

Figure 38. Neuroprotective effects of **MD-MG-02, 14, 04** on retinoic acid-differentiated (left) and undifferentiated (right) SH-SY5Y cells against H_2O_2 toxicity

Additionally, an opposite action was observed for **MD-MG-06**, **03** and **12** increasing H_2O_2 toxicity on both retinoic acid-differentiated and undifferentiated SH-SY5Y cells after H_2O_2 treatment (Figure 39). The results were noteworthy from chemistry point of view as **MD-MG-06**, **03** and **12** had different triterpenoid structures including bi- and tetra-cyclic skeletons. A similar effect was reported for vitamin D derivatives containing steroidal backbone similar to our toxicity increasing compounds.[81] Indeed, the action of these compounds with further analogs should be investigated to shed light on structural requirements and to establish the mechanism(s) at molecular level.

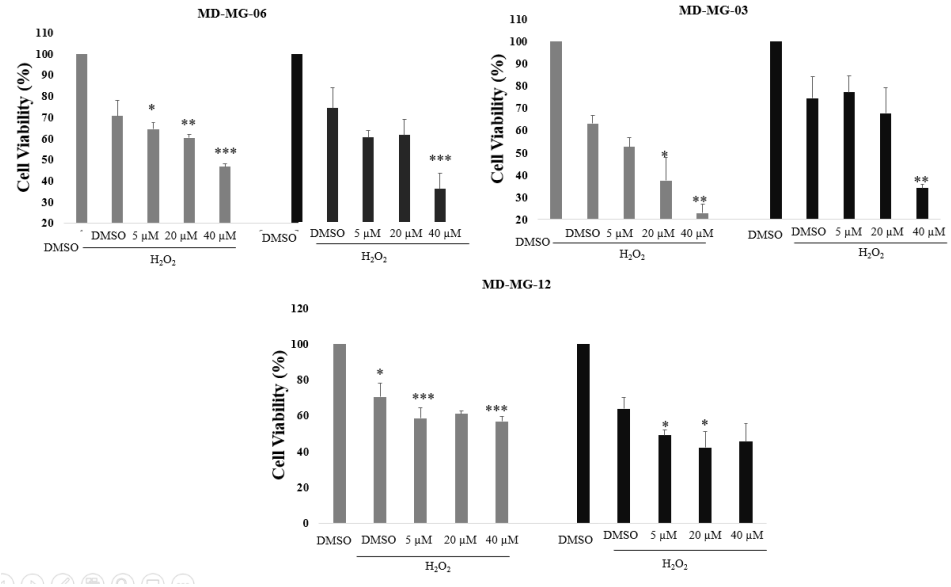

Figure 39. Neuroprotective effects of **MD-MG-06**, **03** and **12** on retinoic acid-differentiated (left) and undifferentiated (right) SH-SY5Y cells against H_2O_2 toxicity.

CHAPTER 4

CONCLUSION

Mastic gum is a complex resin produced by the mastic tree *Pistacia lentiscus* L. var. *chia*. Mastic gum is harvested in Chios Island of Greek and the Çesme and Karaburun region of Turkey. Traditionally used mastic gum has various pharmacological properties, including anti-cancer, antiviral, antioxidant, antibacterial, antidiabetic, and anti-inflammatory.[41,47,51,82–84] Phytochemical components such as terpenoids, phenolic compounds, and essential oils are thought to be responsible for biological activities. Some biological activities are linked with triterpenic compounds, comprising more than 75% of phytochemical components in mastic gum.[38,45,69,83–85]

Besides, there are still unrevealed triterpenoids existing in mastic gum. In addition, the high distribution of mastic tree *Pistacia lentiscus* var. *chia* in the Karaburun region of Turkey and the strong influence of abiotic factors on the secondary metabolite diversity produced in a plant drove us to determine the chemical profile of triterpenoid-rich fractions of the mastic gum extract. Thus, the pure triterpenic compounds were isolated from the powdered mastic gum of *Pistacia lentiscus* var. *chia* collected from the Karaburun peninsula using several chromatographic methodologies. The chemical structures of isolated compounds were elucidated via spectroscopic methods (1D NMR, 2D NMR, and MS spectra) and X-ray diffraction. All elucidated compounds were further screened for neuroprotective properties.

In the thesis, 14 compounds were identified by spectral methods, two of which were new compounds: 3,4-seco-tirucalla-8,24-dien,26-oic acid **(MD-MG-17)** and 3-oxo-17*β*-hydroxy-norolean-12-ene **(MD-MG-13)**. The known compounds were identified as tirucallol, oleanonic acid, 3-O-acetyl masticadienolic acid, isomasticadienonic acid, oleanolic acid, myrrhanol c, moronic acid, dammarenediol, dipterocarpol, 28-norlup-20(29)-en-3-one-17β-hydroperoxide, 17-hydroxy-28-norolean-12-ene-3-one (**MD-MG-24** and **25**). Besides, 28-norlup-20(29)-en-3-one-17β-hydroperoxide was isolated from the mastic gum of *Pistacia lentiscus* var. *chia* for the first time. Also, myrrhanol C with its polypodane-type bicyclic skeleton is a rare triterpene in nature. The selected

compounds in terms of solubility and quantity were examined for neuroprotective effect in SH-SY5Y cell line.

Recent findings indicated that *Pistacia lentiscus* leaf extract had neuroprotective effects.[76] In another study, it was reported that *Pistacia lentiscus* leaf extract might be effective in preventing neuroblastoma by increasing reactive oxygen species production and lipoperoxidation in two human neuroblastoma cell lines (SK-N-BE(2)C, SH-SY5Y).[86] Recently, oleanolic acid (OA), also found in substantial amounts in *Pistacia lentiscus* var. *chia,* was reported to be a novel neuroprotective agent in neurodegenerative diseases as it reinforced the adaptive cell response against oxidative stress and inhibited microglial activation.[87] Although mastic gum is widely used in food and medical sectors, the neuroprotective effect of its triterpene-rich fractions is little known. We hypothesized that some of the triterpenic isolates could be responsible for neuroprotective activities of mastic gum. Accordingly, two compounds (**MD-MG-05**, **MD-MG-13**) showed protective effects against oxidative stress on undifferentiated cells, implying once more that mastic gum as a valuable natural product in medicinal applications especially towards degenerative diseases.

This study revealed that plants growing in different regions are affected by abiotic factors such as air, soil, climate, light. As a result, both the secondary metabolites produced by plants and their amounts could be different. Based on our studies, one might say that the triterpenic composition of mastic gum harvested from the Karaburun peninsula is similar to the Greek mastic gum from Chios; however, it is still possible to run into new chemistry as in our studies pointing significance of the ecological factors as mentioned above. From bioactivity perspective, it is hypothesized that the overriding basis of the decrease in protective effects on the differentiated cells treated with retinoic acid, which is a telomerase inhibitor, is due to inhibition of the telomerase enzyme. However, further studies are needed to find the interaction between telomerase activation and neuroprotective effects in the treatment of neurodegenerative diseases.

REFERENCES

(1) Bouta, W.; Bouda, S.; Rasafi, T. El; Hansali, M. El; Haddioui, A. Morphological Diversity in Wild Populations of Mastic Tree , Pistacia Lentiscus L . (Anacardiaceae) in Morocco. *Phytomorphology An Int. J. Plant Morphol.* **2020**, *70* (1&2), 17–24.

(2) Al-Saghir, M. G. Evolutionary History of the Genus Pistacia (Anacardiaceae). *International Journal of Botany*. 2009, pp 255–257. https://doi.org/10.3923/ijb.2009.255.257.

(3) Andrés-Hernández, A. R.; Terrazas, T. Leaf Architecture of Rhus s.Str. (Anacardiaceae). *Feddes Repert.* **2009**, *120* (5–6), 293–306. https://doi.org/10.1002/fedr.200911109.

(4) Dimas, K. S.; Pantazis, P.; Ramanujam, R. Chios Mastic Gum: A Plant-Produced Resin Exhibiting Numerous Diverse Pharmaceutical and Biomedical Properties. *In Vivo (Brooklyn).* **2012**, *26* (5), 777–785.

(5) Chinou, I. Assessment Report on Pistacia Lentiscus L., Resin (Mastix). *Eur. Med. Agency* **2015**, *44* (July), 43.

(6) S. Paraschos; S. Mitakou; A.-L. Skaltsounis. Chios Gum Mastic: A Review of Its Biological Activities. *Curr. Med. Chem.* **2012**, *19* (14), 2292–2302. https://doi.org/10.2174/092986712800229014.

(7) Zhang, L.; Song, J.; Kong, L.; Yuan, T.; Li, W.; Zhang, W.; Hou, B.; Lu, Y.; Du, G. The Strategies and Techniques of Drug Discovery from Natural Products. *Pharmacol. Ther.* **2020**, *216*, 107686. https://doi.org/10.1016/j.pharmthera.2020.107686.

(8) Katz, L.; Baltz, R. H. Natural Product Discovery: Past, Present, and Future. *J. Ind. Microbiol. Biotechnol.* **2016**, *43* (2–3), 155–176. https://doi.org/10.1007/s10295-015-1723-5.

(9) Newman, D. J.; Cragg, G. M. Natural Products as Sources of New Drugs from 1981 to 2014. *J. Nat. Prod.* **2016**, *79* (3), 629–661. https://doi.org/10.1021/acs.jnatprod.5b01055.

(10) Boy, H. I. A.; Rutilla, A. J. H.; Santos, K. A.; Ty, A. M. T.; Yu, A. I.; Mahboob, T.; Tangpoong, J.; Nissapatorn, V. Recommended Medicinal Plants as Source of Natural Products: A Review. *Digit. Chinese Med.* **2018**, *1* (2), 131–142.

https://doi.org/10.1016/s2589-3777(19)30018-7.

(11) Pachi, V. K.; Mikropoulou, E. V.; Gkiouvetidis, P.; Siafakas, K.; Argyropoulou, A.; Angelis, A.; Mitakou, S.; Halabalaki, M. Traditional Uses, Phytochemistry and Pharmacology of Chios Mastic Gum (Pistacia Lentiscus Var. Chia, Anacardiaceae): A Review. *J. Ethnopharmacol.* **2020**, *254* (December 2019), 112485. https://doi.org/10.1016/j.jep.2019.112485.

(12) Bijay-Singh; Varinderpal-Singh; Ali, A. M. *Site-Specific Fertilizer Nitrogen Management in Cereals in South Asia*; 2020. https://doi.org/10.1007/978-3-030-38881-2_6.

(13) Onay, A.; Yildirim, H.; Yavuz, M. A. Sakız Ağacı (Pistacia Lentiscus L .) Yetiştiriciliği ve Reçinesi. **2016**, *6* (2), 133–144.

(14) Dietemann, P.; Kälin, M.; White, R.; Sudano, C.; Knochenmuss, R.; Zenobi, R. Chios Gum Mastic: Freshly Harvested vs. Commercial Resin and Its Implications to Aging of Varnishes. *Zeitschrift für Kunsttechnologie und Konserv.* **2005**, *19* (1), 117–128.

(15) Paraskevopoulou, A.; Kiosseoglou, V. Functional Properties of Traditional Foods. *Funct. Prop. Tradit. Foods* **2016**, 271–287. https://doi.org/10.1007/978-1-4899-7662-8.

(16) Andrikopoulos, N. K.; Kaliora, A. C.; Assimopoulou, A. N.; Papapeorgiou, V. P. Biological Activity of Some Naturally Occurring Resins, Gums and Pigments against in Vitro LDL Oxidation. *Phyther. Res.* **2003**, *17* (5), 501–507. https://doi.org/10.1002/ptr.1185.

(17) Nahida; Ansari, S. H.; Siddiqui, A. N. Pistacia Lentiscus: A Review on Phytochemistry and Pharmacological Properties. *Int. J. Pharm. Pharm. Sci.* **2012**, *4* (SUPPL. 4), 16–20.

(18) Barton, D. H. R.; Seoane, E. Triterpenoids. Part XXII.* The Constitution and Stereochemistry of Masticadienonic Acid.†. *J. Chem. Soc.* **1956**, No. 4150, 4133–4135. https://doi.org/10.1039/jr9560004150.

(19) Van Der Doelen, G. A.; Van Den Berg, K. J.; Boon, J. J.; Shibayama, N.; René De La Rie, E.; Wim, W. J. Analysis of Fresh Triterpenoid Resins and Aged Triterpenoid Varnishes by High-Performance Liquid Chromatography-Atmospheric Pressure Chemical Ionisation (Tandem) Mass Spectrometry. *J. Chromatogr. A* **1998**, *809* (1–2), 21–37. https://doi.org/10.1016/S0021-9673(98)00186-1.

(20) Assimopoulou, A. N.; Papageorgiou, V. P. GC-MS Analysis of Penta- and Tetra-Cyclic Triterpenes from Resins of Pistacia Species. Part II. Pistacia Terebinthus Var. Chia. *Biomed. Chromatogr.* **2005**, *19* (8), 586–605. https://doi.org/10.1002/bmc.484.

(21) Paraschos, S.; Magiatis, P.; Mitakou, S.; Petraki, K.; Kalliaropoulos, A.; Maragkoudakis, P.; Mentis, A.; Sgouras, D.; Skaltsounis, A. L. In Vitro and in Vivo Activities of Chios Mastic Gum Extracts and Constituents against Helicobacter Pylori. *Antimicrob. Agents Chemother.* **2007**, *51* (2), 551–559. https://doi.org/10.1128/AAC.00642-06.

(22) Van Den Berg, K. J.; Van Der Horst, J.; Boon, J. J.; Sudmeijer, O. O. Cis-1,4-Poly-β-Myrcene; The Structure of the Polymeric Fraction of Mastic Resin (Pistacia Lentiscus L.) Elucidated. *Tetrahedron Lett.* **1998**, *39* (17), 2645–2648. https://doi.org/10.1016/S0040-4039(98)00228-7.

(23) Gao, J. B.; Li, G. Y.; Huang, J.; Wang, H. Y.; Zhang, K.; Wang, J. H. A New Tetracyclic Triterpenoid Compound from Mastich. *J. Asian Nat. Prod. Res.* **2013**, *15* (4), 400–403. https://doi.org/10.1080/10286020.2013.769524.

(24) Sharifi, M. S.; Hazell, S. L. Fractionation of Mastic Gum in Relation to Antimicrobial Activity. *Pharmaceuticals* **2009**, *2* (1), 2–10. https://doi.org/10.3390/ph2010002.

(25) Xynos, N.; Termentzi, A.; Fokialakis, N.; Skaltsounis, L. A.; Aligiannis, N. Supercritical CO2 Extraction of Mastic Gum and Chemical Characterization of Bioactive Fractions Using LC-HRMS/MS and GC–MS. *J. Supercrit. Fluids* **2018**, *133*, 349–356. https://doi.org/10.1016/j.supflu.2017.10.011.

(26) Paraschos, S.; Magiatis, P.; Gousia, P.; Economou, V.; Sakkas, H.; Papadopoulou, C.; Skaltsounis, A. L. Chemical Investigation and Antimicrobial Properties of Mastic Water and Its Major Constituents. *Food Chem.* **2011**, *129* (3), 907–911. https://doi.org/10.1016/j.foodchem.2011.05.043.

(27) Tabanca, N.; Nalbantsoy, A.; Kendra, P. E.; Demirci, F.; Demirci, B. Chemical Characterization and Biological Activity of the Mastic Gum Essential Oils of Pistacia Lentiscus Var. Chia from Turkey. *Molecules* **2020**, *25* (9), 1–19. https://doi.org/10.3390/molecules25092136.

(28) Koutsoudaki, C.; Krsek, M.; Rodger, A. Chemical Composition and Antibacterial Activity of the Essential Oil and the Gum of Pistacia Lentiscus Var. Chia. *J. Agric. Food Chem.* **2005**, *53* (20), 7681–7685. https://doi.org/10.1021/jf050639s.

(29) Barra, A.; Coroneo, V.; Dessi, S.; Cabras, P.; Angioni, A. Characterization of the Volatile Constituents in the Essential Oil of Pistacia Lentiscus l. from Different Origins and Its Antifungal and Antioxidant Activity. *J. Agric. Food Chem.* **2007**, *55* (17), 7093–7098. https://doi.org/10.1021/jf071129w.

(30) Assimopoulou, A. N.; Zlatanos, S. N.; Papageorgiou, V. P. Antioxidant Activity of Natural Resins and Bioactive Triterpenes in Oil Substrates. *Food Chem.* **2005**, *92* (4), 721–727. https://doi.org/10.1016/j.foodchem.2004.08.033.

(31) Tassou, C. C.; Nychas, G. J. E. Antimicrobial Activity of the Essential Oil of Mastic Gum (Pistacia Lentiscus Var. Chia) on Gram Positive and Gram Negative Bacteria in Broth and in Model Food System. *Int. Biodeterior. Biodegrad.* **1995**, *36* (3–4), 411–420. https://doi.org/10.1016/0964-8305(95)00103-4.

(32) Duru, M. E.; Cakir, A.; Kordali, S.; Zengin, H.; Harmandar, M.; Izumi, S.; Hirata, T. Chemical Composition and Antifungal Properties of Essential Oils of Three Pistacia Species. *Fitoterapia* **2003**, *74* (1–2), 170–176. https://doi.org/10.1016/S0367-326X(02)00318-0.

(33) Hill, R. A.; Connolly, J. D. Triterpenoids. *Nat. Prod. Rep.* **2020**, *37* (7), 962–998. https://doi.org/10.1039/c9np00067d.

(34) Seoane, E. Further Crystalline Constituents of Gum Mastic. *J. Chem. Soc.* **1956**, No. 4158, 4135–4143. https://doi.org/10.1039/jr9560004158.

(35) Marner, F. J.; Freyer, A.; Lex, J. Triterpenoids from Gum Mastic, the Resin of Pistacia Lentiscus. *Phytochemistry* **1991**, *30* (11), 3709–3712. https://doi.org/10.1016/0031-9422(91)80095-I.

(36) Sharifi, M. S.; Hazell, S. L. Isolation, Analysis and Antimicrobial Activity of the Acidic Fractions of Mastic, Kurdica, Mutica and Cabolica Gums from Genus Pistacia. *Glob. J. Health Sci.* **2012**, *4* (1), 217–228. https://doi.org/10.5539/gjhs.v4n1p217.

(37) Jin, Y.; Zhao, J.; Jeong, K. M.; Yoo, D. E.; Han, S. Y.; Choi, S. Y.; Ko, D. H.; Kim, H. ji; Sung, N. H.; Lee, J. A Simple and Reliable Analytical Method Based on HPLC–UV to Determine Oleanonic Acid Content in Chios Gum Mastic for Quality Control. *Arch. Pharm. Res.* **2017**, *40* (1), 49–56. https://doi.org/10.1007/s12272-016-0853-2.

(38) Liu, W.; Gao, J.; Li, M.; Aisa, H. A.; Yuan, T. Tirucallane Triterpenoids from the Mastic (Pistacia Lentiscus) and Their Anti-Inflammatory and Cytotoxic Activities. *Phytochemistry* **2021**, *182* (August 2020), 112596.

https://doi.org/10.1016/j.phytochem.2020.112596.

(39) Kaliora, A. C.; Mylona, A.; Chiou, A.; Petsios, D. G.; Andrikopoulos, N. K. Detection and Identification of Simple Phenolics in Pistacia Lentiscus Resin. *J. Liq. Chromatogr. Relat. Technol.* **2004**, *27* (2), 289–300. https://doi.org/10.1081/JLC-120027100.

(40) Kivçak, B.; Akay, S. Quantitative Determination of α-Tocopherol in Pistacia Lentiscus, Pistacia Lentiscus Var. Chia, and Pistacia Terebinthus by TLC-Densitometry and Colorimetry. *Fitoterapia* **2005**, *76* (1), 62–66. https://doi.org/10.1016/j.fitote.2004.09.021.

(41) Qiao, J.; Li, A.; Jin, X.; Wang, J. Mastic Alleviates Allergic Inflammation in Asthmatic Model Mice by Inhibiting Recruitment of Eosinophils. *Am. J. Respir. Cell Mol. Biol.* **2011**, *45* (1), 95–100. https://doi.org/10.1165/rcmb.2010-0212OC.

(42) Kaliora, A. C.; Stathopoulou, M. G.; Triantafillidis, J. K.; Dedoussis, G. V. Z.; Andrikopoulous, N. K. Chios Mastic Treatment of Patients with Active Crohn's Disease. *World J. Gastroenterol.* **2007**, *13* (5), 748–753. https://doi.org/10.3748/wjg.v13.i5.748.

(43) Kaliora, A. C.; Stathopoulou, M. G.; Triantafillidis, J. K.; Dedoussis, G. V. Z.; Andrikopoulos, N. K. Alterations in the Function of Circulating Mononuclear Cells Derived from Patients with Crohn's Disease Treated Withmastic. *World J. Gastroenterol.* **2007**, *13* (45), 6031–6036. https://doi.org/10.3748/wjg.13.6031.

(44) Zhou, L.; Satoh, K.; Takahashi, K.; Watanabe, S.; Nakamura, W.; Maki, J.; Hatano, H.; Takekawa, F.; Shimada, C.; Sakagami, H. Re-Evaluation of Anti-Inflammatory Activity of Mastic Using Activated Macrophages. *In Vivo (Brooklyn).* **2009**, *23* (4), 583–590.

(45) Loizou, S.; Paraschos, S.; Mitakou, S.; Chrousos, G. P.; Lekakis, I.; Moutsatsou, P. Chios Mastic Gum Extract and Isolated Phytosterol Tirucallol Exhibit Anti-Inflammatory Activity in Human Aortic Endothelial Cells. *Exp. Biol. Med.* **2009**, *234* (5), 553–561. https://doi.org/10.3181/0811-RM-338.

(46) Papada, E.; Amerikanou, C.; Torović, L.; Kalogeropoulos, N.; Tzavara, C.; Forbes, A.; Kaliora, A. C. Plasma Free Amino Acid Profile in Quiescent Inflammatory Bowel Disease Patients Orally Administered with Mastiha (Pistacia Lentiscus); a Randomised Clinical Trial. *Phytomedicine* **2019**, *56* (April 2018), 40–47. https://doi.org/10.1016/j.phymed.2018.08.008.

(47) He, M. L.; Yuan, H. Q.; Jiang, A. L.; Gong, A. Y.; Chen, W. W.; Zhang, P. J.;

Young, C. Y. F.; Zhang, J. Y. Gum Mastic Inhibits the Expression and Function of the Androgen Receptor in Prostate Cancer Cells. *Cancer* **2006**, *106* (12), 2547–2555. https://doi.org/10.1002/cncr.21935.

(48) Dimas, K.; Hatziantoniou, S.; Wyche, J. H.; Pantazis, P. A Mastic Gum Extract Induces Supression of Growth of Human Colorectal Tumor Xenografts in Immunodeficient Mice. *In Vivo (Brooklyn).* **2009**, *23* (1), 63–68.

(49) Huang, X. Y.; Wang, H. C.; Yuan, Z.; Li, A.; He, M. L.; Ai, K. X.; Zheng, Q.; Qin, H. L. Gemcitabine Combined with Gum Mastic Causes Potent Growth Inhibition and Apoptosis of Pancreatic Cancer Cells. *Acta Pharmacol. Sin.* **2010**, *31* (6), 741–745. https://doi.org/10.1038/aps.2010.54.

(50) Al-Habbal, M. J.; Al-Habbal, Z.; Huwez, F. U. A Double-Blind Controlled Clinical Trial of Mastic and Placebo in the Treatment of Duodenal Ulcer. *Clin. Exp. Pharmacol. Physiol.* **1984**, *11* (5), 541–544. https://doi.org/10.1111/j.1440-1681.1984.tb00864.x.

(51) Marone, P.; Bono, L.; Leone, E.; Bona, S.; Carretto, E.; Perversi, L. Bactericidal Activity of Pistacia Lentiscus Mastic Gum against Helicobacter Pylori. *J. Chemother.* **2001**, *13* (6), 611–614. https://doi.org/10.1179/joc.2001.13.6.611.

(52) Kottakis, F.; Lamari, F.; Matragkou, C.; Zachariadis, G.; Karamanos, N.; Choli-Papadopoulou, T. Arabino-Galactan Proteins from Pistacia Lentiscus Var. Chia: Isolation, Characterization and Biological Function. *Amino Acids* **2008**, *34* (3), 413–420. https://doi.org/10.1007/s00726-007-0554-8.

(53) Aksoy, A.; Duran, N.; Koksal, F. In Vitro and in Vivo Antimicrobial Effects of Mastic Chewing Gum against Streptococcus Mutans and Mutans Streptococci. *Arch. Oral Biol.* **2006**, *51* (6), 476–481. https://doi.org/10.1016/j.archoralbio.2005.11.003.

(54) Karygianni, L.; Cecere, M.; Skaltsounis, A. L.; Argyropoulou, A.; Hellwig, E.; Aligiannis, N.; Wittmer, A.; Al-Ahmad, A. High-Level Antimicrobial Efficacy of Representative Mediterranean Natural Plant Extracts against Oral Microorganisms. *Biomed Res. Int.* **2014**, *2014*. https://doi.org/10.1155/2014/839019.

(55) Koychev, S.; Dommisch, H.; Chen, H.; Pischon, N. Antimicrobial Effects of Mastic Extract Against Oral and Periodontal Pathogens. *J. Periodontol.* **2017**, *88* (5), 511–517. https://doi.org/10.1902/jop.2017.150691.

(56) Yildiz-Unal, A.; Korulu, S.; Karabay, A. Neuroprotective Strategies against

Calpain-Mediated Neurodegeneration. *Neuropsychiatr. Dis. Treat.* **2015**, *11*, 297–310. https://doi.org/10.2147/NDT.S78226.

(57) Gao, H. M.; Hong, J. S. Why Neurodegenerative Diseases Are Progressive: Uncontrolled Inflammation Drives Disease Progression. *Trends Immunol.* **2008**, *29* (8), 357–365. https://doi.org/10.1016/j.it.2008.05.002.

(58) Mohamed, Z. A.; Eliaser, E. M.; Jaafaru, M. S.; Nordin, N.; Ioannides, C.; Razis, A. F. A. Neuroprotective Effects of 7-Geranyloxycinnamic Acid from Melicope Lunu Ankenda Leaves. *Molecules* **2020**, *25* (16). https://doi.org/10.3390/molecules25163724.

(59) Mohd Sairazi, N. S.; Sirajudeen, K. N. S. Natural Products and Their Bioactive Compounds: Neuroprotective Potentials against Neurodegenerative Diseases. *Evidence-based Complement. Altern. Med.* **2020**, *2020*, 5–7. https://doi.org/10.1155/2020/6565396.

(60) Cenini, G.; Lloret, A.; Cascella, R. Oxidative Stress in Neurodegenerative Diseases: From a Mitochondrial Point of View. *Oxid. Med. Cell. Longev.* **2019**, *2019*. https://doi.org/10.1155/2019/2105607.

(61) Singh, A.; Kukreti, R.; Saso, L.; Kukreti, S. Oxidative Stress: A Key Modulator in Neurodegenerative Diseases. *Molecules* **2019**, *24* (8), 1–20. https://doi.org/10.3390/molecules24081583.

(62) Aumeeruddy, M. Z.; Aumeeruddy-Elalfi, Z.; Neetoo, H.; Zengin, G.; Blom van Staden, A.; Fibrich, B.; Lambrechts, I. A.; Rademan, S.; Szuman, K. M.; Lall, N.; Mahomoodally, F. Pharmacological Activities, Chemical Profile, and Physicochemical Properties of Raw and Commercial Honey. *Biocatal. Agric. Biotechnol.* **2019**, *18* (January), 101005. https://doi.org/10.1016/j.bcab.2019.01.043.

(63) Huang, S.; Zhang, C. P.; Wang, K.; Li, G. Q.; Hu, F. L. Recent Advances in the Chemical Composition of Propolis. *Molecules* **2014**, *19* (12), 19610–19632. https://doi.org/10.3390/molecules191219610.

(64) Cheng, Z.; Zhang, M.; Ling, C.; Zhu, Y.; Ren, H.; Hong, C.; Qin, J.; Liu, T.; Wang, J. Neuroprotective Effects of Ginsenosides against Cerebral Ischemia. *Molecules* **2019**, *24* (6). https://doi.org/10.3390/molecules24061102.

(65) Morais, T. R.; Da Costa-Silva, T. A.; Tempone, A. G.; Borborema, S. E. T.; Scotti, M. T.; De Sousa, R. M. F.; Araujo, A. C. C.; De Oliveira, A.; De Morais, S. A. L.; Sartorelli, P.; Lago, J. H. G. Antiparasitic Activity of Natural and Semi-Synthetic

Tirucallane Triterpenoids from Schinus Terebinthifolius (Anacardiaceae): Structure/Activity Relationships. *Molecules* **2014**, *19* (5), 5761–5776. https://doi.org/10.3390/molecules19055761.

(66) Shirane, N.; Hashimoto, Y.; Ueda, K.; Takenaka, H.; Katoh, K. Ring-A Cleavage of 3-Oxo-Olean-12-En-28-Oic Acid by the Fungus Chaetomium Longirostre. *Phytochemistry* **1996**, *43* (1), 99–104. https://doi.org/10.1016/0031-9422(96)00266-X.

(67) Seebacher, W.; Simic, N.; Weis, R.; Saf, R.; Kunert, O. Complete Assignments of 1H and 13C NMR Resonances of Oleanolic Acid, 18α-Oleanolic Acid, Ursolic Acid and Their 11-Oxo Derivatives. *Magn. Reson. Chem.* **2003**, *41* (8), 636–638. https://doi.org/10.1002/mrc.1214.

(68) Assimopoulou, A. N.; Papageorgiou, V. P. GC-MS Analysis of Penta- and Tetra-Cyclic Triterpenes from Resins of Pistacia Species. Part I. Pistacia Lentiscus Var. Chia. *Biomed. Chromatogr.* **2005**, *19* (4), 285–311. https://doi.org/10.1002/bmc.454.

(69) Domingo, V.; Lorenzo, L.; Quilez Del Moral, J. F.; Barrero, A. F. First Synthesis of (+)-Myrrhanol C, an Anti-Prostate Cancer Lead. *Org. Biomol. Chem.* **2013**, *11* (4), 559–562. https://doi.org/10.1039/c2ob26947c.

(70) Rios, M. Y.; Salinas, D.; Villarreal, M. L. Cytotoxic Activity of Moronic Acid and Identification of the New Triterpene 3,4-Seco-Olean-18-Ene-3,28-Dioic Acid from Phoradendron Reichenbachianum. *Planta Med.* **2001**, *67* (5), 443–446. https://doi.org/10.1055/s-2001-15823.

(71) Hidayat, A. T.; Farabi, K.; Harneti, D.; Nurlelasari; Maharani, R.; Nurfarida, I.; Supratman, U.; Shiono, Y. Cytotoxic Triterpenoids from the Stembark of Aglaia Argentea (Meliaceae). *Indones. J. Chem.* **2018**, *18* (1), 35–42. https://doi.org/10.22146/ijc.25052.

(72) Sugiyama, Y.; Hazama, M.; Iwakami, N. Patent Application Publication. *United States Pat. Appl.* **2005**, *1*, 1–24.

(73) Kim, G. S.; Jeong, T. S.; Kim, Y. O.; Baek, N. I.; Cha, S. W.; Lee, J. W.; Song, K. S. Human Acyl-CoA:Cholesterol Acyltransferase-Inhibiting Dammarane Triterpenes from Rhus Chinensis. *J. Appl. Biol. Chem.* **2010**, *53* (4), 417–421. https://doi.org/10.3839/jksabc.2010.064.

(74) Almeida, A.; Dong, L.; Appendino, G.; Bak, S. Plant Triterpenoids with Bond-Missing Skeletons: Biogenesis, Distribution and Bioactivity. *Nat. Prod. Rep.* **2020**,

37 (9), 1207–1228. https://doi.org/10.1039/c9np00030e.

(75) Ayers, S.; Benkovics, T.; Marshall, J.; Tan, Y.; Strotman, N. A.; Kiau, S. Autoxidation Products of Betulonaldehyde. *J. Nat. Prod.* **2016**, *79* (10), 2758–2761. https://doi.org/10.1021/acs.jnatprod.6b00735.

(76) Pacifico, S.; Piccolella, S.; Marciano, S.; Galasso, S.; Nocera, P.; Piscopo, V.; Fiorentino, A.; Monaco, P. LC-MS/MS Profiling of a Mastic Leaf Phenol Enriched Extract and Its Effects on H2O2 and Aβ(25-35) Oxidative Injury in SK-B-NE(C)-2 Cells. *J. Agric. Food Chem.* **2014**, *62* (49), 11957–11966. https://doi.org/10.1021/jf504544x.

(77) Kondo, T.; Oka, T.; Sato, H.; Shinnou, Y.; Washio, K. Accumulation of Aberrant CpG Hypermethylation by Helicobacter Pylori Infection Promotes Development. *Int. J. Oncol.* **2009**, *35*, 547–557. https://doi.org/10.3892/ijo.

(78) Zhang, T.; Gygi, S. P.; Paulo, J. A. Temporal Proteomic Profiling of SH-SY5Y Differentiation with Retinoic Acid Using FAIMS and Real-Time Searching. *J. Proteome Res.* **2021**, *20* (1), 704–714. https://doi.org/10.1021/acs.jproteome.0c00614.

(79) Pendino, F.; Sahraoui, T.; Lanotte, M.; Ségal-Bendirdijian, E. A Novel Mechanism of Retinoic Acid Resistance in Acute Promyelocytic Leukemia Cells through a Defective Pathway in Telomerase Regulation. *Leukemia* **2002**, *16* (5), 826–832. https://doi.org/10.1038/sj.leu.2402470.

(80) Tsoukalas, D.; Fragkiadaki, P.; Docea, A. O.; Alegakis, A. K.; Sarandi, E.; Thanasoula, M.; Spandidos, D. A.; Tsatsakis, A.; Razgonova, M. P.; Calina, D. Discovery of Potent Telomerase Activators: Unfolding New Therapeutic and Anti-Aging Perspectives. *Mol. Med. Rep.* **2019**, *20* (4), 3701–3708. https://doi.org/10.3892/mmr.2019.10614.

(81) Piotrowska, A.; Wierzbicka, J.; Ślebioda, T.; Woźniak, M.; Tuckey, R. C.; Slominski, A. T.; Zmijewski, M. A. Vitamin D Derivatives Enhance Cytotoxic Effects of H2O2 or Cisplatin on Human Keratinocytes. *Steroids* **2016**, *110*, 49–61. https://doi.org/10.1016/j.steroids.2016.04.002.

(82) Kottakis, F.; Kouzi-Koliakou, K.; Pendas, S.; Kountouras, J.; Choli-Papadopoulou, T. Effects of Mastic Gum Pistacia Lentiscus van Chia on Innate Cellular Immune Effectors. *Eur. J. Gastroenterol. Hepatol.* **2009**, *21* (2), 143–149. https://doi.org/10.1097/MEG.0b013e32831c50c9.

(83) Bouslama, L.; Benzekri, R.; Nsaibia, S.; Papetti, A.; Limam, F. Identification of

an Antiviral Compound Isolated from Pistacia Lentiscus. *Arch. Microbiol.* **2020**, *5* (0123456789). https://doi.org/10.1007/s00203-020-01980-2.

(84) Vuorinen, A.; Seibert, J.; Papageorgiou, V. P.; Rollinger, J. M.; Odermatt, A.; Schuster, D.; Assimopoulou, A. N. Pistacia Lentiscus Oleoresin: Virtual Screening and Identification of Masticadienonic and Isomasticadienonic Acids as Inhibitors of 11 β -Hydroxysteroid Dehydrogenase 1. *Planta Med.* **2015**, *81* (6), 525–532. https://doi.org/10.1055/s-0035-1545720.

(85) Giner-Larza, E. M.; Máez, S.; Recio, M. C.; Giner, R. M.; Prieto, J. M.; Cerdá-Nicolás, M.; Ríos, J. L. Oleanonic Acid, a 3-Oxotriterpene from Pistacia, Inhibits Leukotriene Synthesis and Has Anti-Inflammatory Activity. *Eur. J. Pharmacol.* **2001**, *428* (1), 137–143. https://doi.org/10.1016/S0014-2999(01)01290-0.

(86) Piccolella, S.; Nocera, P.; Carillo, P.; Woodrow, P.; Greco, V.; Manti, L.; Fiorentino, A.; Pacifico, S. An Apolar Pistacia Lentiscus L. Leaf Extract: GC-MS Metabolic Profiling and Evaluation of Cytotoxicity and Apoptosis Inducing Effects on SH-SY5Y and SK-N-BE(2)C Cell Lines. *Food Chem. Toxicol.* **2016**, *95*, 64–74. https://doi.org/10.1016/j.fct.2016.06.028.

(87) Castellano, J. M.; Garcia-Rodriguez, S.; Espinosa, J. M.; Millan-Linares, M. C.; Rada, M.; Perona, J. S. Oleanolic Acid Exerts a Neuroprotective Effect against Microglial Cell Activation by Modulating Cytokine Release and Antioxidant Defense Systems. *Biomolecules* **2019**, *9* (11). https://doi.org/10.3390/biom9110683.

APPENDIX

1.

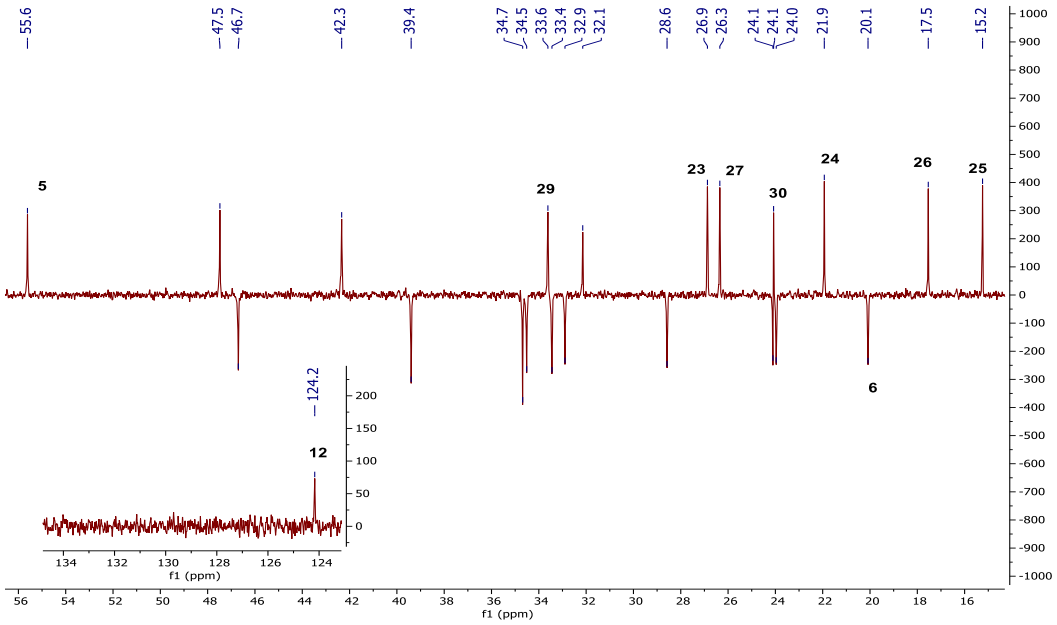

Spectrum 48. DEPT-135 spectrum of MD-MG-02

2.

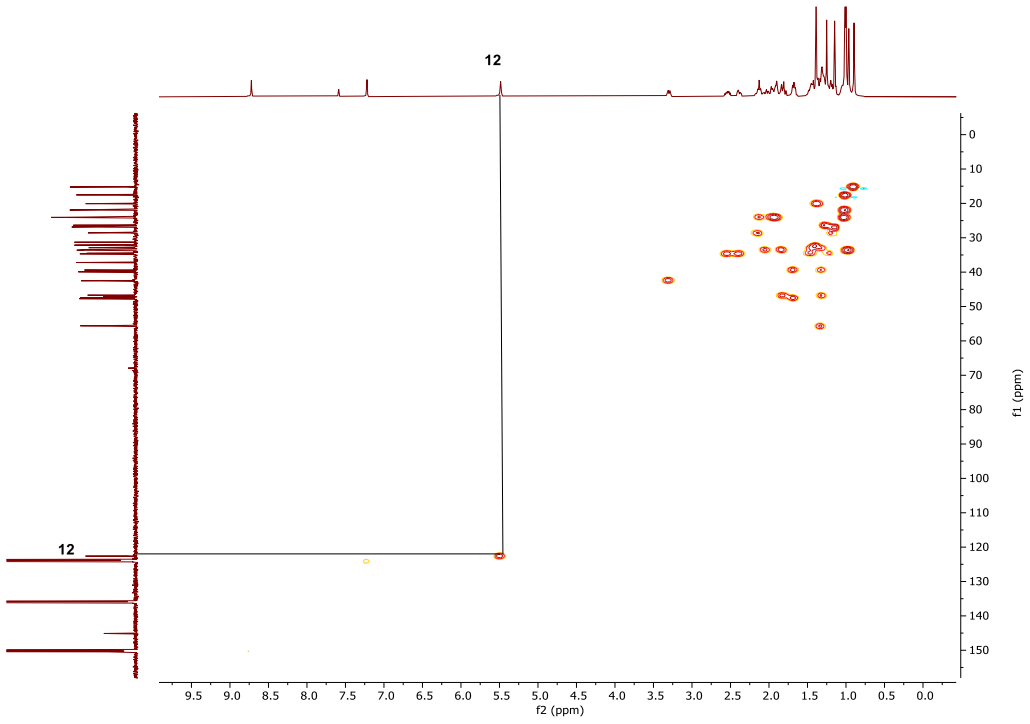

Spectrum 49. HSQC spectrum of MD-MG-02

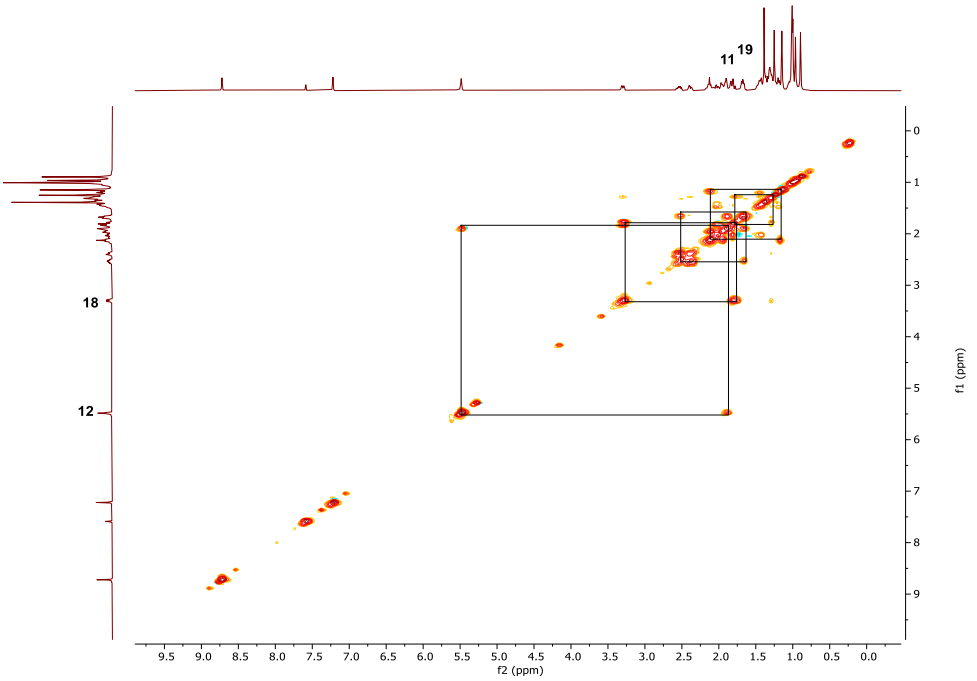

Spectrum 50. COSY spectrum of MD-MG-02

3.

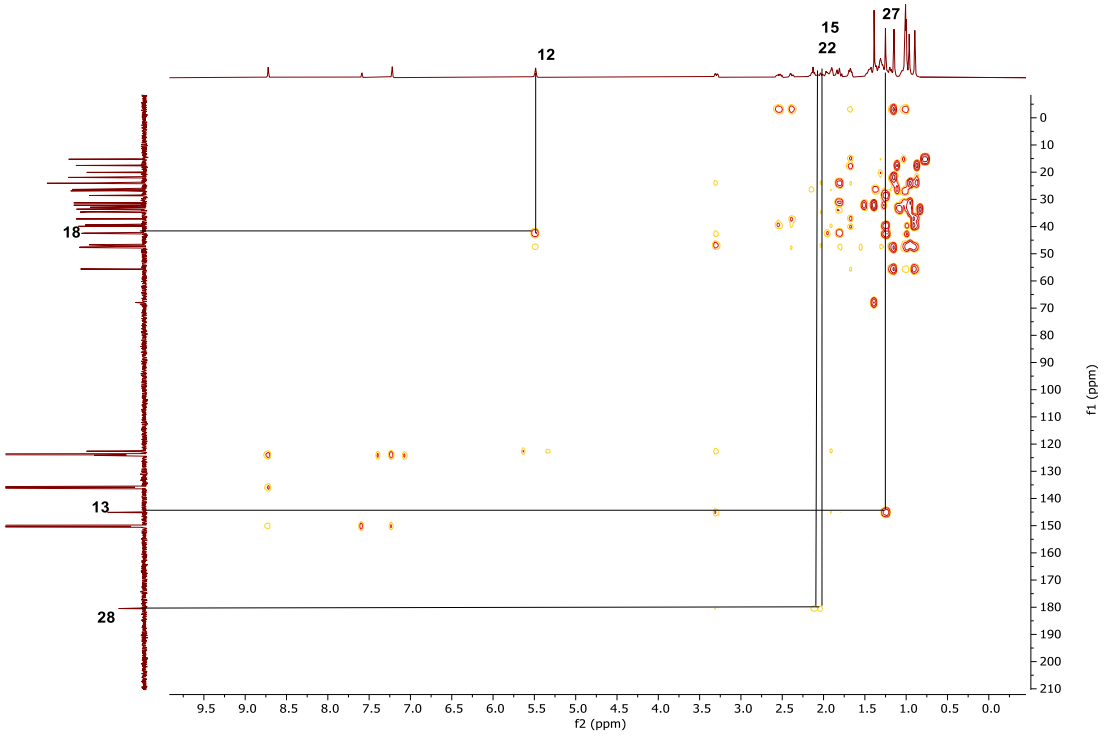

Spectrum 51. HMBC spectrum of MD-MG-02

5.

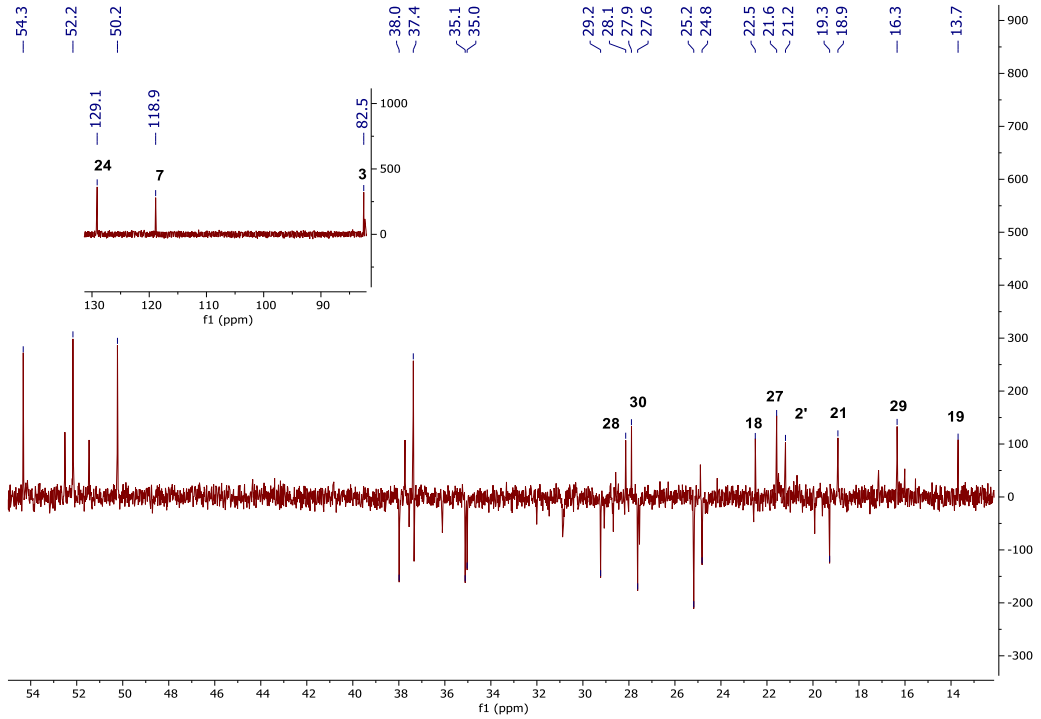

Spectrum 52. DEPT-135 spectrum of MD-MG-03

6.

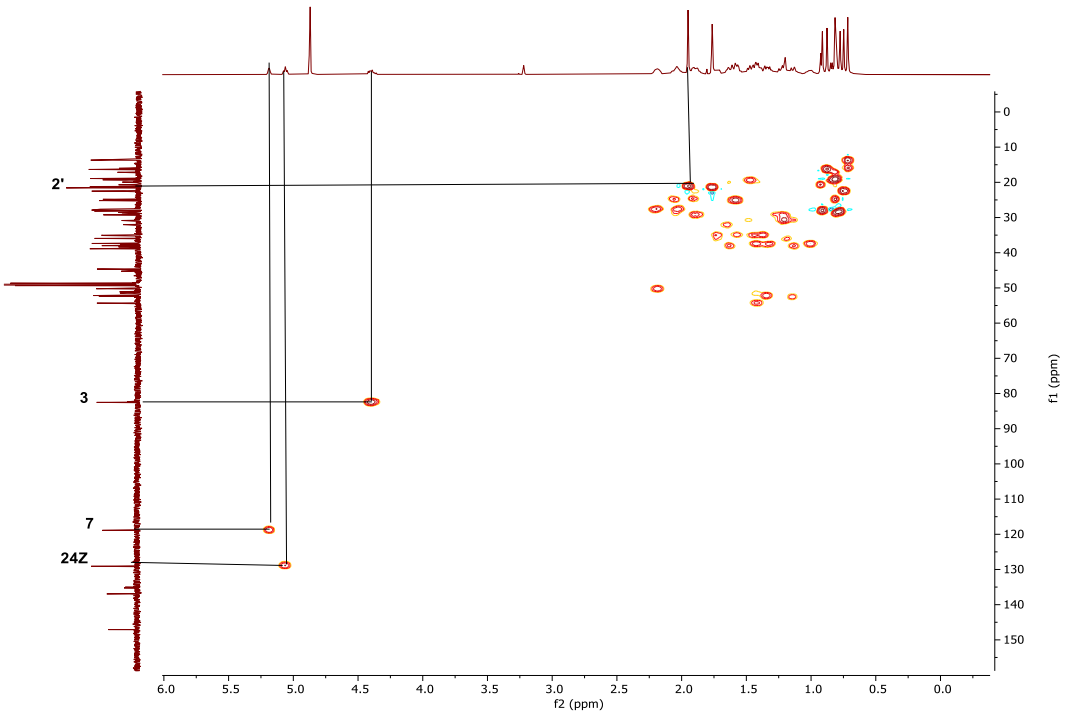

Spectrum 53. HSQC spectrum of MD-MG-03

7.

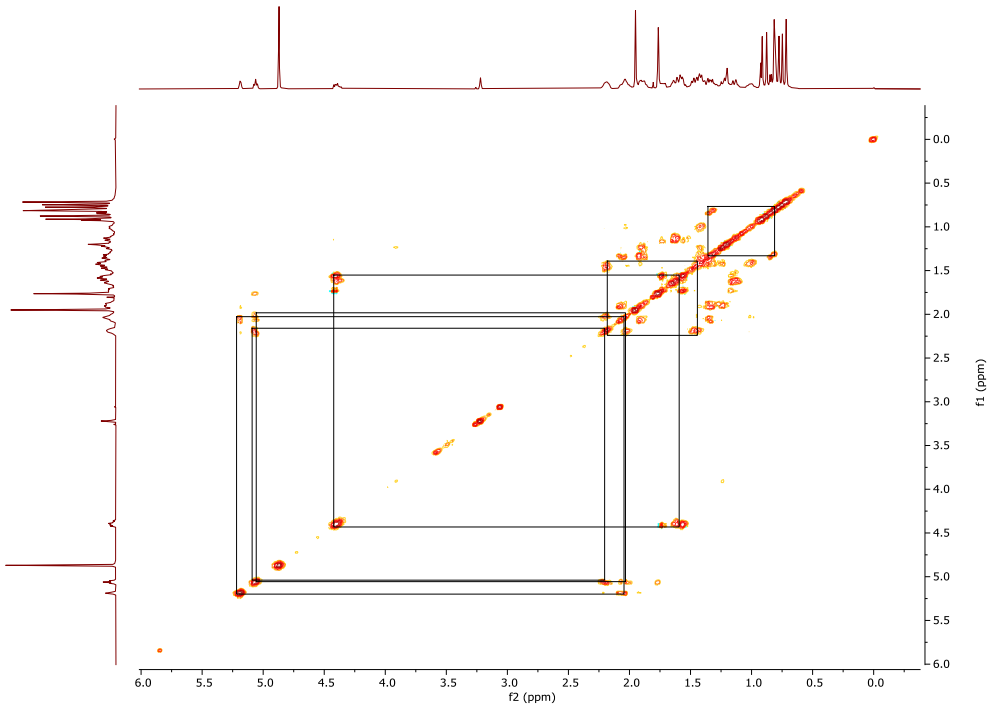

Spectrum 54. COSY spectrum of MD-MG-03

8.

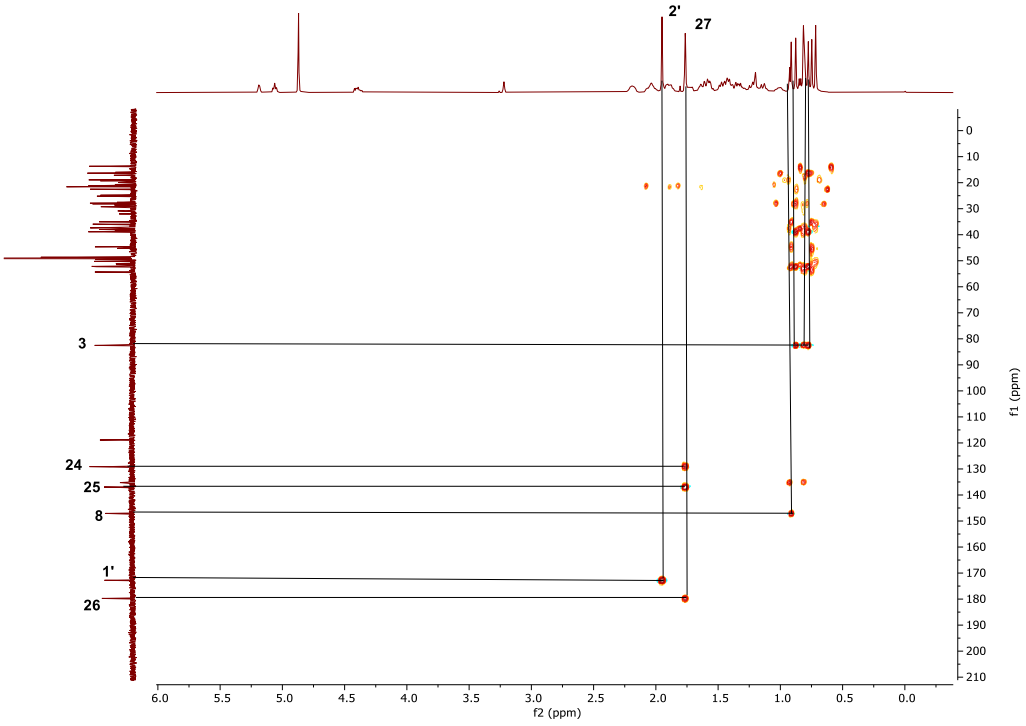

Spectrum 55. HMBC spectrum of MD-MG-03

9.

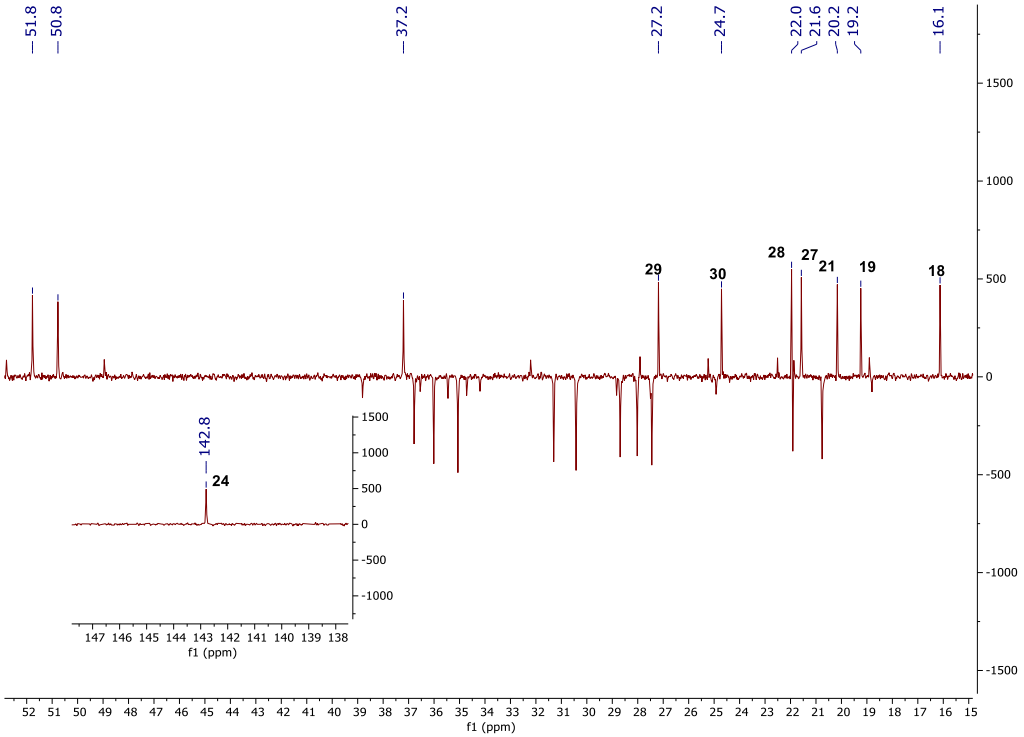

Spectrum 56. DEPT-135 spectrum of MD-MG-04

10.

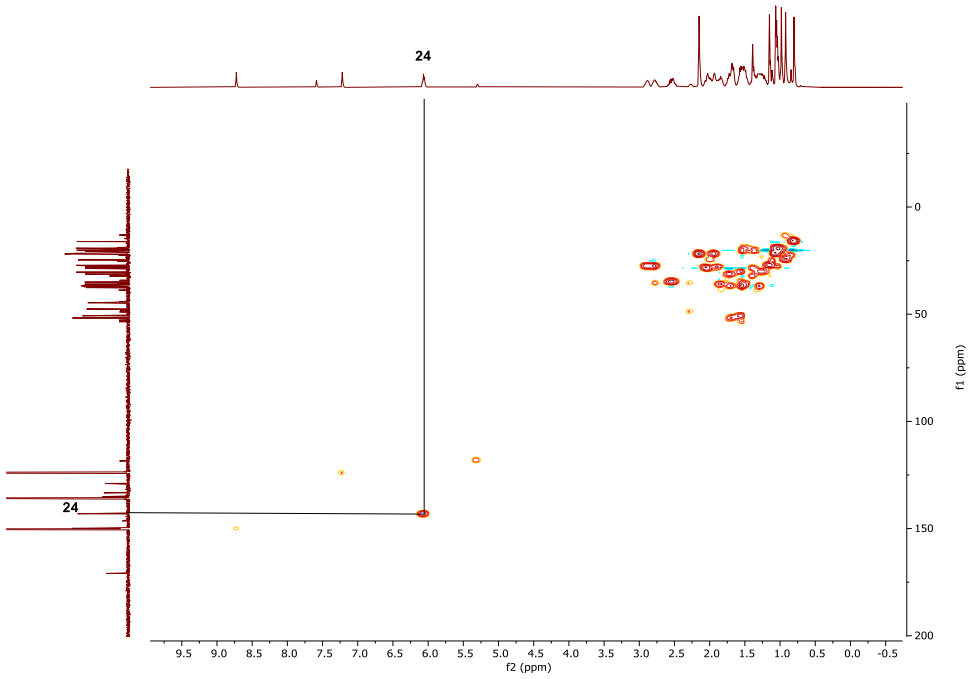

Spectrum 57. HSQC spectrum of MD-MG-04

11.

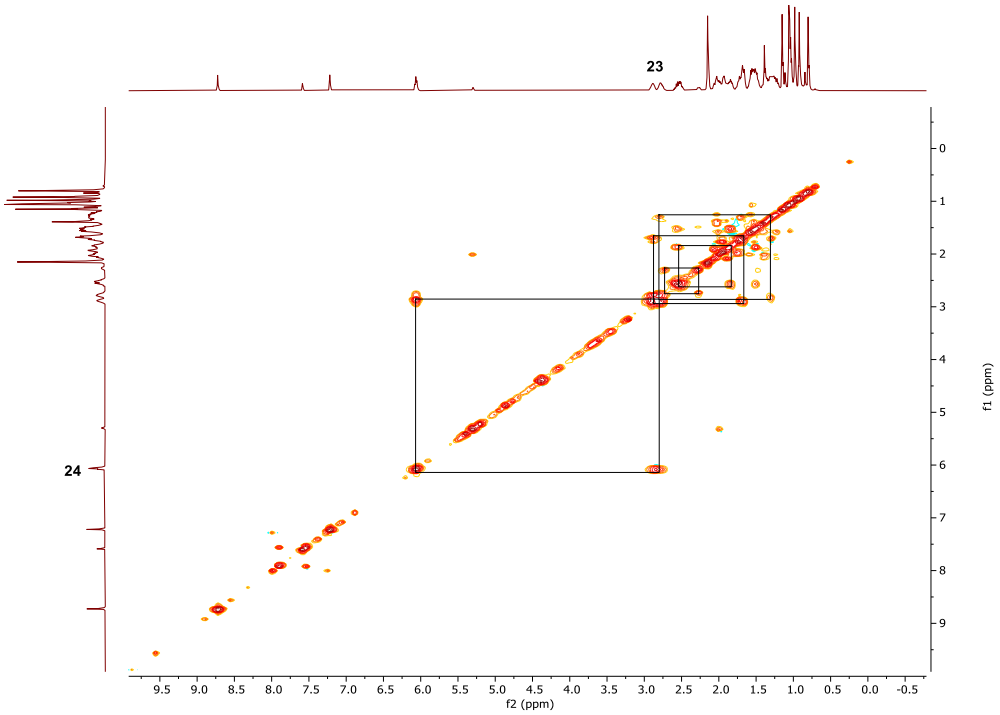

Spectrum 58. COSY spectrum of MD-MG-04

12.

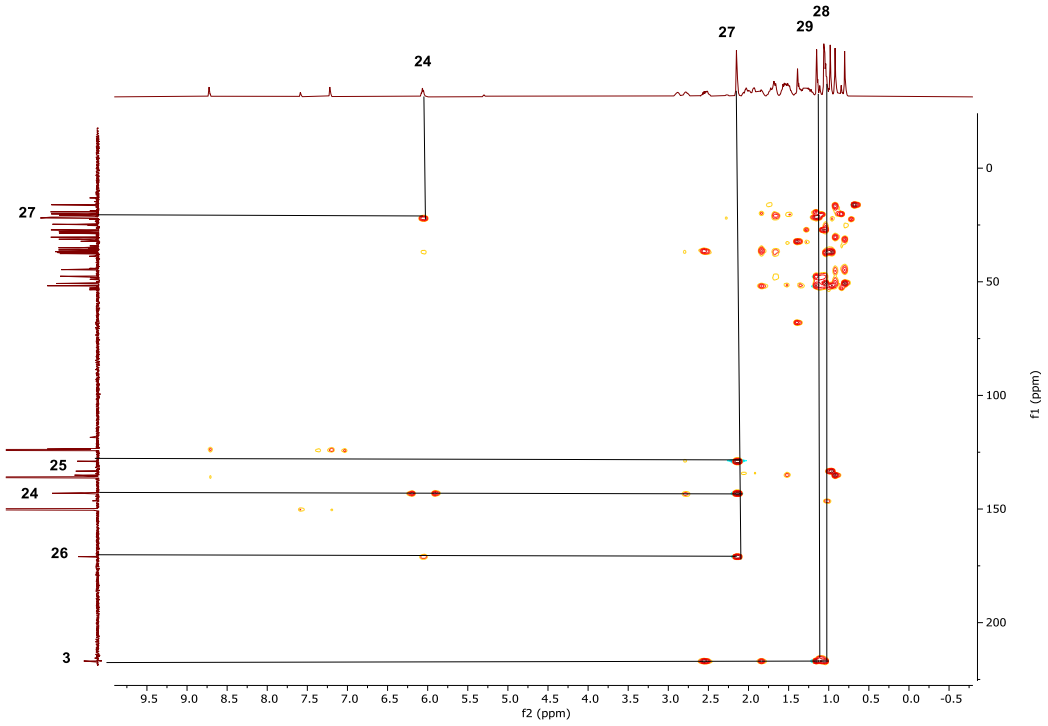

Spectrum 59. HMBC spectrum of MD-MG-04

13.

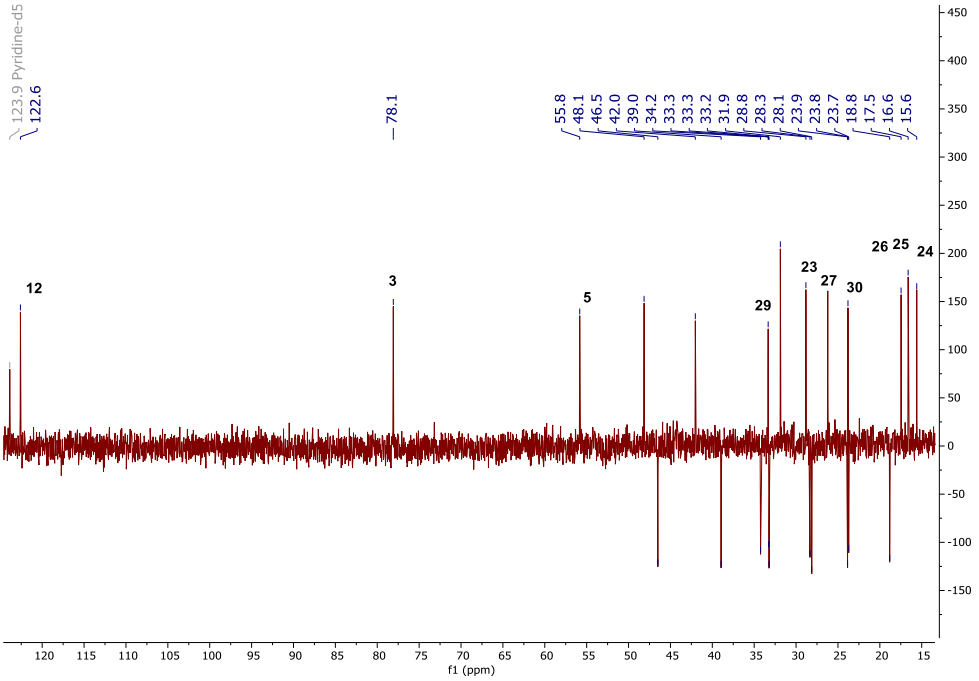

Spectrum 60. DEPT-135 spectrum of MD-MG-05

14.

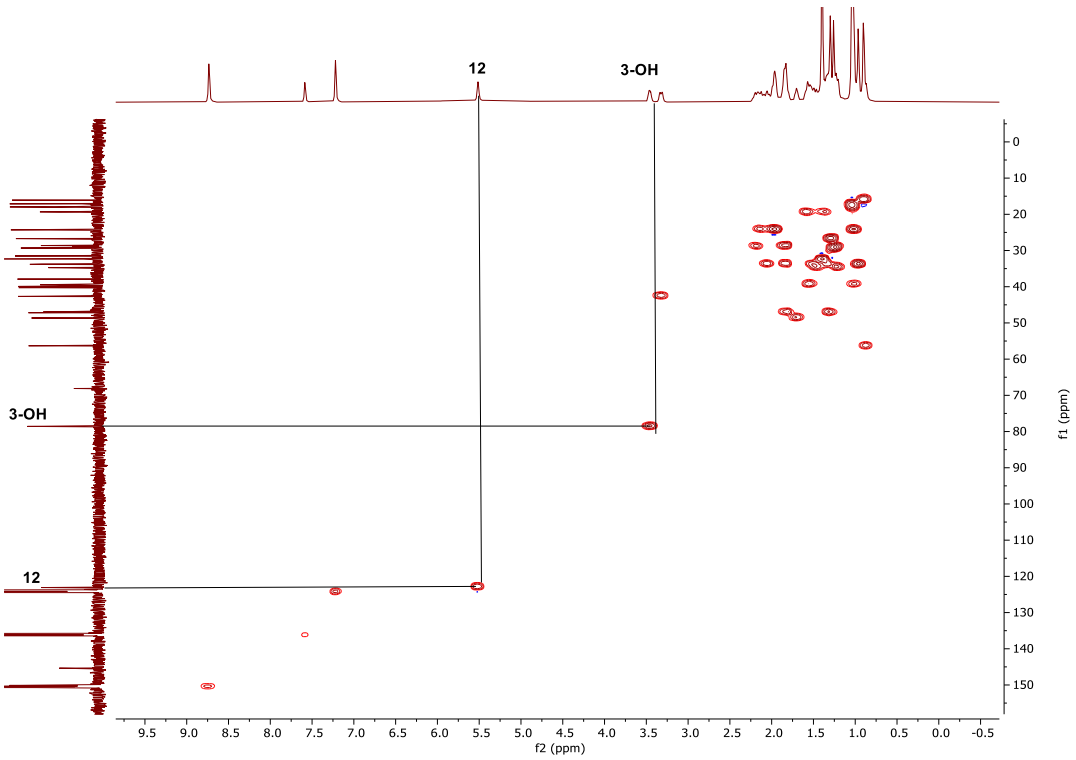

Spectrum 61. HSQC spectrum of MD-MG-05

15.

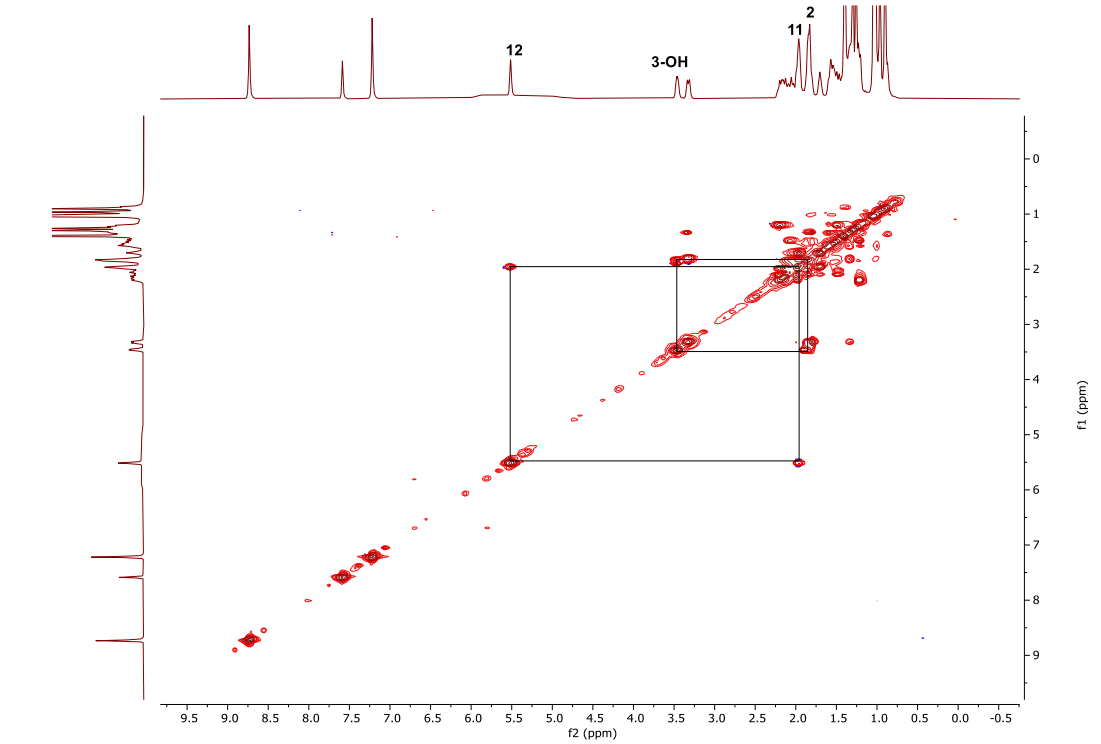

Spectrum 62. COSY spectrum of MD-MG-05

16.

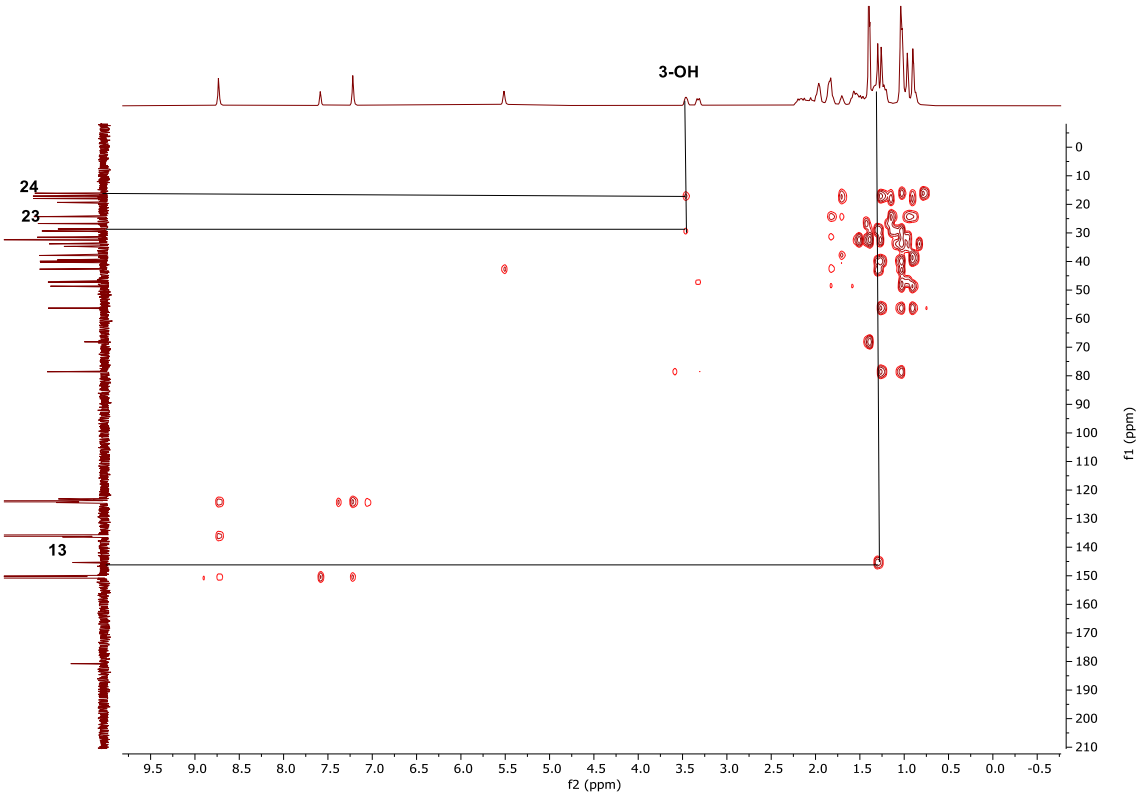

Spectrum 63. HMBC spectrum of MD-MG-05

17.

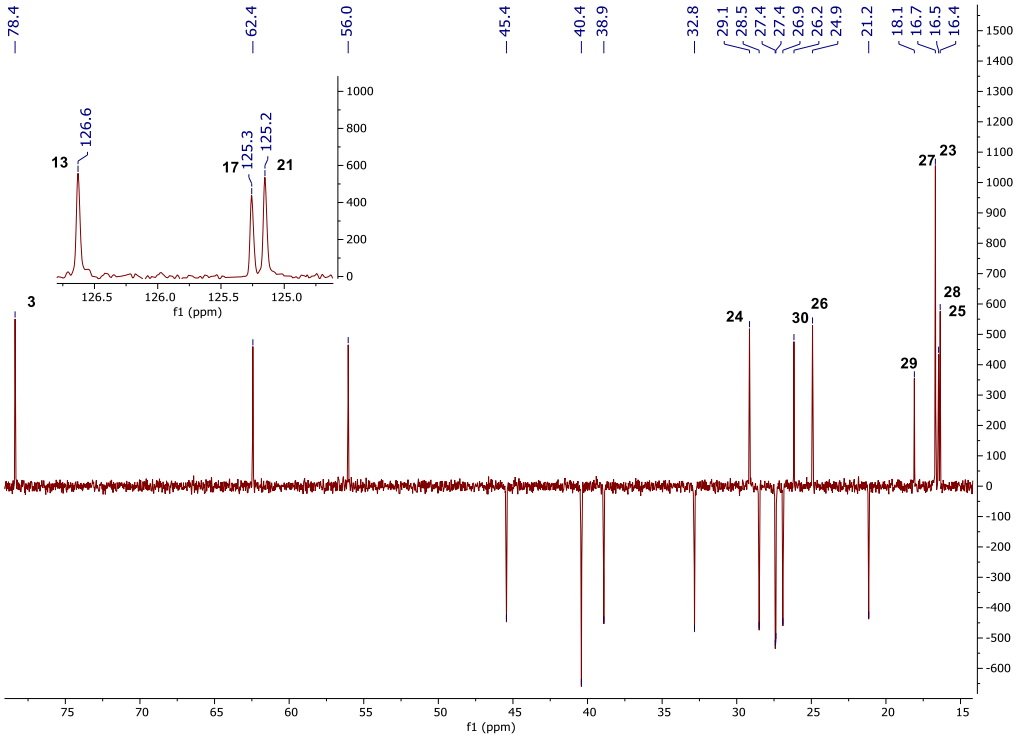

Spectrum 64. DEPT-135 spectrum of MD-MG-06

18.

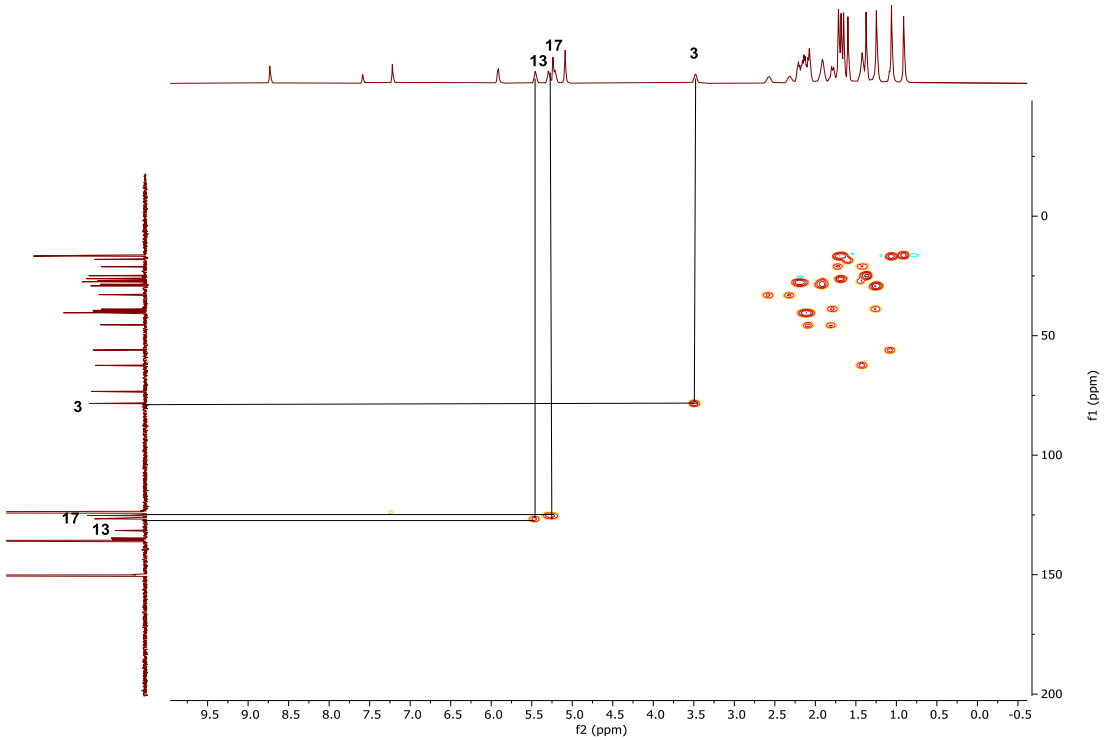

Spectrum 65. HSQC spectrum of MD-MG-06

19.

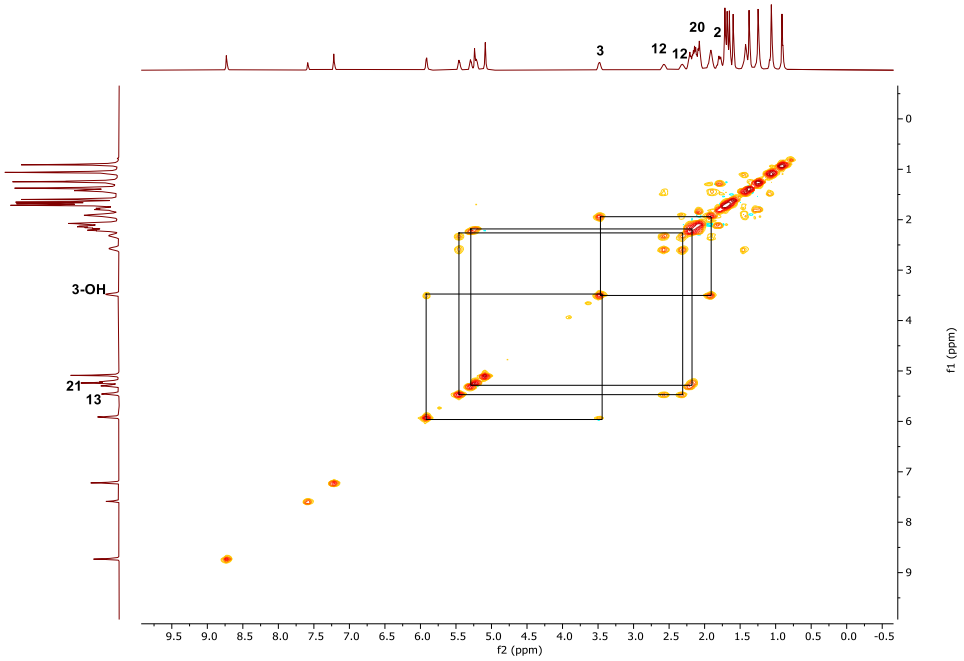

Spectrum 66. COSY spectrum of MD-MG-06

20.

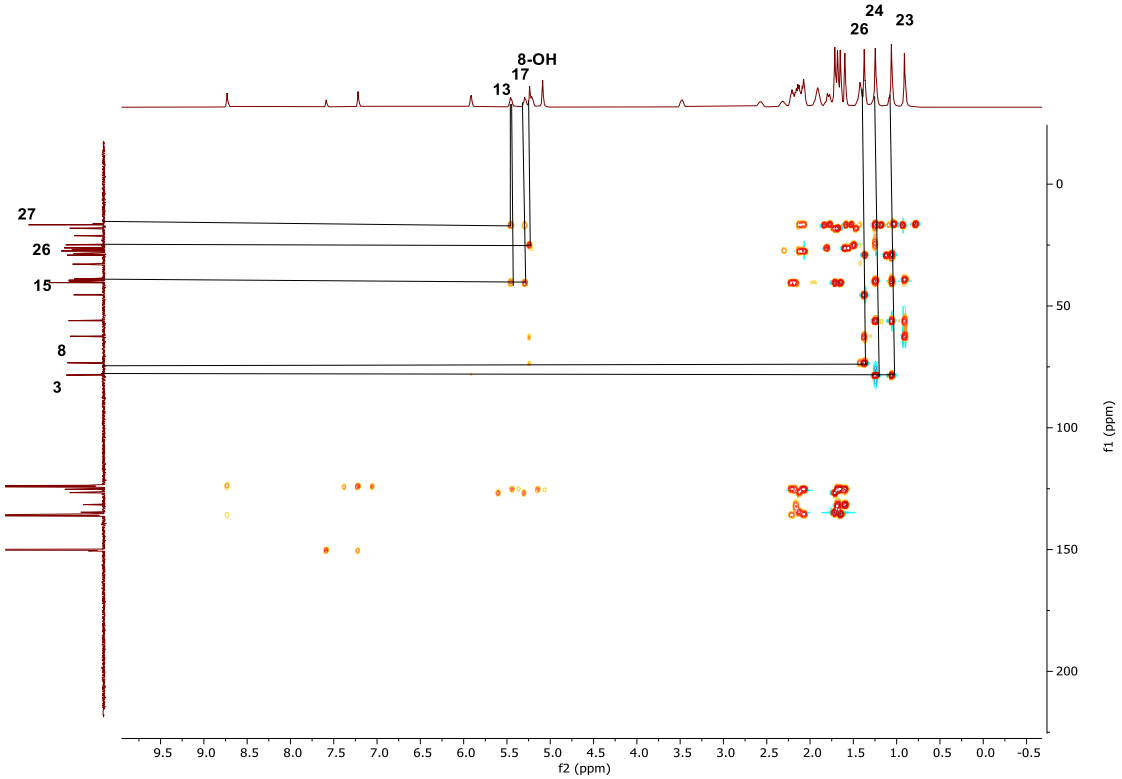

Spectrum 67. HMBC spectrum of MD-MG-06

21.

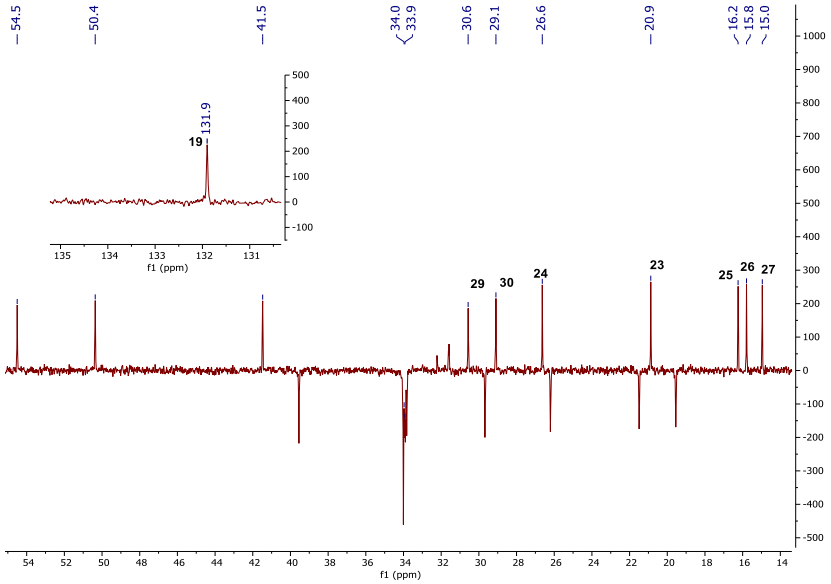

Spectrum 68. DEPT-135 spectrum of MD-MG-07

22.

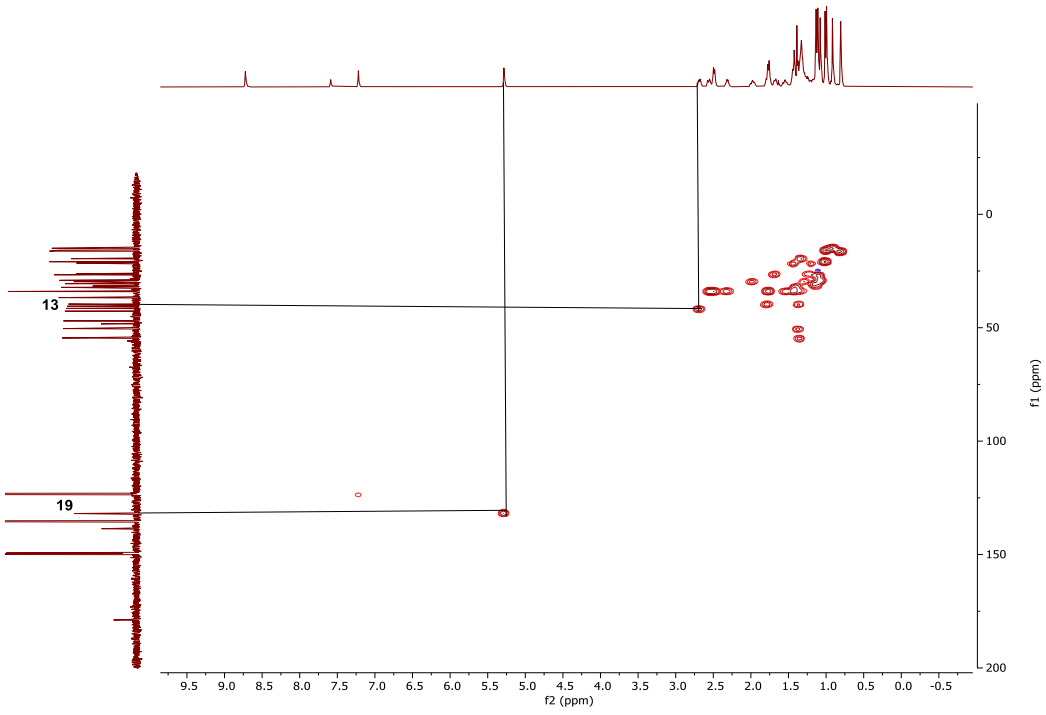

Spectrum 69. HSQC spectrum of MD-MG-07

23.

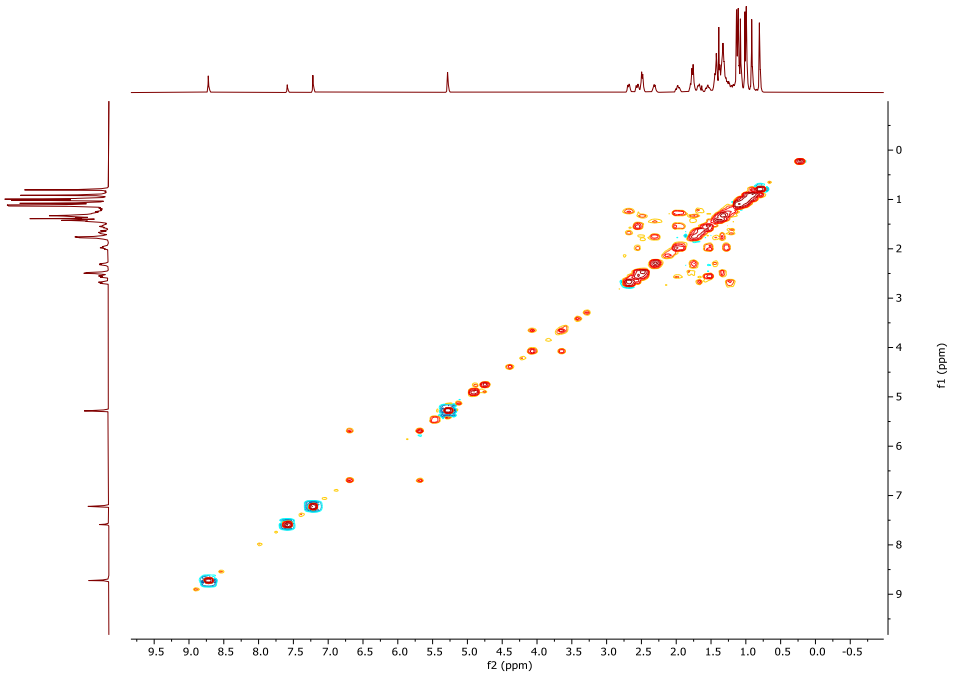

Spectrum 70. COSY spectrum of MD-MG-07

24.

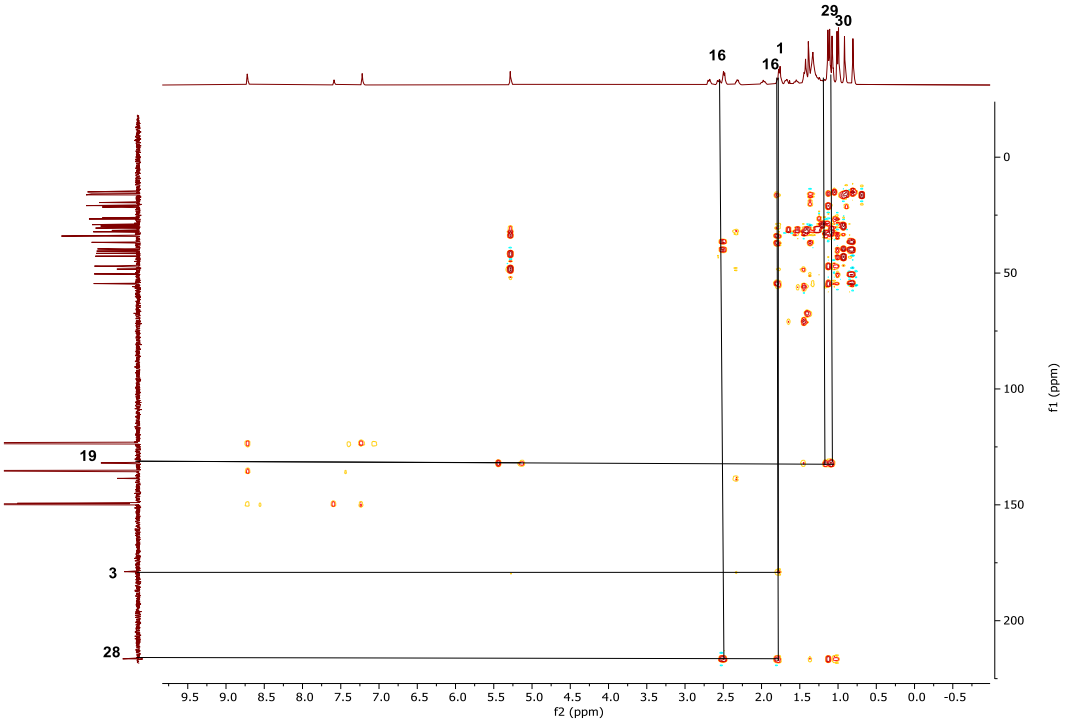

Spectrum 71. HMBC spectrum of MD-MG-07

25.

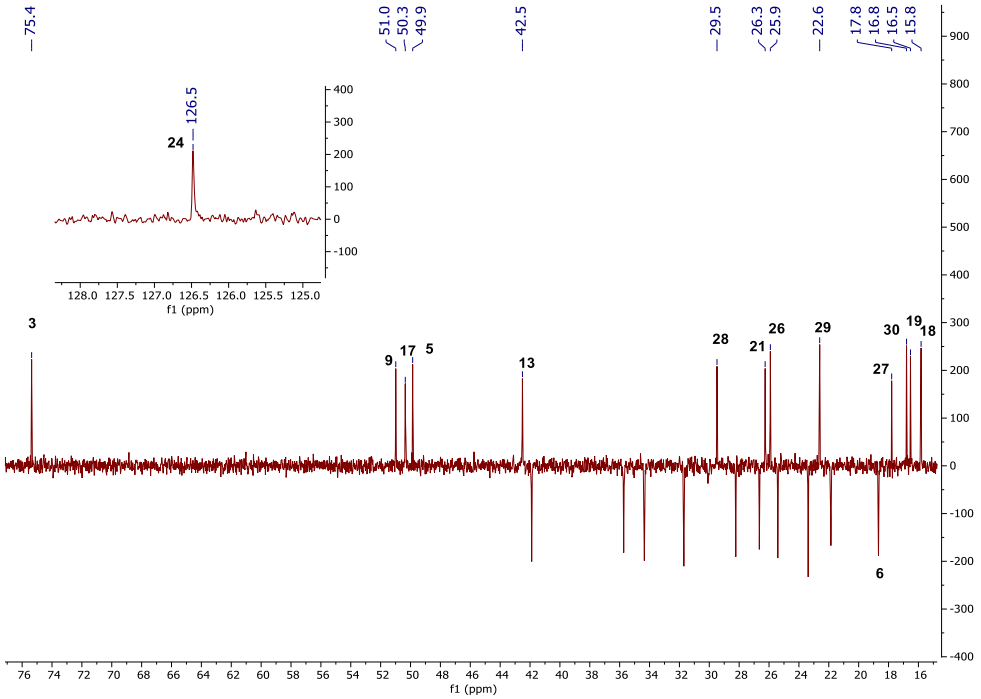

Spectrum 72. DEPT-135 spectrum of MD-MG-12

26.

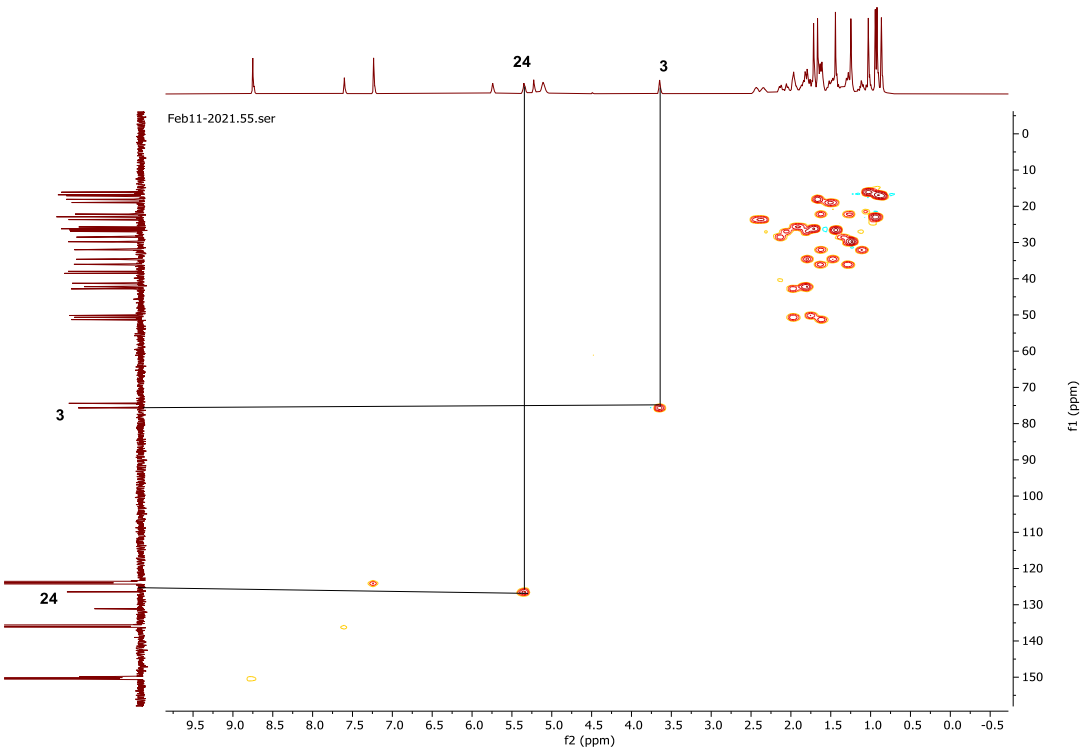

Spectrum 73. HSQC spectrum of MD-MG-12

27.

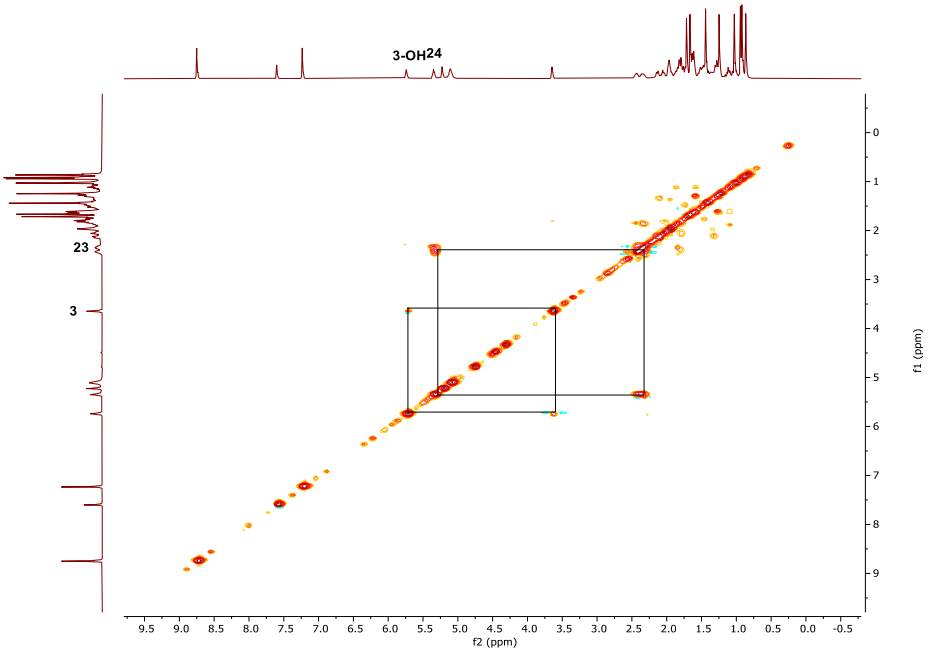

Spectrum 74. COSY spectrum of MD-MG-12

28.

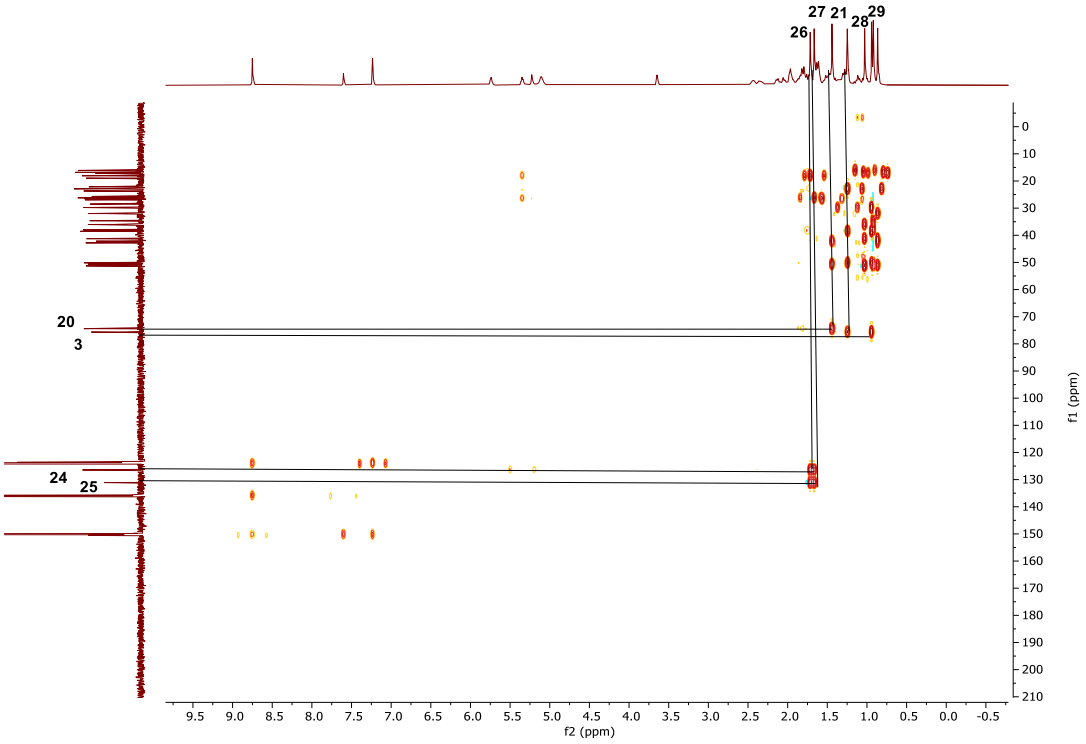

Spectrum 75. HMBC spectrum of MD-MG-12

29.

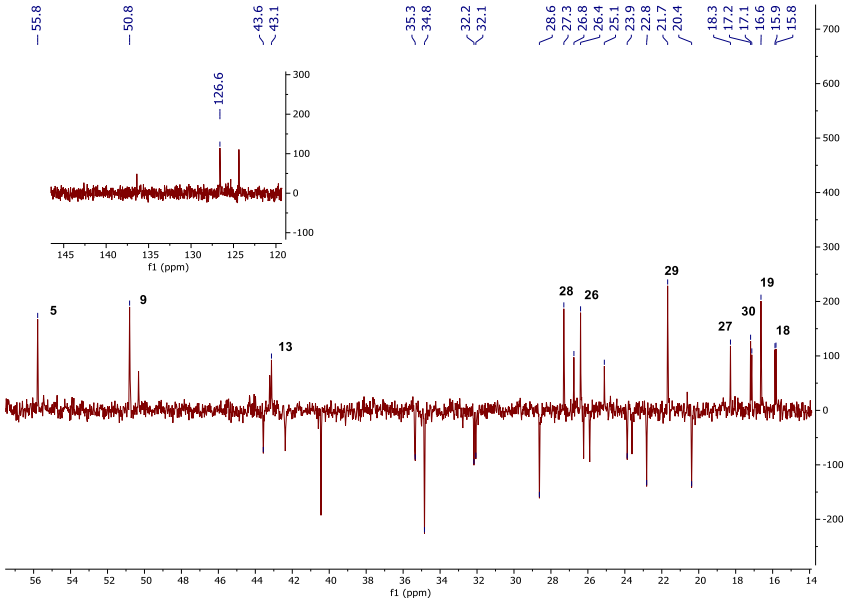

Spectrum 76. DEPT-135 spectrum of MD-MG-14

30.

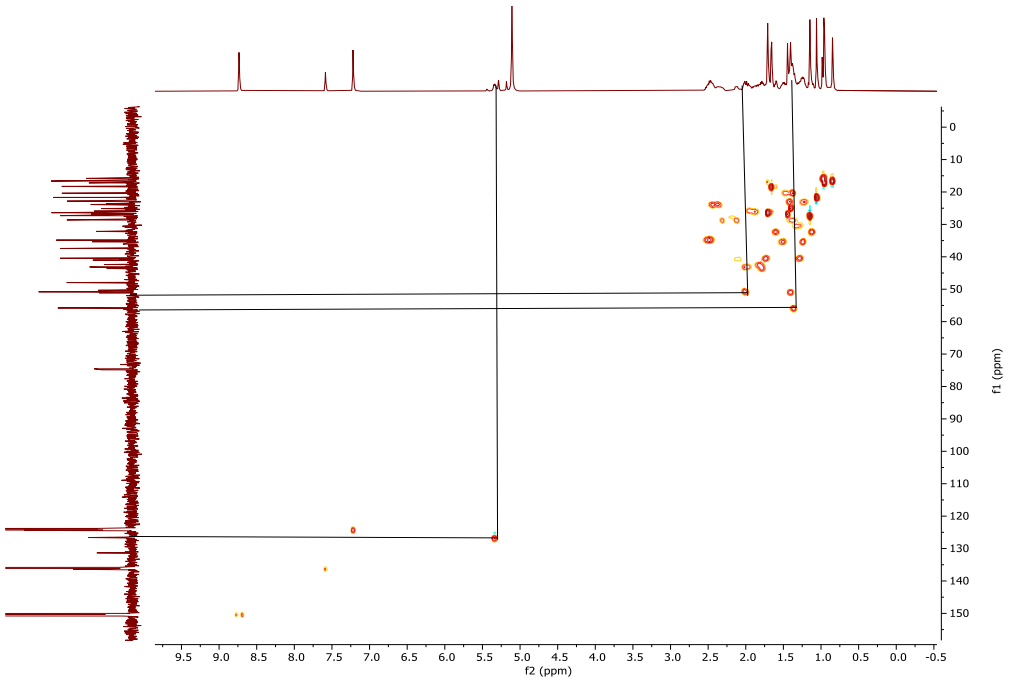

Spectrum 77. HSQC spectrum of MD-MG-14

31.

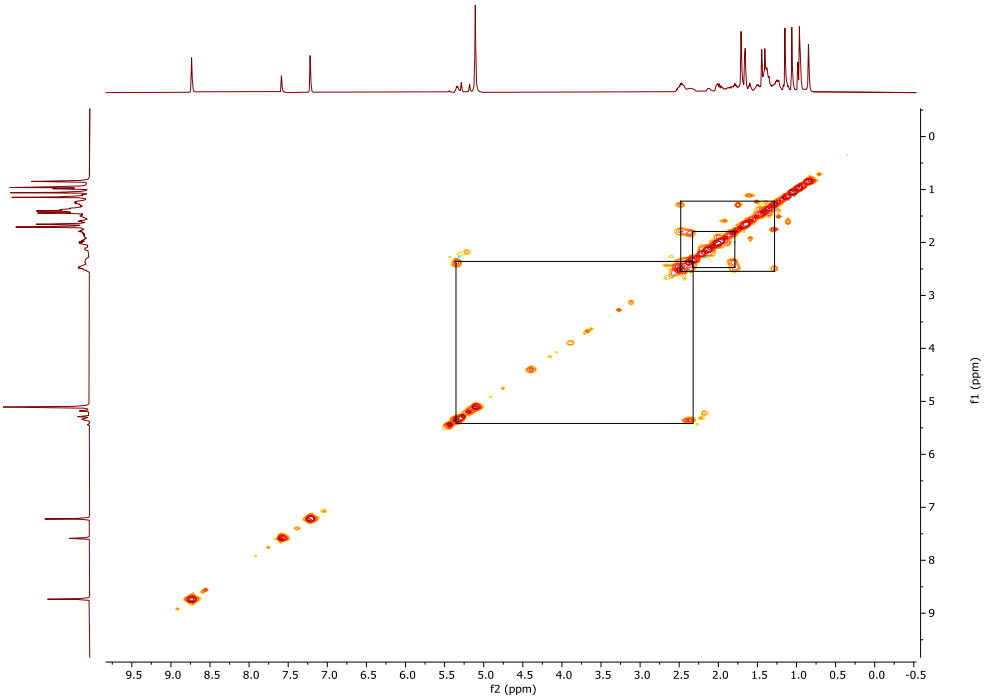

Spectrum 78. COSY spectrum of MD-MG-14

32.

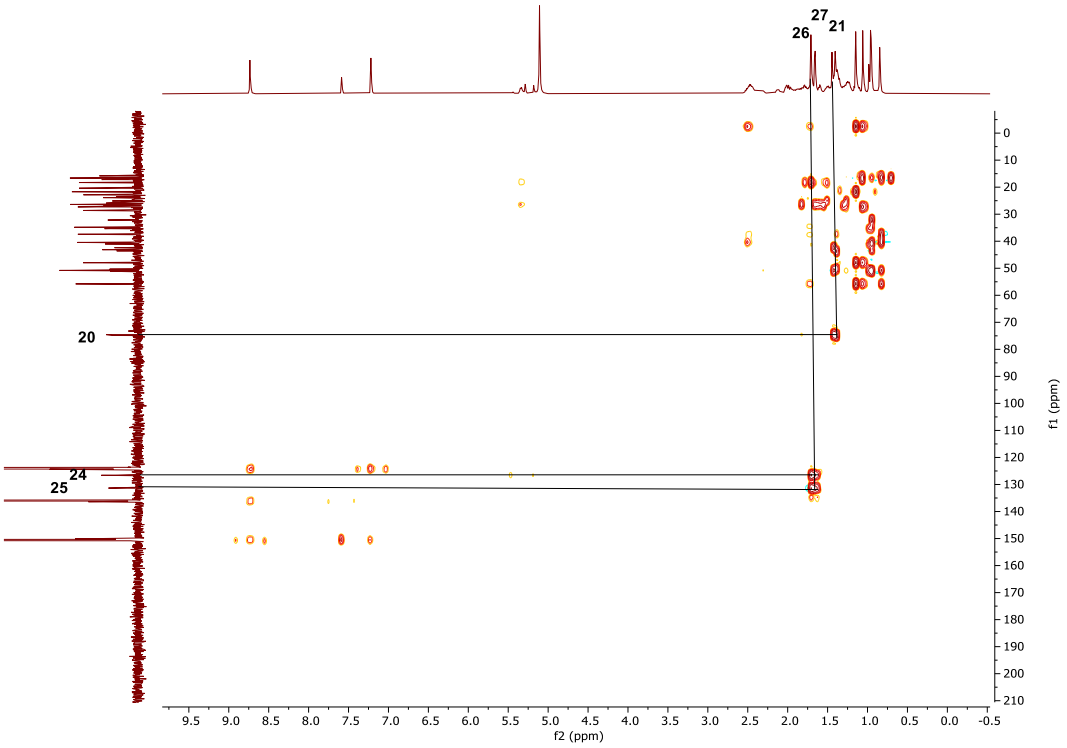

Spectrum 79. HMBC spectrum of MD-MG-14

33.

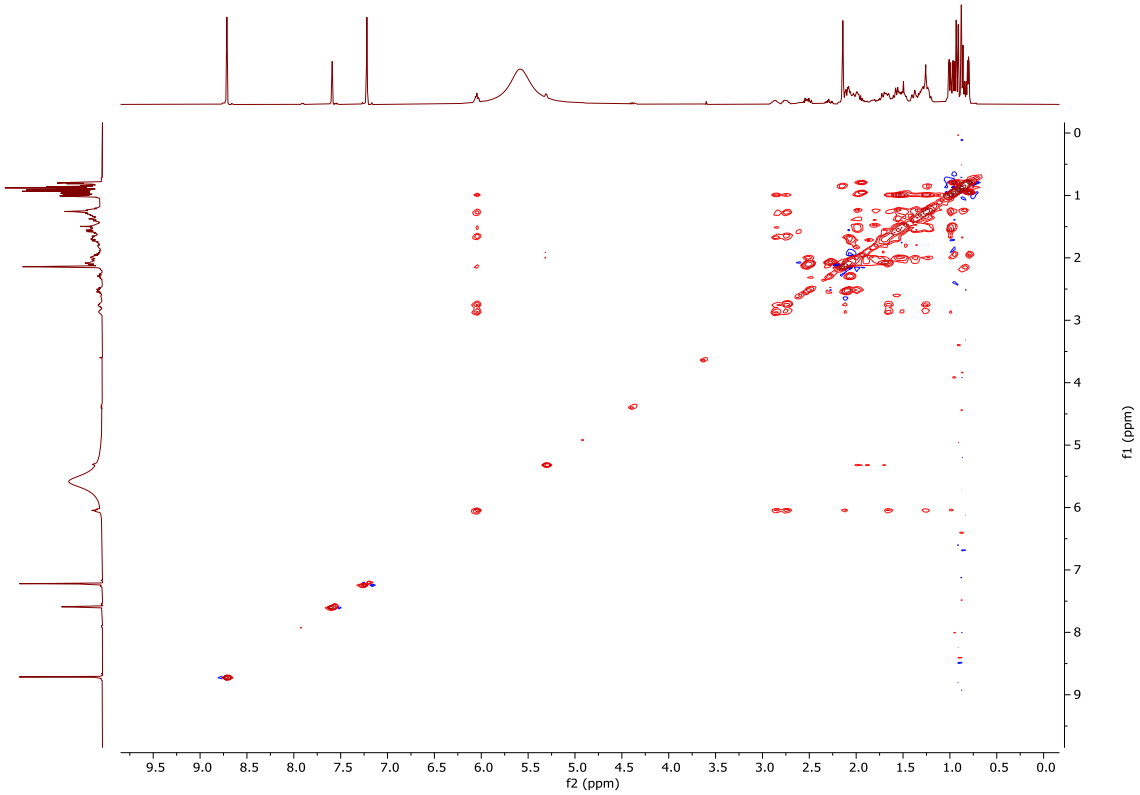

Spectrum 80. TOCSY spectrum of MD-MG-17

34.

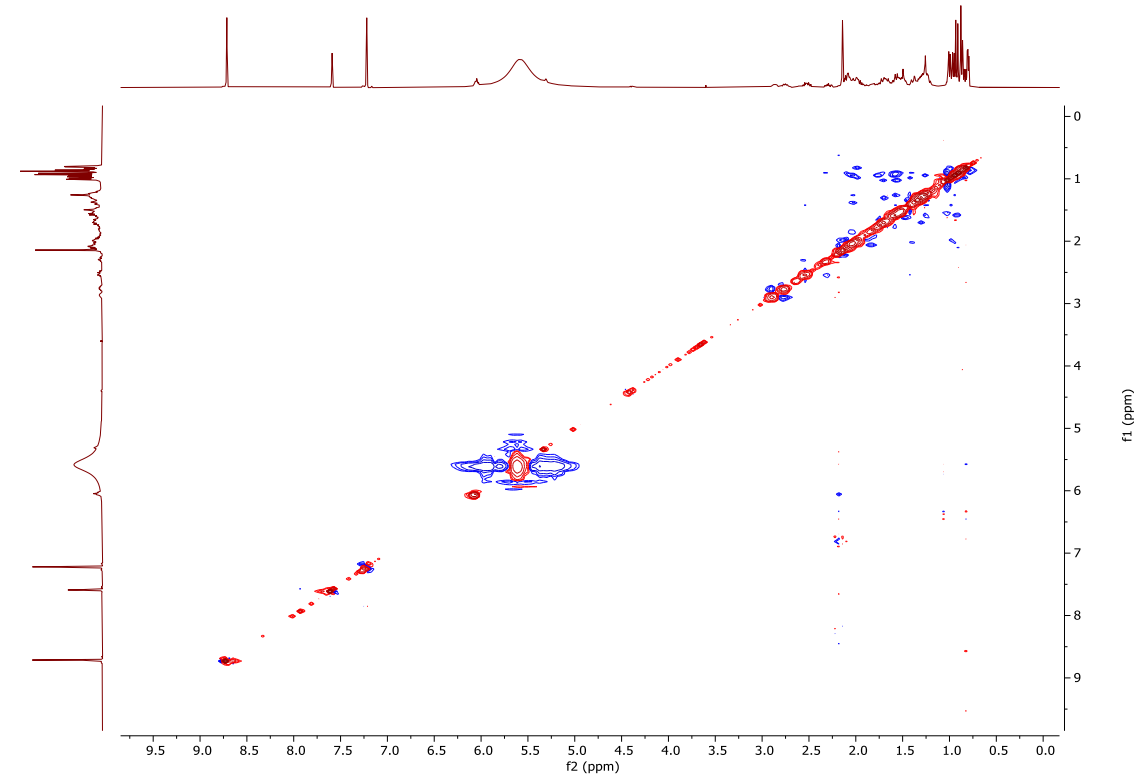

Spectrum 81.NOESY spectrum of MD-MG-17

35.

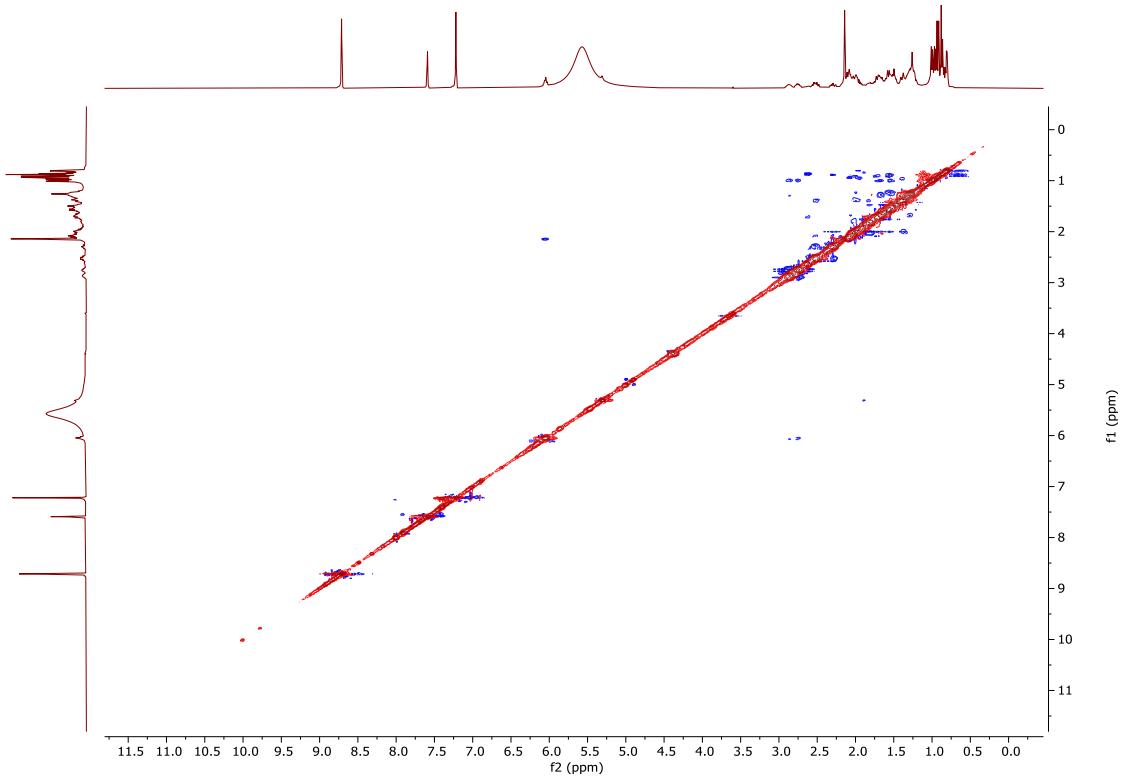

Spectrum 82. ROESY spectrum of MD-MG-17

36.

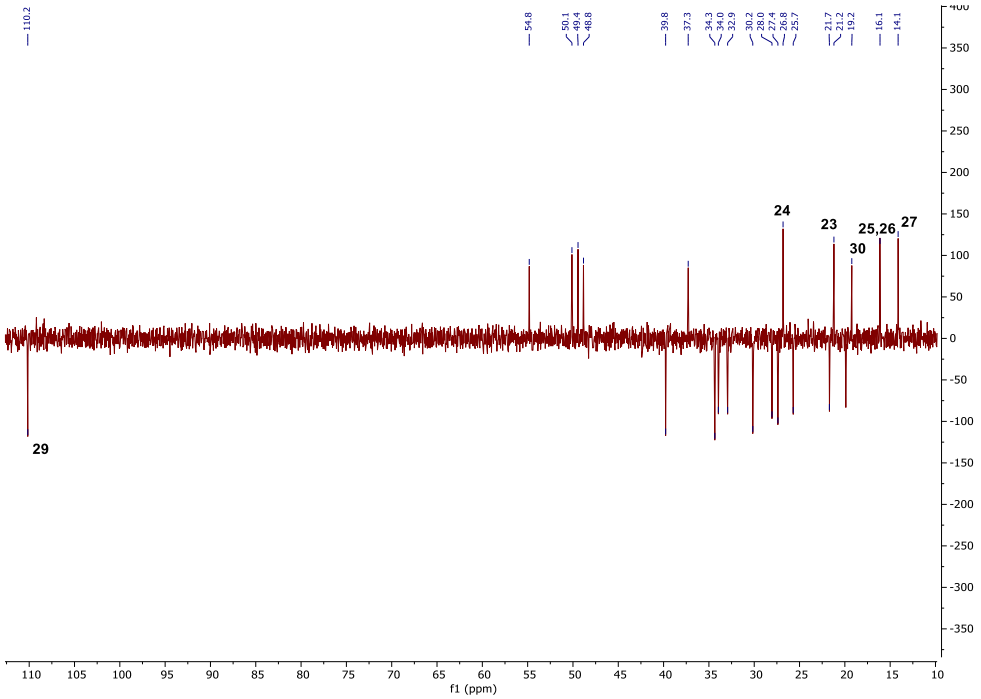

Spectrum 83. DEPT-135 spectrum of MD-MG-19

37.

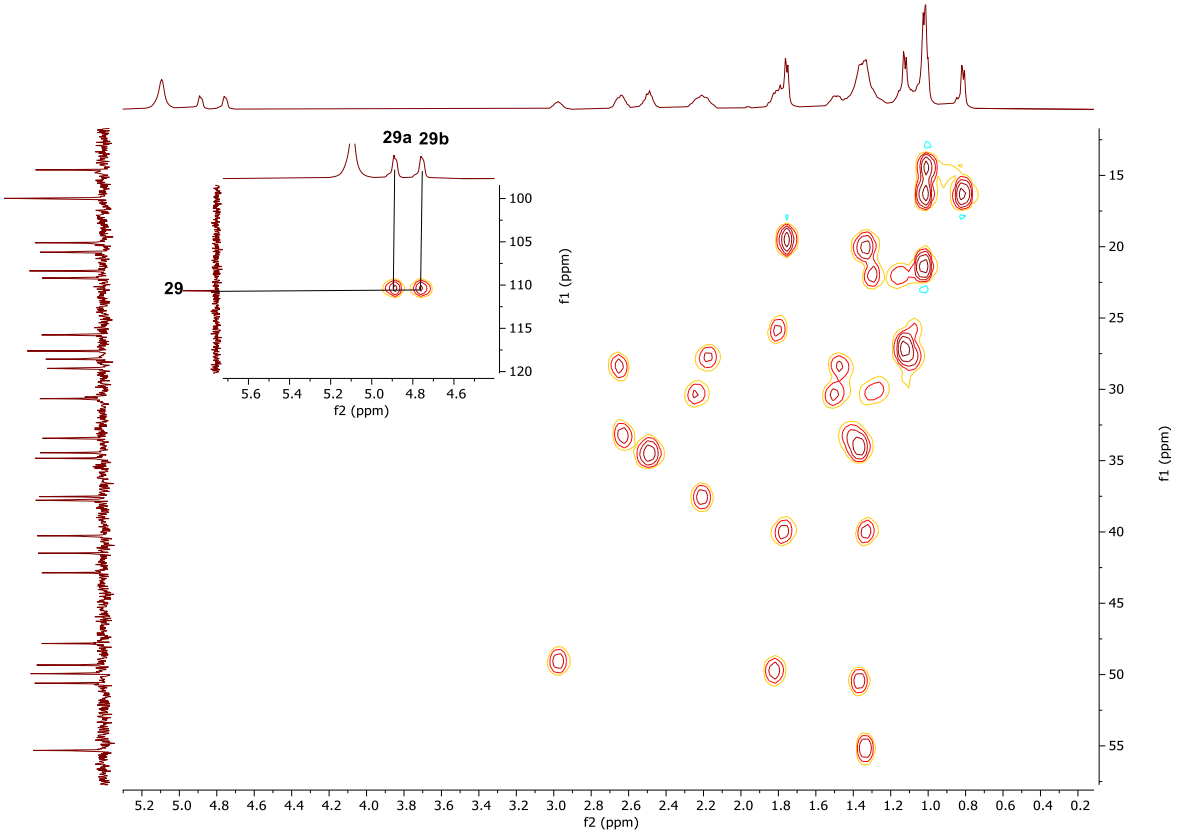

Spectrum 84. HSQC spectrum of MD-MG-19

38.

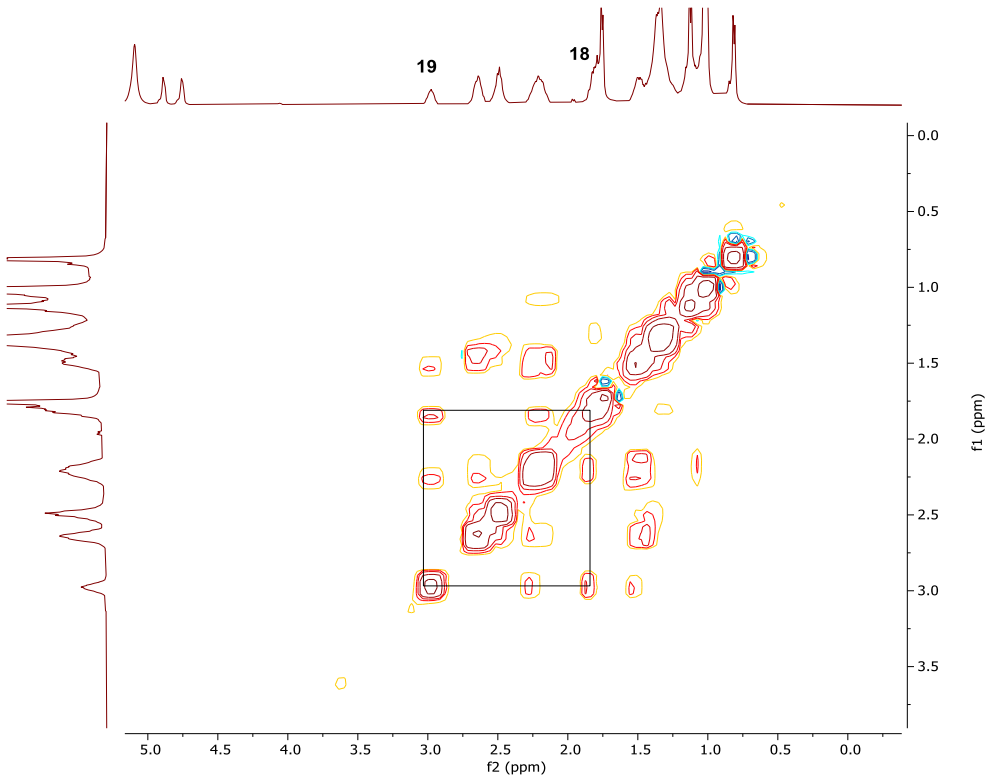

Spectrum 85. COSY spectrum of MD-MG-19

39.

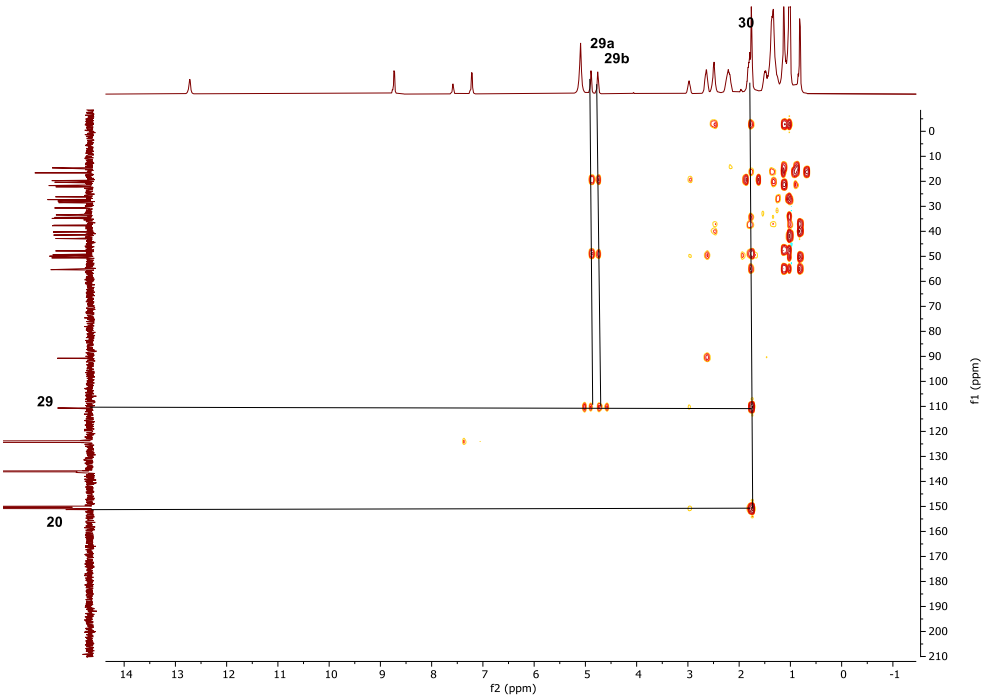

Spectrum 86. HMBC spectrum of MD-MG-19